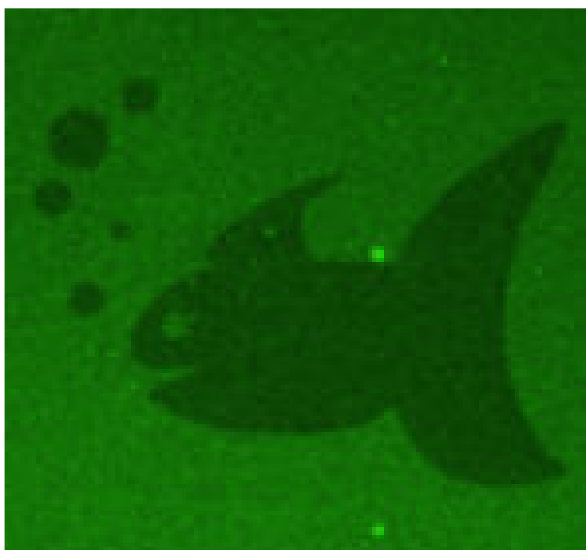# DOCTORAATSPROEFSCHRIFT

2010 | Instituut voor Materiaalonderzoek

Development of diamond-based biosensors

Proefschrift voorgelegd tot het behalen van de graad van
Doctor in de Wetenschappen, te verdedigen door:

Pieter CHRISTIAENS

Promotor: prof. dr. Patrick Wagner
Copromotor: prof. dr. Miloš Nesládek

universiteit
►►hasselt

... meten is weten ...

Volkswijsheid

Acknowledgement

At last, I thank my wife, daughter, parents, brothers, family and friends for the necessary amusing distraction and just being there for me.

Pieter Christiaens,

Brugge,

December 2009.

Composition of the jury

Chairman   Prof. Dr. J. Manca

Dean Faculty of Science,
UHasselt, Belgium

Promoter: Prof. Dr. P. Wagner

IMO, UHasselt, Belgium

Co-promoter: Prof. Dr. M. Nesládek

IMO, UHasselt, Belgium

Members of the jury: Prof. Dr. M. J. Schöning

Laboratory for Chemical Sensors and Biosensors,
Aachen University of Applied Sciences,
Jülich, Germany

Prof. Dr. P. Bienstman

Department of Information Technology,
Ghent University, Belgium

Dr. N. Bijnens

Biomedical Engineering Materials Technology,
Eindhoven University of Technology,
the Netherlands

Prof. Dr. W. De Ceuninck

IMO, UHasselt, Belgium

Prof. Dr. L. Michiels

BIOMED, UHasselt, Belgium

Prof. Dr. M. Ameloot

BIOMED, UHasselt, Belgium

Contents

Figures

Abbreviations

a.u.	arbitrary units
AC	alternating current ($\sim$)
AFM	atomic force microscope
CBM	conduction band minimum
CH_4	methane gas
CNT	carbon nanotube
CVD	chemical vapour deposition
Da	Dalton (unit of molecular weight (MW))
DC	direct current (=)
DNA	deoxyribonucleic acid
EDX	energy dispersive X-ray imaging
EDC	1-ethyl-3-(3-dimethylaminopropyl)carbodiimide, a zero-length crosslinker
EDIS	electrolyte-diamond-insulator-semiconductor (sensor)
EIS	electrolyte-insulator-semiconductor (sensor)
ELISA	enzyme-linked immunosorbent assay
EOSFET	electrolyte oxide semiconductor field effect transistor
eV	electron volt
FET	field effect transistor
H_2SO_4	sulphuric acid
HNO_3	nitric acid
ISFET	ion-sensitive field effect transistor
KNO_3	saltpeter (potassium nitrate)
MW	molecular weight (Da)
NCD	nanocrystalline diamond
PAH	poly(allylamine hydrochloride), a positively charged PE
PCD	polycrystalline diamond
PCR	polymerase chain reaction
PE	polyelectrolyte, a charged macromolecule
PEM	polyelectrolyte multilayer
PSS	poly(sodium 4-styrene sulfonate), a negatively charged PE
SCD	single-crystal diamond
SEM	scanning electron microscope
SGFET	solution-gate field effect transistor
SSMCC	sulfo-succinimidyl 4- (N- maleimidomethyl) cyclohexane -1-carboxylate, a crosslinker

STP	standard temperature and pressure
SU-8	two-component epoxy casting polymer
TFAAD	trifluoroacetic acid-protected 10-aminodec-1-ene
UA	undecylenic acid (= undecenoate)
UNCD	ultrananocrystalline diamond
UV	ultraviolet
VBM	valence band maximum
XPS	X-ray photoelectron spectroscopy

Nederlandstalige samenvatting

De behoefte om (biologische) stoffen op te sporen en te meten, wordt steeds groter; niet alleen door een groeiende aandacht voor gezondheid en leefmilieu, maar ook als ondersteuning voor politietaken als sporenonderzoek, drugs- en terrorismebestrijding. Naast medische diagnostiek worden voedselveiligheid (Salmonella, BSE, …) en dierziektebestrijding belangrijker. Ook moet de keuzevrijheid van de consument in onze vrije markt gegarandeerd kunnen worden: hij moet kunnen kiezen voor voedsel dat volledig biologisch geteeld werd of vrij is van genetisch gemodificeerde organismen. Sensoren vormen een antwoord op deze steeds groter wordende vraag om kwalitatief en kwantitatief aan te geven wat en hoeveel van een bepaalde stof aanwezig is (meten is weten!). Op basis van deze kennis kan men onderbouwde beslissingen nemen.

In hoofdstuk 1 wordt beschreven dat biosensoren ten opzichte van chemische en fysische sensoren het voordeel hebben dat ze, net omdat ze uit biologisch materiaal gemaakt worden, heel snel, specifiek en gevoelig reageren. Ze functioneren op de overgang van de levende (biologie) naar de dode wereld (elektronica). Rond de gevoelige biologische kern zitten fysische of chemische componenten die het biologische signaal omzetten en versterken naar een door de gebruiker waarneembaar signaal.

Vroeger werden kanaries als verklikker voor mijngas ingezet. Tegenwoordig doen moleculen zoals enzymen het opsporingswerk op microschaal. De eerste échte biosensor was de Clark-elektrode waar een zuurstofsensor gecombineerd werd met een enzymmembraan voor het opsporen en meten van glucose. Vandaag variëren de toepassingen van goedkope, draagbare, doe-het-zelf glucosemeters voor diabetici (vb. Accu-Chek® van Roche) tot dure, volledig geautomatiseerde laboratoriumtoestellen (vb. GeneChip® microarray van Affymetrix). Meten en benoemen van eiwitten door immunosensoren en van DNA door DNA-sensoren, in combinatie met de kennis die vergaard werd bij het menselijke genoomproject, maken het vandaag mogelijk om ziekten en erfelijke aandoeningen in een vroeg stadium op te sporen, zodat erger voorkomen kan worden.

Diamant ligt omwille van zijn biocompatibiliteit voor de hand als basismateriaal voor implanteerbare biosensoren. In hoofdstuk 2 wordt uitgelegd hoe diamant kunstmatig kan aangemaakt worden en hoe de eigenschappen

aangewend en zelfs veranderd kunnen worden. Zulke stabiele sensoren zouden gedurende een lange periode in het lichaam werkzaam blijven, waardoor herhaaldelijke monstername kan achterwege blijven en er voortdurende monitoring kan plaatsvinden van bvb. de zuurtegraad van het bloed. Diamant kan immers als dunne laag kunstmatig afgezet worden op verschillende ondergronden, gaande van glas tot halfgeleidend silicium. Zo ontstaat een afschermende diamantlaag die lichaam en sensor scheidt. Een deel van de sensor wordt dan het gevoelig sensoroppervlak door functionalisering met biologische componenten. De chemische inertheid maakt het echter net moeilijk om het oppervlak te functionaliseren met een biologische component tot een gevoelige laag.

Overtuigd van het belang van biosensoren en het potentieel van diamant als dragermateriaal, werden in hoofdstuk 5 en 6 van deze doctoraatsstudie de grenzen van een nieuw multidisciplinair onderzoeksdomein afgetast, waarbij natuurkundige kennis gecombineerd wordt met biologie: de eerste onderzoeksstappen op weg naar een biosensor met diamant als basismateriaal werden gezet.

Ten eerste onderzocht op welke manier DNA aan diamant kan gehecht worden met het oog op een latere toepassing in een biosensor die gevoelig is voor DNA-hybridisatie. Deze aanhechting moet een evenwicht vinden tussen enerzijds de nabijheid van het sensormateriaal (dichtbij zodat de sensor gevoelig is), en anderzijds de sterische bereikbaarheid (bewegingsvrijheid zodat hybridisatie makkelijk kan plaatsvinden). In hoofdstuk 5 wordt uitgelegd op welke manier we er in slagen DNA aan diamant te bevestigen door middel van ω-onverzadigde vetzuren, ultraviolet licht en de chemische stof EDC die kruisverbindingen maakt.

Ten tweede werd nagegaan hoe diamant als actief sensormateriaal kan ingezet worden. Als benadering voor een echte DNA-sensor werd eerst de gevoeligheid voor veranderingen van zuurtegraad (pH) bepaald, en daarna werden laagjes polyelektrolyt als model voor hybriserend DNA opgemeten. In hoofdstuk 6 wordt de ConCap-meetmethode uitgelegd: De condensatoreigenschap van een silicium plaatje met een laagje diamant wordt gebruikt om ladingsopbouw aan het oppervlak door pH-verandering op te sporen. Deze meetopstelling werd verder uitgebreid met geladen polyelektrolytketens die model staan voor DNA.

De technische beschrijving van de aangewende onderzoekstechnieken voor het karakteriseren van diamantstalen staat in hoofdstuk 3: achtereenvolgens worden contacthoekbepaling, atoomkrachtmicroscopie, elektronenmicroscopie, fluorescentiemicroscopie en foto-elektronmicroscopie uit de doeken gedaan. Hoofdstuk 4 beschrijft in welke materialen en methoden gebruikt werden in het onderzoek. Er wordt aangegeven hoe de diamantstalen geprepareerd worden, hoe het DNA bereid en vastgehecht wordt. Hier wordt ook de opstelling voor de concap-meting uit de doeken gedaan.

In het laatste hoofdstuk (7) besluiten we deze thesis met beschouwingen over welke verschillende richtingen verder onderzoek kan uitgaan.

De doctoraatsthesis werd in het Engels opgesteld omdat die taal op dit moment de *lingua franca* van de wetenschappelijke wereld is.

Preface

The need to detect and measure (biological) substances has increased dramatically; not only by the growing attention for good practices and quality assurance in health and environmental management, but also as support for high-tech police tasks, like crime scene investigation, narcotics and terrorism control. Apart from medical diagnostics, food safety (Salmonella, BSE, …) and animal health become more important. Also the free choice of consumers in our free market economy must be guaranteed: it must be possible to choose for biological or genetically-modified-organism-free food.

Biosensors are the answer to these new emerging questions. With respect to chemical and physical sensors, they have the advantage that they, because they are made of biological materials, react very fast, specific and sensitive. They operate at the interface between the living (biology) and the dead world (electronics). Around the sensitive biological core, there are physical or chemical components that transform and amplify the biological signal to a signal that can be observed by the user.

Canary birds used to function as mine gas indicator. Nowadays, active molecules, like enzymes do this detection at a much smaller level. The first real biosensor was the Clark electrode, combining an oxygen sensor with an enzyme membrane for the detection and measurement of glucose (1962). Today applications range from cheap portable do-it-yourself glucose meters for diabetics (e.g., Accu-Chek® from Roche), to expensive, fully automated laboratory equipment (e.g., GeneChip® microarray of Affymetrix). Measurement and identification of proteins by immunosensors and DNA by DNA sensors in combination with knowledge gathered by the human genome project, enable us now to detect diseases and hereditary disorders in an early stage, thus preventing worse.

Diamond is an obvious choice as building material for implantable sensors because of its biocompatibility, chemical inertness, and the ability to make it electrical semiconducting, allowing connection with integrated circuits. Such implantable sensors would stay active in the body for a long time, thus replacing repeated sampling and enabling continuous monitoring of e.g., the pH of the blood. Diamond can be artificially deposited as a thin layer on different substrates, ranging from glass to semi-conducting silicon. This way, an inert physical separator layer between body and the electronic part of the sensor is

created. Part of the sensor surface however can be functionalized with biological components to become a sensitive layer. However, the chemical inertness of diamond makes this a difficult task.

In this doctoral study, the boundaries of a new multidisciplinary research domain were explored. Knowledge about physics and biology was merged to build prototype sensors showing how diamond can be used as base material for biosensors. The first research steps towards a diamond-based biosensor were made: DNA was successfully bound to a diamond surface, and diamond was used as sensing material for pH and polyelectrolytes, the latter as a model for DNA.

Chapter 1 is a general introduction to biosensors. It describes the biological, transducer and electronic components.

Chapter 2 deals with diamond growth in the laboratory and how its properties can be used and manipulated.

Chapter 3 explains the analysis techniques that were used to assess the properties of the diamond samples.

Chapter 4 describes the used materials and methodologies.

Chapter 5 describes in detail the method we developed to attach DNA to diamond using ω-unsaturated fatty acids, UV light and an EDC crosslinker.

Chapter 6 explains the ConCap measurement method as a refined impedimetric detection technique for charged molecules. It describes pH sensitivity of hybrid diamond-silicon EDIS structures when measured with the ConCap method. The setup was further extended with adsorbed polyelectrolytes as a model for DNA molecules.

Chapter 7 concludes this thesis with considerations about which research is left to be unravelled.

1. Biosensors

1.1. Introduction

A biosensor consists of a biological sensitive component that is the active core of the device, completed by a transducer and an electronic part that measures, amplifies and decodes the recognition events [figure 1.1] [1]. These three parts will be discussed in the paragraphs below.
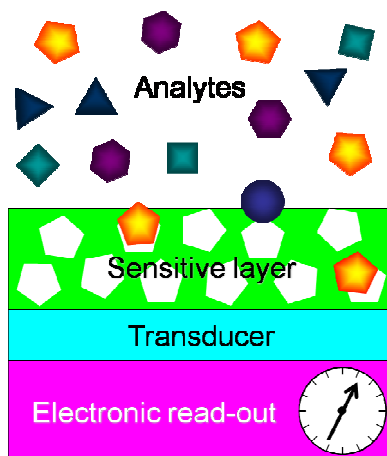
Figure 1.1.   General biosensor scheme.

The challenge for biosensor development is to reduce the time required for a biochemical assay and to provide an easier way of analyzing. The ideal biosensor should be cheap (as a result of a simple fabrication process), fast, reliable, reusable, robust, small, stable and user-friendly [2]. These properties are necessary for 'point of care' use by medical practitioners in the field [3].

1.2. Biological component

The most important part of a biosensor is a sensitive biological element that exhibits highly specific interactions and is derived from the nanomachinery in the biological cell. Therefore, molecular-scale nanotechnology is needed to investigate functionalized surfaces (see chapter 3: Characterisation techniques

for functional surfaces, p. 55). Depending on the design, the wanted sensitivity and desired specificity, this sensitive biological element can be a small molecule, like a specific enzyme, an immunoreceptor or DNA, or a much larger biological component, like a whole cell or cell culture [4,5]. In this broad definition even whole animals can be used. An older example are canaries for mine gas detection and water fleas as sentinel species for intoxication in veterinary pathology [5]. There was even a sensor made with a whole Colorado potato beetle acting as gate for a field effect transistor (FET) [6]. Nowadays bees and wasps, held in specially designed test containers, can be trained by behavioural conditioning for detection of explosives or disease markers in air, blood or urine samples [7,8]. Sensing organisms can be combined with robotics technology, e.g., a slime mold fungus-driven robot was developed that moves away from light or towards sugar [9].

Biotechnology provides many different types of stable cell lines that can be cultured infinitely with well established conditions. Cells however can be less specific than receptors, but the advantage is that they have a broader spectrum; this is interesting for environmental monitoring for biological threats. E.g., the immunological Toll-like receptor (TLR)-4-mediated reaction to lipopolysaccharide (LPS, a bacterial cell wall component) could be used to detect bacterial presence in a very sensitive way [10,11].

In this work, we focus on biological molecules. These can be grouped in affinity receptors that detect interaction between affinity pairs, and catalytic enzymes that chemically interact with the analytes [12]. In both cases, the biological element has a specific affinity for the analyte [13]. Using biochemical techniques, these components are adsorbed or immobilized by e.g., silanization, covalent cross-linking, encapsulation between membranes or in a matrix close to the transducer [14,15,16]. When immobilizing biomolecules, special attention should also be given to orientation and retention of binding capacity [17], and to prevention of nonspecific biofouling, e.g., by using blocking agents, like bovine serum albumin (BSA) or polyethylene glycol (PEG) [18,19,20].

Charged (bio)molecules on the surface of a semiconductor induce an electrical field in the semiconducting material. This effect can be measured by a change in conduction in a field effect transistor (FET) setup, or by changed surface capacitance or charge transfer resistance resulting in an electrochemical impedance spectroscopy setup [21,22,23]. Detection of DNA-DNA and antibody-antigen interaction in a label-free way is e.g., possible by detecting the field effect induced by molecular charges [24]. The nature of their electrostatic

charge are acidic and basic groups that accept protons from or donate protons to the solvent. The pH of the solution can influence the charge of these molecules: a pH that is higher than the isoelectric point of a protein renders it negative, a pH lower makes it positive. Electrostatic screening of these charges by counter ions complicates direct electrostatic detection, but this can be bypassed by a FET setup [23,25] (see chapter 2.5.2: FET structures, p. 40). Another possibility is the use of positively charged polyelectrolytes, like poly-L-lysine (PLL) that reduce electrostatic repulsion between negatively charged DNA strands, thus decreasing the time required for annealing and allowing hybridization at low ionic strengths. This is the condition where the field effect can best be sensed [25].

1.2.1. Nucleic acids

Nucleic acids are the physical carriers of genetic information. Inheritance of phenotypic traits happens through mediation of the biological cell's nanomachinery. Though many is already known, molecular biologists are still unravelling the details of the complex way how DNA and RNA polymerase enzymes and transcription factors work [26].
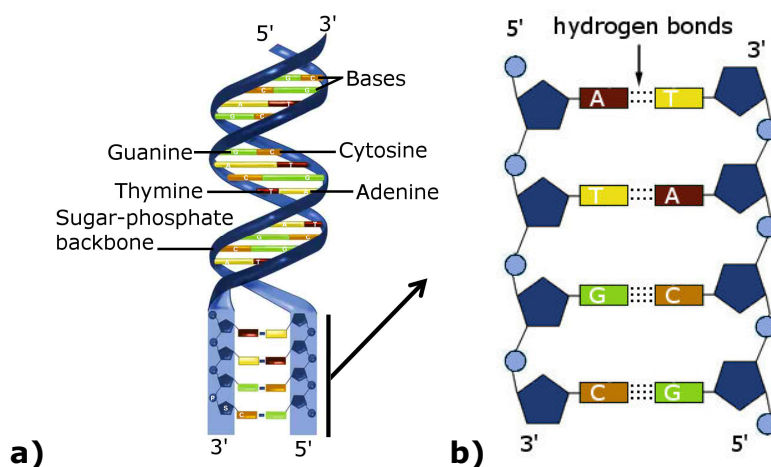
Figure 1.2.   DNA structure.
(a) The nucleotides attached to the deoxyribose-phosphate backbone interact with the complementary antiparallel strand by hydrogen bonds (adapted from: The New Genetics, 2006, National Institutes of Health) (b) Detail of the interaction between complementary nucleotides (adapted from: Scienceaid.co.uk).

DNA consists of two complementary strands that form a duplex [figure 1.2]. Each nucleotide strand has a different sense (5'→3' *vs.* 3'→5') and is composed of a negatively charged backbone of phosphate and deoxyriboses coupled to one of 4 possible basic molecules. The sequence of these bases (Adenine (A), Thymine (T), Guanine (G), Cytosine (C)) encodes the genetic information [27]. The two complementary strands bind in a highly specific way by a process that is called hybridization. Bases A and T interact by 2 hydrogen bonds and bases G and C by 3. These hydrogen bonds must surmount the repulsion force of the negatively charged backbone strands [28]. Therefore, a mismatch makes hybridization less likely to occur. This nanoscale disruption of the DNA helix is the required detection limit of a DNA sensor, because such a single nucleotide polymorphism (SNP) in the genome might already cause a genetic disease [29].

With the completion of the human and other genome projects, a huge treasure of information became available. More than 800 organisms have been sequenced. Not only genomic information of both useful and noxious organisms is now known, also numerous biotechnologically important model species have been sequenced. Also, an immense amount of proteomic data is being derived [30]. This knowledge will allow us to understand disease mechanisms, to predict drug responses and even to prevent and manipulate pathogenesis. The full exploitation of these data in genosensors is very promising.

Applications of DNA technology nowadays reach from DNA fingerprinting for criminal investigations to food-borne pathogen identification [31]. For this purpose, DNA is amplified with the PCR technique using labelled nucleotides and a natural template sample. In a next step, optical readout detects fluorescence alteration when hybridization occurs on commercial DNA chips called DNA microarrays. These chips are fabricated using a combination of photolithography and chemistry [32,33,34]. Each gene is represented by several oligonucleotides to reduce false negatives [35]. DNA microarrays offer the opportunity to analyze multiple genes or their products in parallel [36]. Analyses can be done at relative low cost (e.g., the microarray facility of the Flemish Institute for Biotechnology performs an Affymetrix whole transcript array with a vast number of 26 x 29000 gene sequences for € 490 (year 2009) [34]). Probe DNA is printed in picoliter volumes on a solid support, like glass, Si or plastic, or can be synthesized on the chip by photochemical lithography [28].

Next to the naturally occuring DNA structure, also DNA analogues can be chemically synthesized and attached to biosensors [37]. Base analogues, like

inosine, have a similar basepairing mechanism as their natural counterparts, but the interaction occurs with a lower specificity. These basepairs are called 'wobble' basepairs [28]. Another DNA analogue are dendrimers: branched nucleotide macromolecules that amplify the hybridization capacity by their abundance of single strands [28]. Nucleic acid aptamers on the other hand are short nucleic acid strands (ssRNA or ssDNA) that fold into complex 3D structures. Systematic evolution of these ligands by exponential enrichment (SELEX), which is an iteration of *in vitro* selection and amplification that is similar to phage display, allows engineering of highly specific RNA and DNA receptors for non-nucleic acid targets of 100 Da - 10kDa, like toxins, drugs, proteins or other molecules, organic as well as inorganic [38,39]. Peptide aptamers are the peptide counterparts [40]. Next, ribozymes are naturally occuring enzymes consisting of RNA where, compared to DNA, deoxyribose and thymidine are replaced by ribose and uracil. The RNA determines the binding affinity of the ribozyme. As a last analogue, there is PNA that is a synthetic analogue polymer. The phosphate-deoxyribose backbone is replaced by amide bonds. PNA sensors have the advantage of being chemically more stable. Moreover, the absence of negatively charged phosphate in the backbone results in a lower electrostatic repulsion by the complementary catcher sequence [28,41].

1.2.2. Immunoreceptors

Both immunoreceptors and enzymes are proteins. This group of molecules were the first complex biological molecules that were studied in detail. Because proteins were found to be so diverse in structure and function, they were even suspected to be the bearers of hereditary traits, which later on proved to be wrong by the Hershey-Chase experiment: it was DNA.

Immunoreceptors belong to the immune system. Animals (including humans) have a redundant immune system with many different kinds of molecular receptors and cytokines. Biological coevolution has shaped our immune system through a hide-and-seek game in the parasite-host relationship: for every evasion system that worked well for some parasite (virus, nematode, flagellate, ...), the host developed a suitable answer by the process of evolution [42].

The best known and characterized receptors are the classical antibodies that are present in all mammals species, also called immunoglobulins. They

consist of four protein chains: two light and two heavy chains, tied together by disulphide bonds. The heavy chains are composed of three or more constant domains and one variable domain, while the light chains only have one constant and one variable domain. The variable domains typically have three complementary determining regions (CDR), which determine the binding capacity to its antigen. The CDRs of the light and heavy chain together form the complete antigen binding area. Through so-called somatic recombination, a broad combinatorial diversity of antibody receptors can be produced.
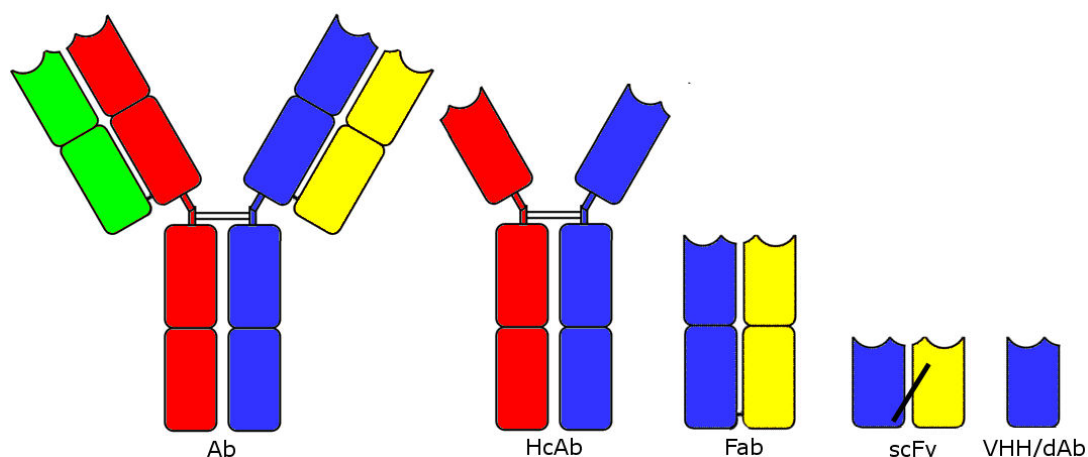
Figure 1.3.   Immunoreceptor size.
From large (left) to small (right): a classical antibody (Ab; 150 kDa), a heavy chain-only (camelid) antibody (HcAb; 75 kDa), an antigen-binding fragment (Fab; 50 kDa), a single chain fragment (scFv; 25 kDa) and a variable domain of a heavy-chain antibody/domain antibody (VHH/dAb; 12.5 kDa) (adapted from: Immunobiology, 2001, Janeway C.A., Garland Science).

Keeping in mind that size of the detecting molecules on a biosensor is important, research has been done to explore smaller kinds of antibodies or antibody fragments because then a wider range of analytes and epitopes can be investigated (explanation: see below). Fab fragments are the antigen-binding parts of the previously described classical antibodies. These are obtained by papain protease digestion, or by recombinant expression. Even smaller are single-chain variable fragments (scFv). These are biotechnologically produced as one chain by expression of the fused sequence of both the heavy and light chain variable domain, connected by an amino acid linker [figure 1.3].

Next to classical antibodies, another type of naturally occuring antibodies exist: the heavy chain-only antibodies (HcAb). These are smaller than the classical antibodies because they are devoid of light chains. They are present in the family *Camelidae* (camel, dromedary, llama, alpaca, ...) next to classical antibodies. Of these HcAb, a new generation of recombinant antibody fragments is derived. These are called VHH or single-domain antibodies and are the smallest functional antigen-binding fragments known. The VHH is commercially known as nanobody® and consists of the variable domain derived from HcAb. They are as active as their conventional counterparts. Moreover, they recognize less accessible epitopes, like catalytic clefts of enzymes because they are so small, enabling them to penetrate further in the conformational structure of the antigen. They are also very denaturation-resistant, favouring their use as immunosorbent. They are even more hydrophylic than the conventional antibody fragments, resulting in an increased solubility. Through phage display selection, their affinity can be enhanced and even toxic antigens can be targeted [43,44]. Single-domain antibodies derived from classical antibodies also exist, but these have to be modified to make them as soluble as naturally occurring camelid VHHs [45].

Whether FET-based detection of antigen-antibody binding is possible, is subject to debate. The conclusion was that small inorganic counter ions from the electrolytic solution screen and bind the protein charges in such a way, that macroscopical detection by ion-sensitive field effect transistors (ISFETs) might be impossible [46]. A way to circumvent this static detection problem, is the use of a dynamic detection method involving an ion concentration pulse [47].

Detection of antigen-antibody binding (e.g., in an ELISA) usually has an immobilized capturing antibody and a free-floating antigen, but the other way round is also possible. This can be detected by an ISFET setup [48] and by electrical impedance spectroscopy [49].

Nowadays, high affinity binding between an affinity pair can also be mimicked by the molecular imprinted polymer (MIP) technology that is inspired by the highly specific binding interactions, like between enzyme-substrate, antigen-antibody and ligand-receptor. Monomers polymerize in the presence of the eventual analyte. After extraction, the polymer shows a high binding specificity to the original analyte because antigen-specific cavities are left [50,51,52]. During addition of the sample, the binding is determined e.g., impedimetrically, by quartz crystal microbalance or by fluorescence quenching. MIPs are especially useful for detection of small molecules for which no biological

ligand can be made. They remain stable at extreme pH, pressure and temperature conditions and can also operate in organic solvents.

1.2.3. Enzymes

Enzymes are active proteins. These active molecules lower the energy barrier in biochemical processes where a substrate is converted into a reaction product. When these enzymes are incorporated in biosensors, they are called 'catalytic' biosensors.

In the first biosensor, the Clark electrode, glucose oxidase was immobilized in a membrane and combined with a Pt oxygen sensor [53,54,55]. When glucose is added, the glucose oxidase facilitates the oxidation of glucose to gluconolacton, thereby lowering the O_2 concentration, which is detected by the oxygen sensor. Another example is a penicillinase-based biosensor [56-60]. The bacterial enzyme penicillinase breaks down the antibiotic penicillin and thereby decreases the pH level, which is detected by the sensor. Such sensors are called first generation biosensors because they use the mobility of small molecules to reach the electrodes.

Second generation sensors make use of chemical mediators, like ferrocyanide to transport electrons. An example is the well known glucosemeter with glucosedehydrogenase.

In third generation biosensors, direct electron exchange is achieved through direct coupling of electronically active enzymes to the electrodes. An example is horseradish peroxidase that is attached to a diamond electrode for cyclic voltammetric detection of H_2O_2 [61].

1.3. Transducer

The transducer uses some physical or chemical property to detect and amplify the biological signal. The basic transducing mechanism can be mechanical (gravimetric/acoustic), optical, thermal or electrochemical.

Gravimetric devices, like quartz crystal microbalance, surface acoustic wave sensor or cantilever arrays have an acoustic eigenfrequency that depends on the oscillating mass [28,62,63]. Specific binding of the analyte induces a mass change that can be detected. The electrically-induced oscillation of a

piezoelectric base material changes by the mass adsorption to immobilised affinity receptors.

Optical spectrometers measure the light that is absorbed or emitted by molecules in solution. Each analyte captures certain typical wavelength energies, exponentially to concentration and the path length (Law of Lambert-Beer), while some molecules emit light at a larger wavelength i.e. lower energetic. A special type of optical sensors are surface plasmon resonance (SPR) systems that measure the change in angle for which a surface plasmon is generated. This change is caused by molecular adsorption altering the interfacial refractory index. The origin of this effect is an evanescent wave field at the interface between two dielectric media [64].

Thermal sensors measure the energy dissipated from many chemical and biological processes in the form of heat that can be measured as a temperature change [65], e.g., thermistors that detect enzymatic reaction heat. Affinity reactions however are usually not exothermic enough. In the other sensor types, heat can be the cause of problems, for example biosensors using SPR detection can be very sensitive to temperature changes. To minimize this effect, temperature stabilization mechanisms, like thermal insulation or constant proportional heating is needed.

To increase sensitivity, sometimes auxiliary techniques, like fluorescent, chemiluminescent, enzymatic, magnetic, redox or radioactive labels, or increased surface area are used [66,67,68,69,70]. Although label-free methods are less sensitive than labelling, they are preferred for fast, low cost and easy real-time detection applications.

Electrochemical sensors measure the electric field (voltammetric) or electron exchange (amperometric) caused by redox reactions between electrodes and molecules. Field effect transistors use sensitive semiconductors to detect field effect changes (see chapter 2.5.2 *FET structures*, p. 40). Impedance sensors record the current and time phase shift between current and induced AC voltage peaks in the frequency spectrum (see chapter 6 *ConCap mode pH measurements on EDIS structures*, p. 81). ConCap sensors reveal the field effect using an impedimetrical measurement (see chapter 6.2 *Introduction to ConCap measurements*, p.84).

1.4. Electronic part

Although the electronic circuit is an important and powerful part of a biosensor, this is not the limiting factor for device fabrication. Microchip technologies are well established, and the necessary minimal requirements are already available since long time.

In a research setup, the electronics part is replaced by full range measuring equipment. The eventual sensing device can do with much less, but it is important to record everything and not discard possibly important information during the research phase. A thorough data analysis after each experiment reveals the most interesting measuring conditions (analyte and buffer concentrations, frequency, voltage, temperature, ...). When the properties of the sensitive component are well characterized, the eventual measuring electronics can be focussed to these important most sensitive regions.

1.5. General application considerations

Besides the three contributing parts (biological, transducer and electronic part), other aspects should also be taken into account. E.g., to increase functionality and reduce costs, the sensitive part of the sensor can be split into several parts, allowing multiple parallel analyses simultaneously. These arrays of e.g., DNA, proteins or antibodies make high-throughput screening possible [71,72].

Biosensors nowadays are mainly used for *in vitro* measurements. For *in vivo* use, long-term implantation stability of the sensors is needed. For this, all parts in contact with the body (fluids) need both biocompatible sensitive surfaces as well as biocompatible passive encapsulation. On the one hand, the sensor should not cause inflammation or allergic reactions. On the other hand, the sensor parts can be damaged by moisture, salts and immunological rejection [73,74,75]. Diamond is in both cases the material of choice because it does not initiate rejection and resists breakdown.

Combining biosensors with microfluidics and micromachined structures results in the creation of a so-called 'Lab on a chip' or biochip [28,76,77]. An example is an implantable glucose sensor that delivers insulin directly into the blood when glucose levels rise [78].

1.6. Summary

Summarizing, biosensors are sensitive devices incorporating biological molecules that capture analytes in a specific way. The most well know example is the glucosemeter for diabetes patients.

A lot of research has already been done to replace laboratory tests by smaller and easier implementations. Repetitive sampling applications however urges the search for *in vivo* measurements. The solution to this problem is the development of biocompatible sensitive surfaces. Diamond is a promising candidate for this purpose.

Our research today shapes tomorrow's world. Therefore, a vision on future needs is required: we foresee a trend towards small and cheap medical devices that are implantable for long times. Several sensors will be combined in arrays. Integration with modern electronics and microfluidic technology will allow fast diagnosis and treatment. Early subclinical detection will even allow preventive medicine. Although all elements for such kind of sensors are already largely available, we still have a long way to go for the full integration, validation, registration and commercialisation.

2.   Diamond synthesis and applications

2.1. Introduction

Diamond is named after the Greek word *adamas* (αδαμας) that means invincible, pointing at the characteristic hardness. Only materials, like ReB_2 (Rhenium diboride) are even harder [79]. Being one of the hardest materials in nature, diamond is used as hardest reference calibration material in the Mohs scale for material hardness and in many industrial power tools. The ultimate reason however for the high value of diamond stones is the rarity of the product, obeying the economical laws of supply and demand on the public market.

a)   **b)**
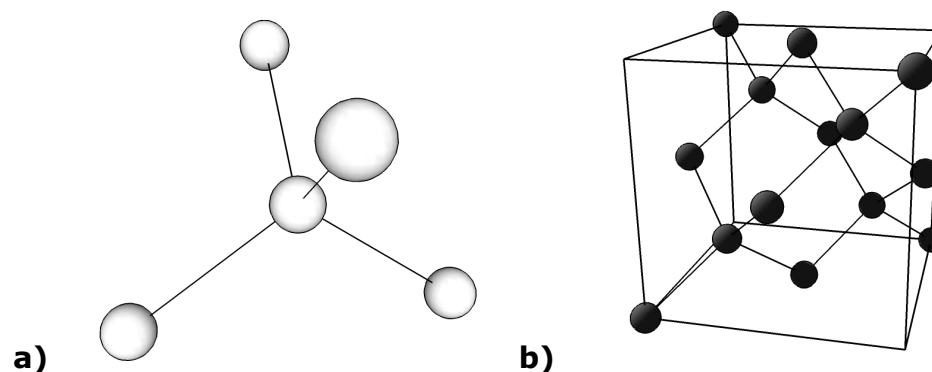
Figure 2.1.   Diamond lattice structure.
(a) spatial orientation of neighbouring C atoms around a central bulk C atom (b) resulting cubic unit cell for diamond (cubic lattice constant 0.356 nm).

Diamond is only one of several allotropic forms of carbon, next to hexagonal graphite and fullerenes (buckyballs and carbon nanotubes), diamond-like carbon (DLC), the rare hexagonal lonsdalite, … [80]. It consists entirely of carbon atoms that form a tetrahedral structure through sp^3 hybridization orbitals that form covalent bonds with neighbouring C atoms [figure 2.1]. The distance between two C atoms is 0.154 nm and this packing results in a density of 3.52 g/cm^3.

Because diamond is entirely composed of carbon, which is the most important building block of biomass, it is very interesting for in vivo applications [81]. Diamond can be implanted within living tissues without rejection reactions or degradation [82]. Chemical vapour depositied (CVD) diamond is as biocompatible as Ti and 316 stainless steel [91]. *In vivo* tests show the absence of connective tissue proliferation, damage to structure tissues or (cyto)toxic responses around nanocrystalline diamond (NCD) implants [83-86]. Diamond can also be used as a more active material than just as coating substance, e.g., for the fabrication of neurochips, since adhesion, growth and excitability of ganglion cells on diamond surfaces can be promoted and patterned using inducing molecules, like poly-D-lysine (PL) or laminin (LN) [87,88,89], or oxygen-termination [90].

Next to being inert and biocompatible [91], diamond is also more resistant to nonspecific DNA adsorption than commonly used materials, like polymethyl methacrylate (PMMA), polydimethyl siloxane (PDMS), SU-8, glass and Si [92].

2.2. Recent advances in diamond-based biosensors

Synthetic diamond has been recognized as an attractive material for biochemical sensing and as an interface to biological systems, giving rise to an entirely new class of electrochemical biosensors and bio-inorganic interfaces [130]. These advances are based on new approaches to functionalize diamond surfaces, and the engineering of new measurement techniques.

The potential of newly identified biomarkers urges the development of high throughput diagnostic biosensor systems with increased sensitivity [130]. Unlike diamond, classical materials in diagnostic applications, like latex beads, polystyrene, carbon electrodes, gold and oxidized silicon or glass, do not have desired properties as flatness, homogeneity, chemical stability, reproducibility and biochemical surface modifications. The required integration of bio-functionalized surfaces with micro-electronics adds even more complexity to this topic.

Takahashi *et al.* [196] have overcome the problem of chemical inertness by introducing a photochemical chlorination, amination and carboxylation process of H-terminated diamond surfaces [130]. Yang *et al.* [214] went further by describing DNA attachment to NCD and demonstrating high stability of this

bio-functionalized surface during hybridization cycles [214]. We described an analogous but simplified DNA attachment method (see chapter 5 *DNA attachment to NCD*, p. 69). Härtl et al. reported on covalent attachment of the more delicate catalase enzyme, preserving the redox activity [218]. Others described functionalization by electrochemical reduction of diazonium salts on boron-doped diamond electrodes. These resulting surfaces have been further modified with DNA, enzymes and proteins. (For more information about surface modifications, see chapter 2.6 *Tuning of properties*, p. 49.) In conclusion, these strategies for surface modifications have paved the way to fully functional bio-interfaces.

Because also surface geometry determines potential application, several structures of diamond electrodes, like microtips, microdiscs, microbands and nanorods were fabricated [130]. Also different detection modes of sensors were investigated. We describe the feasibility of pH and polyelectrolyte sensing with a capacitive EDIS platform that was inspired on a silicon-based setup (see chapter 6 *ConCap mode pH measurements on EDIS structures*, p. 81). Nebel *et al.* [218] describe an electrochemical setup using DNA-functionalized ultra-hard vertically aligned diamond nano-wires for voltammetry and impedance spectroscopy.

In the coming years, advances in diamond-based biosensors will contribute to the progression in diagnostics for health and food industry.

2.3. Artificial diamond growth

Since the middle of the twentieth century, artificial growth of synthetic diamond became possible. In the '50s, attempts were successful at high pressure and high temperature (HPHT), mimicking natural diamond growth in the earth's crust. Later on, in the '70s and '80s, also low pressure growth succeeded (CVD and PECVD) [93,94,95].

Diamond nowadays can be coated as thin films on different materials. E.g., NCD can be deposited as a transparent layer on different substrates, like Si, quartz, and thermally resistant glass [91,96]. CVD is a widely applicable technique, allowing shaping of remarkable structures, including fabrication of microshells [97]. Even microelectromechanical systems (MEMS) and miniaturized reactor chambers can be fabricated with it [98]. Industrial diamond is mainly used for mechanical applications (drilling, cutting, grinding polishing, …). Recently, synthetic diamond is also used in medical, optical (X-ray

windows), electronic (high power/frequency/temperature operation), and thermoconductive (heat sink) applications [99,100,101]. Also in analytical chemistry, diamond can be used. For instance sintered diamond particles are used as stable high performance liquid chromatography (HPLC) column packing with better separation and higher selectivity [102].
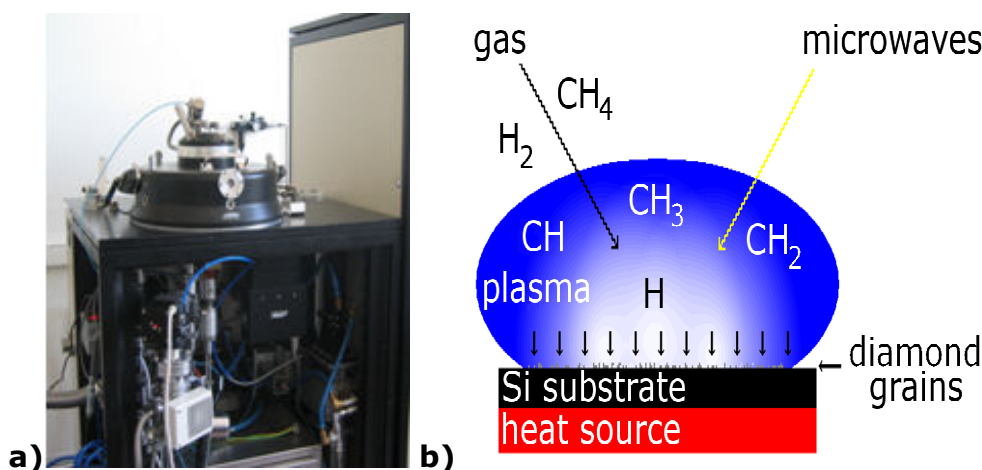
Figure 2.2.   CVD diamond growth.
(a) ASTeX reactor. (b) Nucleation process on a heated substrate.

Because diamond is so rare and suitable experimental samples are even more rare, we used artificially grown samples. At IMO chemical vapour deposition (CVD) coating is performed in an Applied Science and Technology Inc. (ASTeX) reactor at low pressure using 25 sccm CH_4 and 475 sccm H_2 with Si substrates at 5 kPa and 700°C, resulting in nanocrystalline diamond films with a typical thickness between 100 and 500 nm (see chapter 4.1.1 *Synthesis and preparation of NCD*, p. 65). Also larger (1 μm) or smaller (< 10 nm) grains can be obtained using the right growth conditions, like temperature, gas mixing ratio and seeding procedure [103,104]. Unlike NCD, this ultrananocrystalline diamond (UNCD) is renucleated continuously, resulting in much smaller crystal sizes and more grain boundaries with dangling bonds [105], which are the main conductive paths in undoped diamond films [106]. Both hot filament and microwave power can be used as energy source to ignite and maintain the plasma in the low pressure reaction chamber. Crystal lattice defects and graphite inclusions however prevent the use of synthetic diamond as gem stone.

The CVD process combines inorganic nucleation and growth mechanisms with organic chemistry. Plasma radicals originating from H_2 and CH_4 react with the substrate surface and deposit a new carbon layer [figure 2.2]. When H_2 is split by microwaves, hydrogen radicals can react with either CH_4 or the diamond surface, thereby producing reactive sites. These can recombine to form an additional carbon layer to the diamond surface [107]. The hydrogen radicals etch the accidentally formed graphite away, leaving a pure diamond film on the substrate [83] [figure 2.3].
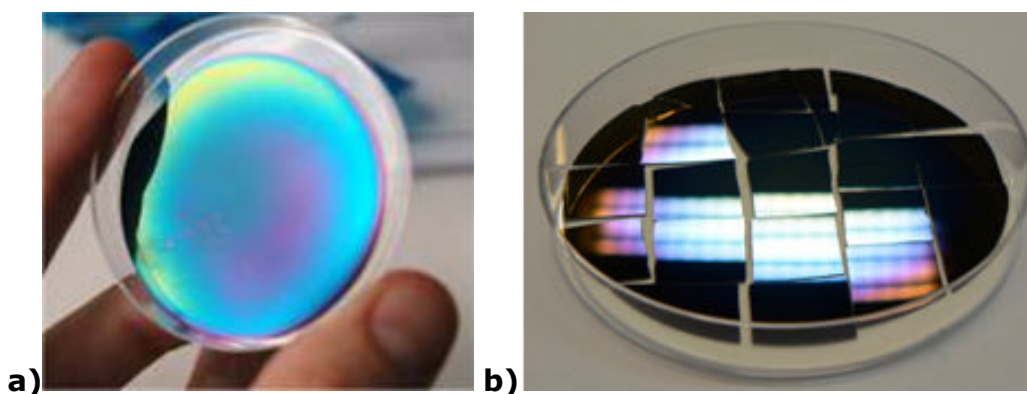
Figure 2.3.   Macroscopic image of CVD diamond substrates.
(a) As-grown wafer and (b) diced wafer chips ($\pm$ 1 cm^2).

For NCD deposition, a Si wafer with Miller index (100) is treated by vibrational abrasion or more homogeneous ultrasonic seeding with detonation nanodiamond powder [105]. Both techniques result in scratches acting as nucleation centers [108,109].

Next, a thin Ti layer with a thickness of $\pm$ 50 nm can be sputtered on top of the Si substrate to enhance seeding [110]. Subsequently, a < 200 nm NCD film was grown on the pre-treated substrate using microwave plasma enhanced CVD (MPECVD) in an ASTeX® reactor with a 2.45 GHz microwave generator (3000 W, 5.3 kPa, 475 sccm H_2, 25 sccm CH_4). Starting from the small diamond grains, NCD grows confluent after 60-100 nm, the largest crystal engulfing the smaller ones [105]. This is illustrated in figure 2.4. After growth, the wafers are cleaned in an oxidizing mixture of boiling H_2SO_4 and KNO_3 for 30 min, followed by an ultrasonic bath in distilled water and drying with N_2 gas.
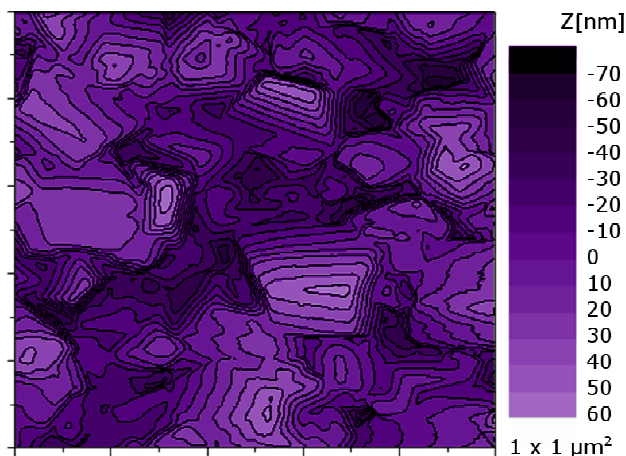
Figure 2.4.   Topographical AFM image.
Contour lines (isohypses) of NCD sample.

2.4. Surface conductivity

Bulk diamond is an electrical insulator with a wide indirect bandgap (5.4 eV), in contrast to as-grown and atomic hydrogen plasma-treated diamond samples that are H-terminated showing a p-type surface conductivity even in undoped samples [111-115]. This property can be used for FET fabrication (see chapter 2.5.2: *FET structures*, p. 40). This conductive layer is only a 10 nm thin [27,116,117]. Exposed to air, surface adsorbate layers induce surface conduction in the H-terminated surface, while annealing in vacuum makes it vanish again [111,116,118,119]. Hydrogen appears to be a necessary but insufficient condition for surface conduction; also adsorbates from ambient air are needed [120]. The mechanism of this hole-induced conductivity is still under investigation [27,121].

Conductive diamond is particularly interesting for electrochemical applications, like redox electroanalysis because of its potential window of 3 to 4 V in aqueous media and resistance to fouling [122]. The latter is important for long-term stability when engulfed by body fluids [123].

One model for this conductivity phenomenon describes that a thin water layer is formed in air, thus facilitating electron transfer, which causes energy band bending near the surface [112] [figure 2.5]. Hydroxonium (H_3O^+) ions are reduced, thus forming water and H_2 near the sample edge. The driving force of

this transfer is the chemical potential difference between the liquid phase and diamond. What is left, are 'holes' that form an accumulation layer, thus inducing a surface band bending. Related to the Nernst equation, the equilibrium value of the chemical potential can be stated as [112]:

$$\mu_e = -4.44\,\text{eV} + \frac{0.058}{2}\,\text{eV}\left[2pH + \log\left(\frac{p_{H_2}}{bar}\right)\right]$$

From this formula, it can be explained why surface conductivity increases in an atmosphere which is rich in HCl, thus reducing the chemical potential and increasing hole accumulation. Vice versa, the surface hole conductivity decreases in NH_3 fumes because the chemical potential is increased.
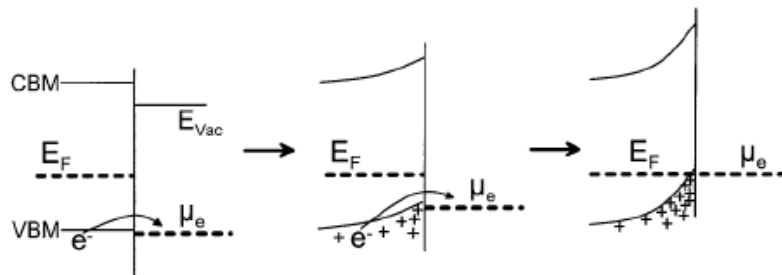
Figure 2.5.   Electron transfer causes hole accumulation near the surface. Valence band maximum (VBM) and conduction band minimum (CBM) of the bulk material deflect upwards due to electron exchange with the solution. This process equals the chemical potential of the electrolyte with the Fermi level of the bulk [112].

Another model explains the phenomenon by a charge transfer doping mechanism from the valence band of diamond to empty adsorbate electronic states [124,125]. By this, electrons are exchanged with adsorbates. They equilibrate the solid state Fermi energy of the diamond with the electrochemical potential of the adsorbates [126,127]. Spatially, this is modelled as a 2D hole gas [128,129].

2.5. Diamond-based field effect transistors

2.5.1. Introduction to diamond sensors

Once a functionalised diamond surface is established, this stable and biocompatible platform can be used as the sensitive part of a sensor to detect biomolecules that are clinically relevant, preferably biomarkers with a high predictive value, like prostate-specific antigen (PSA) or acute phase C-reactive protein (CRP) [130].

Field effect transistor (FET)-based pH sensors were the first type of diamond-based sensors that were demonstrated [*131*]. Protons interacting with the diamond surface induce physicochemical changes that can be detected by the semiconducting channel of the FET. Likewise, charges of molecules, like DNA should be measurable. The first step we had to perform, was to establish our own well-functioning pH sensor platform. The second step was to combine the sensor with nucleotides to obtain a DNA sensor. Several attempts however to take step one were unsuccessful. However, the gathered practical experience was useful in further experiments. Moreover, colleagues gathered knowledge concerning impedimetrical sensors on diamond. These data show a sensitivity of NCD samples for DNA-DNA and antibody-antigen interactions [132,133].

2.5.2. FET structures

Introduction

Field effect transistors (FETs) are electronic components that have three electrical contacts: the voltage on the gate connection determines the resistance of the conduction channel between drain and source contact. This mostly Si-based device has a high input impedance and a low output impedance.

In the beginning, metal-oxide-semiconductor FETs (MOSFETs) were developed [47,134,135] [figure 2.6]. Later on, the metallised gate was replaced by an electrolytic solution, resulting in a more sensitive flat solution-gate FET (SGFET). The feedback loop in the constant current mode regulates the drain-source voltage. The channel current is dependent on the electrical field perpendicular to the channel, which is dependent on the interfacial potential determined by the site-binding model that explains the charging of an oxide

surface as a equilibrium between bound an free ions [47,136,138]. A shift in electrostatic potential implies a label-free detection mechanism.

For a MOSFET, the behaviour and absolute value of the drain-source current (Ids) is dependent on the design and fabrication (see below: *Theoretical model*, p. 42) and the drain-source voltage (Vds) is kept constant by the electronic circuit. The only characteristic variable left is the gate-source voltage (Vgs) [47]. In a SGFET, there is an extra component which is the chemical potential that can also influence the behaviour [47].

This device was found to be not only sensitive for electrical potentials, but also for ion concentrations (Na^+, K^+, Cl^-, NH_4^+, Ca^{2+}). Depending on the gate material, they are also called ion-sensitive field effect transistor (ISFET). They are a broad-range, robust and thermostable alternative for the glass electrode. Applications nowadays range from pH probes for nutrients to neurochips detecting in a non-invasive way neuronal cell action potentials, instead of the invasive patch-clamp technique or using phototoxic voltage-sensitive dyes (VSD) to monitor neuronal potentials [137,140].
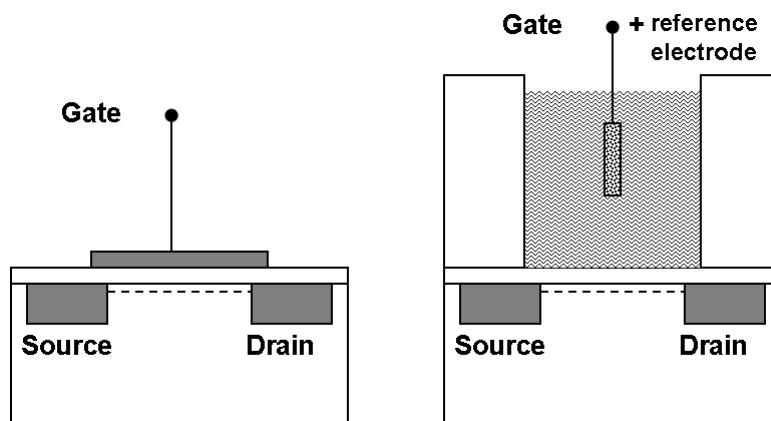
Figure 2.6.   Analogy between MOSFET and SGFET.
The dashed line indicates the conduction channel.

As transducer elements in biosensors, the FET gate is modified with specific sensitive molecules that are attached on the gate surface, close to the conductive channel. These sensitive molecules can be enzymes or antibodies, resulting in respectively an enzyme FET (ENFET) or immuno-FET (IMFET)

[159,138]. E.g., an ENFET can be sensitive to pH changes through enzyme-facilitated basic or acidic dissociation [139]. Whole-cell FETs benefit from the amplification through second messenger molecule transduction of the signal, which is a common way to have cellular mechanisms triggered. A disadvantage is that this might lead to less specific reactions [11,140].

Theoretical model

A classical ISFET consists of a semiconducting Si bulk with a source and drain contact [figure 2.7].
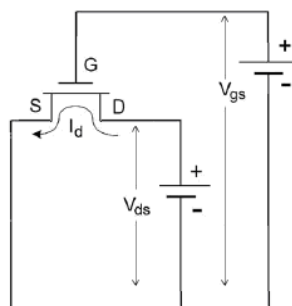
Figure 2.7.   Equivalent circuit of a depletion mode FET.
The gate (G)- source (S) voltage (Vgs) determines the resistance in the conduction channel for the current Id that is generated by a voltage Vds between Drain (D) and Source (S) (adapted from [135]).

As previously stated [figure 2.6], the gate of the MOSFET is replaced by an electrolyte solution with a reference electrode. The linear part of the source-drain current of the ISFET (in non-saturation mode) can be modelled as [135]:

$$i_d = C_{ox} \mu \frac{W}{L} \left[\left(V_{gs} - V_t \right) \cdot V_{ds} - \frac{1}{2} V_{ds}^2 \right]$$

C_{ox} is the oxide electric capacitance per unit area, W and L the width and the length of the channel, and μ is the electron mobility of the channel. The threshold voltage V_t is the gate voltage V_{gs} at which the device starts to be conducting. It can be seen from this equation that the drain current is a unique function of the 'input' voltage V_{gs}, only when the geometric sensitivity parameter $\beta = C_{ox}\mu W/L$ as well as the applied drain-source voltage V_{ds} and the threshold

voltage V_t are constant. The parameter β is a constant, completely determined by the design, and V_{ds} is kept constant by the applied electronic feedback circuit. In reproducible fabrication processes, the threshold voltage V_t is also constant. Thus, V_{gs} is the only input variable. Defining the metal connection of the reference electrode as a remote gate, as shown in figure 2.6, suggests that any interfacial potential in the input circuit should be described in terms of V_t. Therefore the second important MOSFET equation is that of the threshold voltage V_t [135]:

$$V_t = \frac{\Phi_M - \Phi_{Si}}{q} - \frac{Q_{ox} + Q_{ss} + Q_B}{C_{ox}} + 2\phi_f$$

where the first term reflects the difference in workfunction between the gate metal (Φ_M) and the silicon (Φ_{Si}), the second term is due to accumulated charge in the oxide (Φ_{Ox}), at the oxide-silicon interface (Φ_{SS}) and the depletion charge in the silicon (Φ_B), whereas the last term (Φ_f) determines the onset of inversion depending on the doping level of the silicon. All terms are purely physical in nature. In case of the ISFET, the same fabrication process is used, resulting in the same constant physical part of the threshold voltage. However, the workfunction of the gate metal is now 'buried' in the constant potential of the reference electrode, E_{ref}. The interfacial potential at the solution/oxide interface is given by $\Psi + X^{sol}$ of which Ψ is the chemical input parameter, shown to be a function of the solution pH and X^{sol} is the surface dipole potential of the solvent, thus having a constant value. Hence the expression for the ISFET threshold voltage becomes [135]:

$$V_t = E_{ref} - \Psi + \chi^{sol} - \frac{\Phi_{Si}}{q} - \frac{Q_{ox} + Q_{ss} + Q_B}{C_{ox}} + 2\phi_f$$

Ion and pH sensitivity

A semiconductor in an electrolyte establishes a thermodynamic equilibrium. At first contact, electrons are exchanged until the Fermi energy levels are equalled. Thus, a potential drop is formed across the space charge layer of the semiconductor and the Helmholtz double layer of the electrolyte [141,142]. pH sensitivity in devices that exploit the potential drop at the semiconductor-electrolyte interface is classically explained by the 'site-binding

model': the binding of the amphiphilic oxygen groups of the oxide surface is determined by the pH [143].

The interfacial potential Ψ depends on the charge concentration of the site-binding theory [143]. Negative, neutral and positive charges of oxide surfaces originate from the amphiphilic character: the O can have respectively none (-O⁻), one (-OH) or two (-OH$_2^+$) hydrogen atoms, depending on the pH. Moreover, ions gathering at an electrochemically active surface in an electrolyte, accumulate in an anisotropic way due to different size and charge of the larger positive and smaller negative ions involved [144]. They form a so-called double layer in the Gouy-Chapman model. Like buffer molecules, the surface groups can protonate and deprotonate, thus altering the surface charge, which can be sensed by the conductive channel of the ISFET.
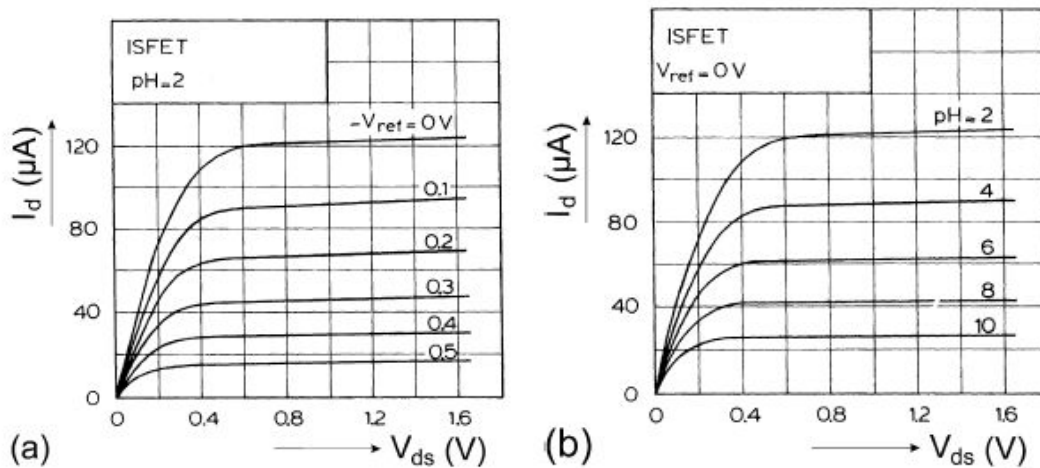
Figure 2.8. pH dependent I/V characteristics of a Si-based ISFET.
(a) At a certain pH, several reference potential series can be distinguished. (b) Likewise, at a certain reference gate potential, several pH series form similar curves [135].

A theoretical description of Ψ as a function of the pH that could also explain the sub-Nernstian (<58 mV/decade) response of the device was developed based on the well-known equation for capacitors $Q=CV$ where Q is the surface charge in the form of protonized (-OH$_2^+$) or deprotonized (-O⁻) -OH groups of the oxide surface, C is the double layer capacitance at the interface and V is the resulting surface potential, denoted as Ψ in previous equations. The surface acts as a source or sink for protons, whereas the load of this source is

the double-layer capacitance. The surface proton buffer capacity as well as the value of the double-layer capacitance determine together the final value of the potential Ψ which can be expressed in a sensitivity factor α resulting in the equation [135]:

$$\Delta\Psi = -2.3\alpha \frac{RT}{F} \Delta pH_{bulk}$$

with
$$\alpha = \frac{1}{(2.3kT/q^2)(C_s/\beta_s)+1}$$

where β_S symbolizes the surface buffer capacitance, e.g., the ability of the oxide to deliver or take up protons, and C_S is the differential double-layer capacitance, of which the value is mainly determined by the ion concentration of the bulk solution via the corresponding Debye length. R is the gas constant, and F the Faraday constant. The equation of ΔΨ shows that only in case that α approaches 1, the maximum Nernstian sensitivity of 58.2 mV per decade (at 20°C) can be obtained, whereas for oxides having a value α < 1 a sub-Nernstian response can be expected. The value α = 1 is reached for oxides with a large value of the surface buffer capacitance β_S and a low value of the double layer capacitance C_S.
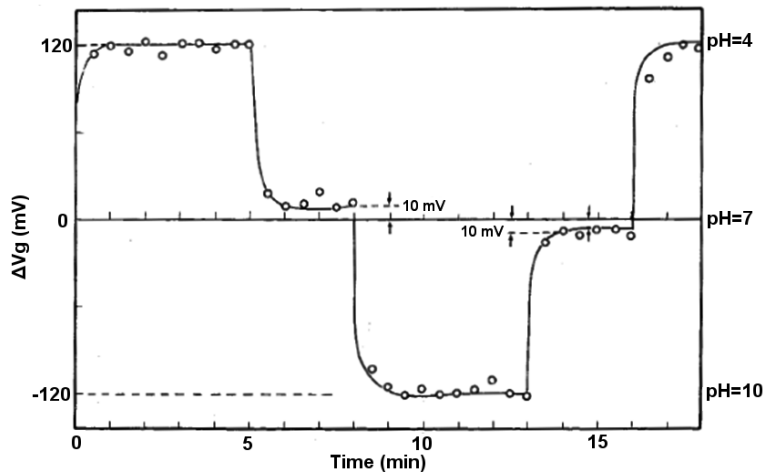
Figure 2.9.   Stepwise gate voltage feedback response of a SiO₂ gate ISFET. pH-induced changes show a sub-Nernstian sensitivity of 40 mV/pH [adapted from 134].

Sensor characteristics

In the case the ISFET is treated as a MOSFET with the reference electrode connected to the V_{gs} port, i_d/V_{ds} curves can be recorded as function of V_{gs} as is usually done with MOSFETs [figure 2.8a]. However, with the reference electrode connected to the source ($V_{gs}=0$), different curves can be achieved by changing the pH of the solution due to the relation $\Psi=f(pH)$ [figure 2.8b].

Using these characteristics, a linear response to pH can be obtained in a setup where the current is kept constant. This is achieved by a feedback loop mechanism that controls the gate potential V_{gs}, resulting in a stepwise response [figure 2.9].
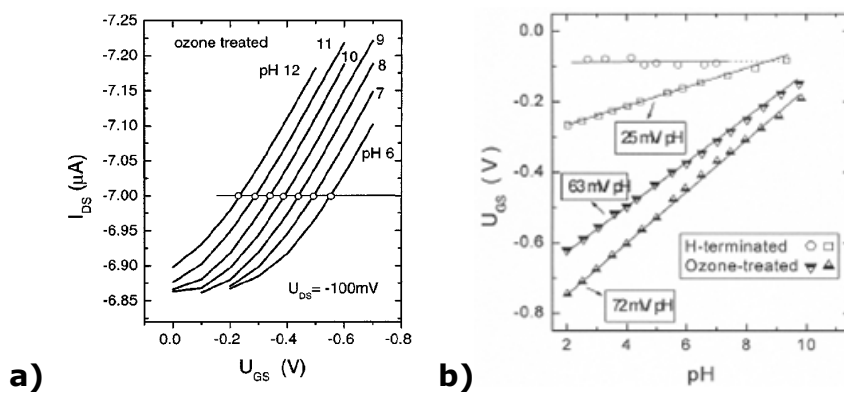
Figure 2.10.   Characteristics of a diamond-based ISFET.
(a) Ids/Ugs characteristics for different pH series (b) Difference in pH sensitivity of H-terminated devices versus ozone-treated devices (from [147]).

Attempts to make diamond-based FETs

Diamond FET devices have the advantage over Si-based devices that they do not need doped regions for the source and drain contacts; Only two metallic contacts on a hydrogenated diamond surface and a reference electrode in the buffer solution are needed. The surface conductivity forms the conduction channel (see chapter 2.4 *Surface conductivity*, p.38).

Diamond SGFET sensors exploit the properties of the conductive channel in hydrogenated diamond surfaces [145-149]. A large advantage is that no

complicating passivation is needed (e.g., SU-8 photoresist, oxide-nitride-oxide (ONO), SiO_2, Si_3N_4, Al_2O_3, or Ta_2O_5 [150,151]). This can be explained by the large potential window (wide bandgap) of diamond, together with the strong Coulomb repulsion between electrolyte and H-terminated surface forming a 'virtual gate insulator'. This allows a closer interaction and thus a stronger field effect influence from electrolytic ions on the conduction channel [146,152,153,168,192].

Recently, sensitivities above the Nerstian limit were observed on ozone-treated diamond [147] [figure 2.10]. Though the sensitivity model is valid, the high values that were obtained have to be corrected downwards because of the pH-dependent potential of the used Pt reference electrode [154]. To increase the sensitivity, amphiphilic groups, like amine can be introduced, thus expanding the range of chemical groups that can be protonated or deprotonated [155]. Combination of these binding sites with the 2D hole accumulation gas surface conduction model describes pH-sensitive islands that pinch off conduction in hydrogenated non-sensitive regions through lateral electrostatic modulation, resulting in an overall pH sensitivity [147,156] [figure 2.11]. However, pH sensitivity occurs experimentally also in (apparently) non-oxidised hydrogenated diamond [126].
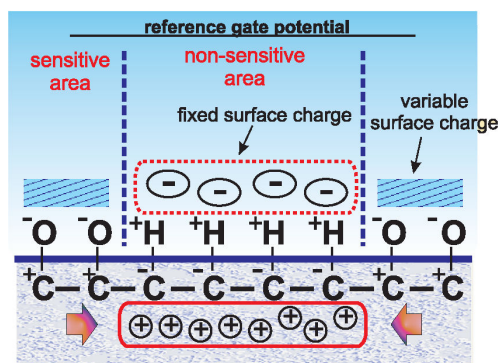
Figure 2.11.   2D hole conduction model.
Surface regions can be selectively oxidized and hydrogenated. Hole accumulation at the hydrogenated area is influenced by protons adsorbing to the oxidized area ([147]).

Both film quality (grain boundaries) and sample preparation are major influencing factors for device characteristics [147,155,157-159]. Miniaturisation is needed to reduce the sample volume and requires nanolithography channels

as narrow as 500 nm [145,146]. This indicates the importance of local surface quality [126]. There are even sensors that use as sensitive element biotin-modified Au nanowires, Si nanowires (SiNW) or DNA-single-walled carbon nanotubes (swCN) with less than 10 nm diameter [160-162]. Next to the p-type H-terminated surface channel, also the p-type nm-range B-doped channel can be used [163].

The small sensing area and the miniaturisation make device fabrication difficult, and because the measuring techniques are so sensitive, it is also prone to influences, like temperature, ion strength, volume, … , resulting in a difficult controllable drift signal. E.g., diamond ISFETs are sensitive to pH through amphiphilic O an N groups [155] that are also sensitive to Br^-, Cl^- and I^- ions [153,164]. Moreover, when using biological material, the system seldom stabilises (or it must be dead). Partial stabilization can be obtained by the use of an electromagnetically and thermally insulated oven box. Normalization for such effects can be fulfilled by using a differential setup that suppresses noise [3]: next to the real sensing cell, there is also a control cell that records the background signal to relate the positive measurement to the reference FET (REFET). [138,148]. Another way of improving sensitivity is miniaturisation, e.g., carbon nanotube (CNT) sensors whose cross-sectional conduction pathway is affected by binding of charged biomolecules [165]. Like microarrays, multiplexing of ISFETs on one chip is possible [166].
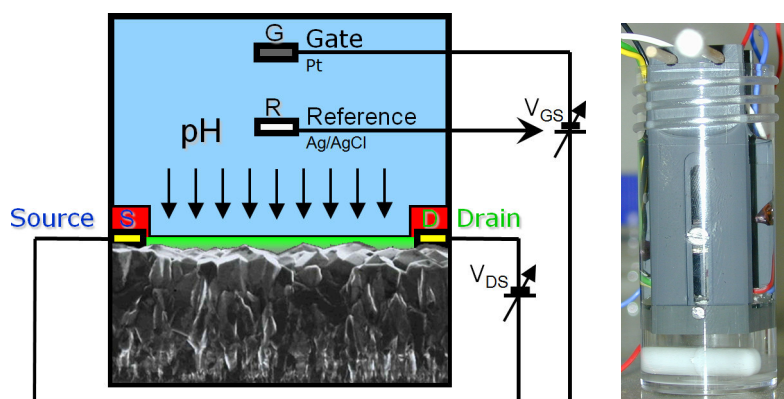
Figure 2.12.   Solution-gate FET (SGFET) setup in theory and in practice.

At our laboratory, FET mode measurements were performed with a combination of a Keithley 2400 sourcemeter with a PalmSens potentiostat, both

synchronised via home-made LabVIEW software. The concept of a constant current mode (analogous with electrolyte-insulator-semiconductor (EIS) constant-capacitance mode) was programmed. This implies that the current is regulated by the gate voltage in a feedback loop.

Lacking miniaturised manufacturing techniques during the time span of my PhD project, such as nanolithography or electron beam lithography (EBL), larger scale diamond SGFET designs were made and investigated [figure 2.12]. Difficulties with water infiltration in the polymer shielding the electrical contacts were overcome. Unfortunately no satisfactory reproducible pH sensitivity could be observed due to the high temperature dependence of the sensitive FET setup [figure 2.13].
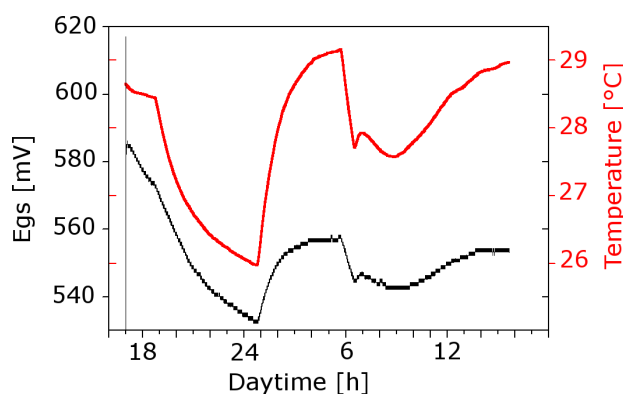
Figure 2.13.   Temperature-dependent conduction properties.
The time chart illustrates the strong temperature dependence of the ISFET Egs signal that keeps Ids constant (at pH=7). To reduce the temperature-dependence, later experiments were performed in a closed oven box.

2.6. **Tuning of properties**

Due to the large bandgap, diamond exhibits a high stability with respect to chemical reagents and corrosion [167,168]. In electrochemistry, this wide potential window can be capitalized for the production of electrodes operating in hostile environments [169-172]. Both H- and O-terminated diamond surfaces are very stable in aqueous solutions [173], contrary to silicon gate material that is sensitive to invasion of interfering cations, like K^+, Na^+ and Ca^{2+} [159].

Applications of diamond in biosensors, demanding such chemical stability, are therefore obvious.

Although undoped diamond is a good electrical insulator, besides the aforementioned surface conductivity, doping with small molecule impurities, like B (p-type) and N, Li or P (n-type) turns the material into a semiconductor [111,174-182]. Thus, junction FETs and UV light-emitting diodes (LEDs) can be fabricated [183-185].

2.6.1. Surface termination

There are two stable termination states of the diamond surface possible [figure 2.14]. On the one hand as-grown and hydrogen-plasma treated CVD diamond is hydrogenated and therefore electrically conductive (see chapter 2.4 *Surface conductivity*, p.38) On the other hand, wet chemically oxidized or oxygen plasma treated surfaces are insulating. The changes caused by hydrogen and oxygen plasma treatment are reversible [126].
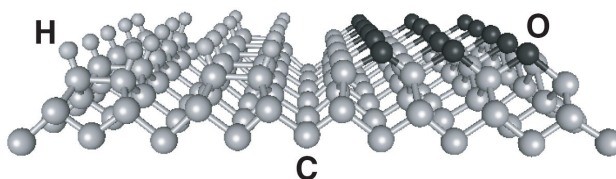
Figure 2.14.   3D model for the diamond lattice.
H- (left) and O-terminated (right) surface [27].

There is a charge polarization in the covalent bond between the foreign atoms (H or O) and the carbon as a result of their electronegativity (EN) difference (H: 2.3, C: 2.5, O: 3.6). These properties are the origin of a different reactivity (e.g., during functionalisation). E.g., H-termination protects the diamond surface against the phase transition to graphite that proceeds slowly at room temperature [111,186,187].

Surface oxidation can be done by boiling the diamond samples in an acid mixture of H_2SO_4 and KNO_3 for 30 minutes [188]. Gentler and better defined oxygenation can be obtained by ozonisation [147,164,189,190]. FTIR (Fourier transform infrared spectroscopy) analysis shows that carbonyl (>C=O), lactone () and carboxyl () and cyclic ethers () are present [191].

Diamond conductivity can also be manipulated by patterning hydrogenated and oxidised regions: a hydrogenated sample can be treated by local anodic oxidation in a Kelvin probe force microscope (KPFM; nm scale) or reactive ion etching (µm-mm scale), which allows fabrication of in-plane-gate FETs and ISFETs [111,129,148,156,192-195].

H-terminated surfaces can be used for further treatments, like amination, chlorination, carboxylation or peroxidation [196,197,198]. E.g., for polycrystalline diamond, it has been shown that direct amination can be done by 254 nm UV irradiation in ammonia atmosphere, and patterning is possible by passivation through fluorination with an Au mask [199].

The XPS technique (see chapter 3.1.5 X-ray photoelectron spectroscopy (XPS), 60) was used for determination of the surface termination state.

2.6.2. Surface activation and functionalisation
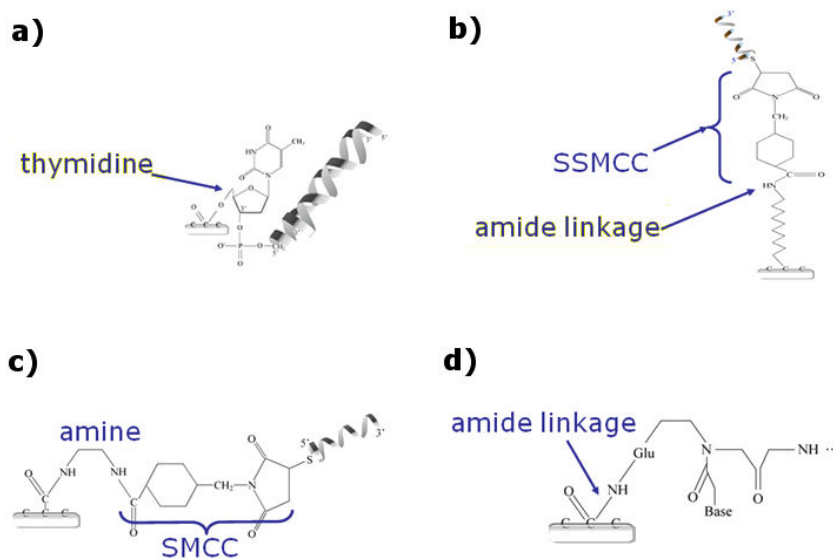
Figure 2.15. Methods for attachment of DNA and PNA to diamond and nanotubes.
a) direct connection between bulk diamond and the last thymidine of DNA (Ushizawa et al., 2002 [213]) b) SSMCC linker (Yang et al., 2002 [246] & Härtl et al., 2004 [218]) c) SMCC linker between CNT and DNA (Baker et al., 2002 [200]) d) amide links CNT to PNA (Williams et al., 2002 [201])

Though some modification procedures make the diamond surface more stable under extreme conditions [202], most make it more reactive, which is desired for further covalent functionalisation of this surface, guaranteeing a strong fixation of the molecules to the surface [203,204,205,206,207].

Silanisation of oxidized UNCD could be demonstrated analogously to Si surfaces with electrochemically active enzymes [13,208]. Other functionalisation procedures imply grafting of aryl diazonium derivatives, or dicarboxylic acids [209,210,211]. Still other methods for activation with nitrophenyl imply electrochemical reduction of aryl diazonium salts (grafting) of nitrophenyl, involving a radical-mediated cascade with 4'-nitro-1,1-biphenyl-4-diazonium (NBD) tetrafluoroborate [212].

Several activation procedures were studied [figure 2.15]. A promising technique, published by Ushizawa *et al.*, for activation and functionalisation of diamond powder was thionyl chloride-mediated reaction of surface oxides with thymidine, followed by enzymatic attachment of dsDNA molecules [188,213]. Our experience learns it is difficult to reproduce on polycrystalline diamond with the grain size ranging between tens to several hundreds of microns, probably because of lower content of grain boundaries. These boundaries contain the necessary dangling bonds for the attachment mechanism, resulting in an insufficient availability of carboxyl groups on the polycrystalline diamond surface.

The Baker method oxidizes nanotubes to form carboxylic groups at the edges, followed by thionylchloride an ethylenediamine-mediated amination [200]. The amine residues are further reacted with crosslinker SSMCC to produce maleimide groups. Finally, thiol-modified DNA is bond to these groups, resulting in DNA-modified nanotubes.

The Williams method exposes nanotubes to sulphuric acid and nitric acid to produce carboxylic groups that react with PNA using EDC and NHS [201].

A method first published by Yang *et al.* showed growth by photoattachment of vinyl groups of ω-unsaturated TFAAD to hydrogenated diamond films, amorphous carbon and Si [49,214,215,216,217,223]. This was followed by SSMCC-mediated thiol-modified DNA attachment. The proposed reaction mechanism is the formation of anions that directly react with surface H or that adsorb to H, thereby creating sites reacting to other alkenes [218,223]. A protecting group prevents intramolecular and other unwanted reactivity,

necessitating deprotection afterwards. The method results in a very stable bond allowing reuse for up to 30 hybridization-denaturation cycles [214] [figure 2.16]. Also, biologically activity of enzymes could be maintained using this immobilization technique [218]. Advantages of this TFAAD pathway is the formation of a strong C-C bond, the possibility of photopatterning and the high stability of the resulting covalent functionalisation [49]. This approach also allows preventing nonspecific protein adsorption by analogous photochemical modification of diamond films with triethylene glycol [219].
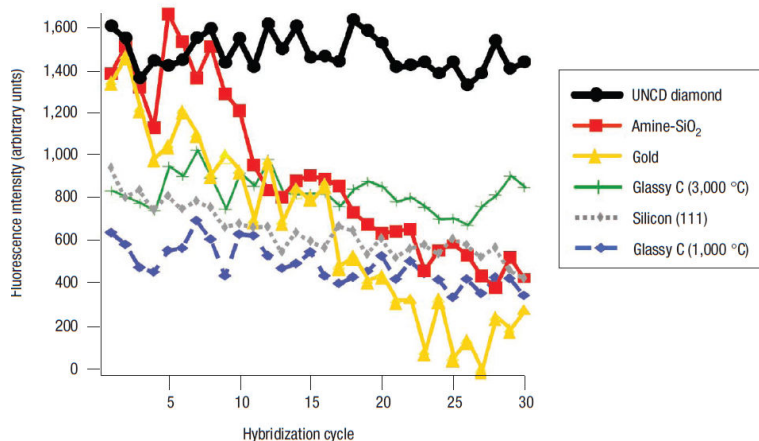
Figure 2.16.   Superior stability of diamond as a rehybridization platform.
TFAAD-modified diamond substrates show a high chemical stability: up to 30 denaturation and rehybridization cycles can be performed without loss of binding efficiency (adapted from [214]).

The Yang comparison experiment [figure 2.16] describes several surfaces that were amino-modified and were further reacted with SSMCC and thiol-modified DNA to form a hybridization platform. The experiment demonstrates the high stability of the diamond platform.

The development of a new two-step procedure for diamond functionalisation with DNA, which is entirely attributable to this PhD, can be found in chapter 5: *DNA attachment to NCD*, p. 69). [248].

2.6.3. Further steps

After activation and functionalisation of the diamond surface, organic chemistry is used to build a fully functional surface with biologically interacting molecules. Organic chemistry and biotechnology provides us with a wide range of possibilities to tether biomolecules to diamond, e.g., DNA, peptides, enzymes or antibodies [220,221].

The diamond surface is a stable platform with a high packing density [196,222]. Both probe density and orientation play an important role in the accessibility to the target [223]. Depending on the used transducer, simple adsorption, thiolated DNA self-assembled monolayers (SAMs) on Au, biotin-avidin labels or covalent binding can be used to attach biomolecules [224].

Adsorption of the sensitive receptor molecules to the surface, can be enhanced by some adsorption matrix [225]. After the incubation period the remaining nonspecific binding sites should be blocked for adsorption of other molecules. Cell adhesion to the diamond surface, which is mediated by electrostatic interactions and H bonds, works better with UV- and 10-undecenoic acid (UA)-treated surfaces [242].

IgG antibodies can simply be adsorbed to the NCD surface [89]; After washing and blocking with BSA, hydrophilic surfaces (air plasma treated; comparable to our acid-oxidized state) show a higher specific affinity for their complementary antigen than the hydrophobic (hydrogen plasma treated) NCD [226].

Covalent coupling can be done directly or by mediation of a crosslinker (like SSMCC, EDC, or a dicarboxylic linker (like adipic acid, terephthalic acid or trimesic acid) [227,228]).

3. Characterisation techniques for functional surfaces

3.1. Characterisation techniques

3.1.1. Scanning electron microscopy (SEM)
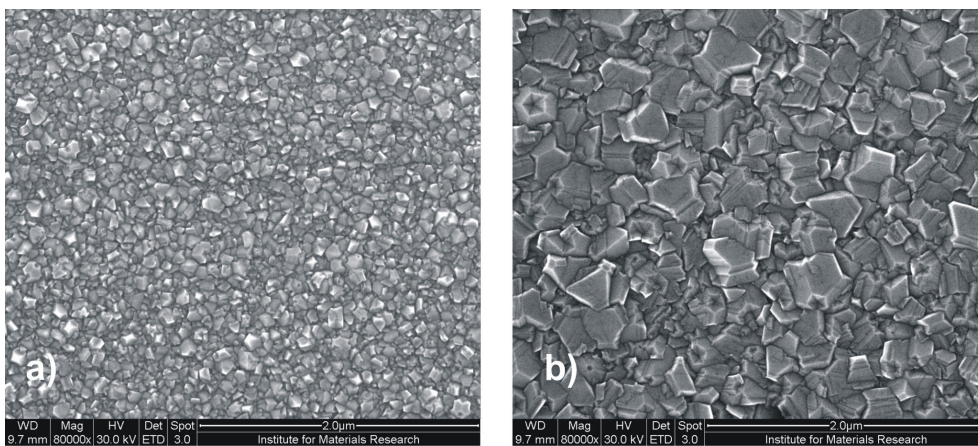
Figure 3.1.   Scanning electron micrograph of NCD.
(a) a 100 nm and (b) 500 nm thick NCD film deposited on a p-Si-SiO$_2$ substrate.

NCD films have been characterized using a scanning electron microscope (SEM) (FEI Quanta 200F FEG and Philips XL30-FEG). This technique produces a tophographical image of the sample surface. The SEM micrograph in figure 3.1 demonstrates an example of the morphology of a 100 nm and a 500 nm thick NCD film deposited on a p-Si-SiO$_2$ substrate. As can be seen, the films comprise randomly oriented fine grains. The average grain size of the 100 nm thick NCD film, as determined by the SEM image, was around 100 nm.

In the SEM's vacuum chamber, a beam of electrons (1-50 keV) is directed to the sample. The substrate should preferably be conductive because electrostatic charging effects complicate imaging due to uncontrolled beam deflection. The high energy electrons are reflected and consequently detected, giving a topographic image with a resolution up to 5 nm. Recorded SEM images

and subsequent EDX analysis of secondary electron energies allow a determination of surface element composition up to 1 µm depth, depending on the acceleration voltage [figure 3.2].
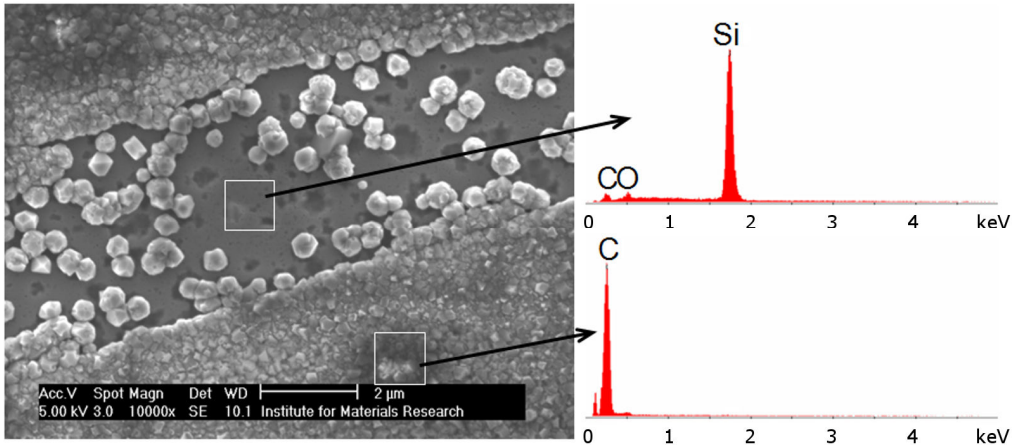
Figure 3.2.   SEM sample imaging and element analysis.
(Left) SEM image of an NCD growth defect (Right) EDX element analysis of selected regions: (Top) uncovered substrate region with mainly Si and traces of C and O (Bottom) C peak for a region with confluent growth.

3.1.2. Atomic force microscopy (AFM)

We used AFM for topographical characterisation of hydrogenated and oxygenated diamond surfaces. It scans a small surface (1-100 µm^2) and records conformational relief information [figure 3.3 and figure 2.4, p. 38]. A 10 nm-wide and 10 µm-long Si tip on a mm-long cantilever oscillates above the surface of the sample that is laying on a high resolution piezo tube scanner block. Some AFMs can even be used as a biosensor by functionalization of the tip surface [229]. Other AFMs actively alter the chemical surface structure: using bias voltages of the tip with respect to the sample, H atoms can be replaced by O [230].

An optoelectronical feedback loop controls the net movement of the cantilever that results from the summation of several forces, such as van der Waals attraction at a distance in the order of a few atomic diameters, repulsion at a distance smaller than an atomic diameter, capillary forces and Hooke's spring force of the cantilever. A laser beam detects the position of the cantilever

and repositions the sample vertically through the piezo element. This information is used to reconstruct a height image. Non-contact mode is used for both hard materials, like diamond, and soft materials with e.g., fragile biofunctionalisation. The typical distance between tip and sample is 1-10 nm for non-contact mode.
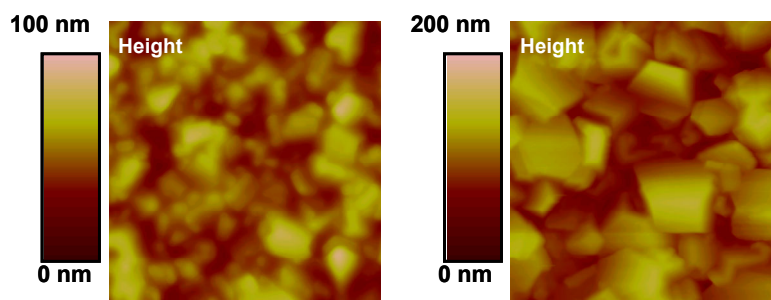
Figure 3.3.   AFM roughness comparison of NCD growth: thicker films have a higher surface roughness.
The 100 nm NCD (left) and 500 nm NCD (right) films were grown on a p-Si-SiO$_2$ (native oxide) structure. The scan area was 1 µm^2.

Our images were recorded by a Veeco Multimode microscope equipped with the Nanoscope III controller and Quadrex module. The intermittent contact (tapping mode) measurements were perfomed using Nanosensors GmbH etching Si probes (tip radius around 5 nm).

3.1.3. Contact angle measurement (CA)

The contact angle measurement shows the hydrophobicity and hydrophilicity of the surface, giving a non-quantitative indication of the overall chemical surface properties [figure 3.4]. The more a material is repellent to (the polar liquid) water, the higher the CA between the applied drop and the surface will be. H-terminated diamond surfaces have light polar covalent bonds at the surface and show a larger CA (90°) than O- (30-60°) or 10-undecenoic acid (UA)-terminated (70-80°) diamond surfaces [242,231]. UA is used as the first functionalisation step for the presented DNA attachment to DNA (see chapter 5, *DNA attachment to NCD*, p. 69).

CA measurements were performed at the Katholieke Hogeschool Limburg, campus Diepenbeek. The setup, an OCA 20 from Dataphysics, consists of a CCD

camera coupled to a computer, an injection needle for 1 µl drop delivery, a lamp and a movable platform where the samples can be put. The goniometer software determines the internal angle α in the drop between the surface and the drop tangential using the lateral image [figure 3.5].
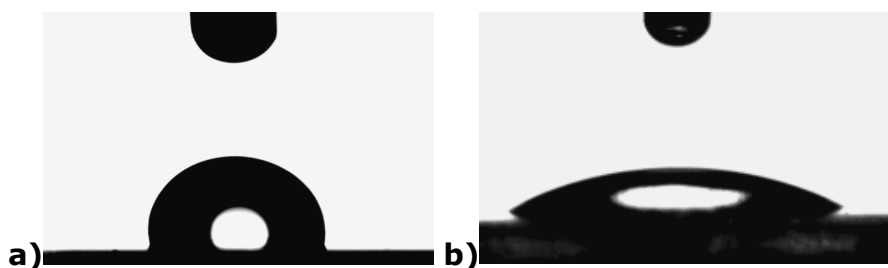
Figure 3.4.   The hydrophilicity of the surface determines water drop shape. Drops on a hydrophobic hydrogenated (a) and on a hydrophilic oxygenated NCD surface (b).
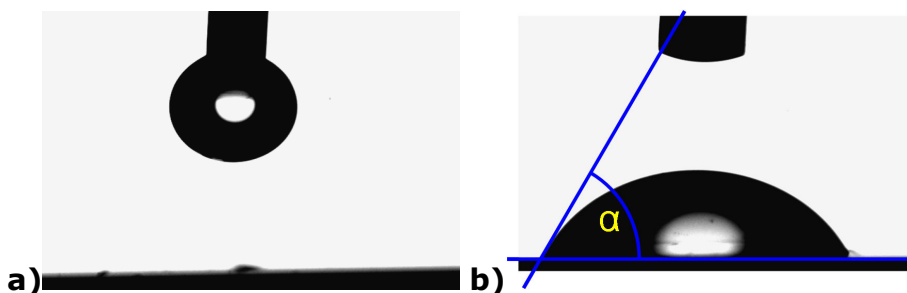
Figure 3.5.   Contact angle measurements for fast macroscopical assessment. Application of a 1 µl drop (a) and contact angle α determination (b)

3.1.4. Laser scanning confocal fluorescence microscopy (LSCFM)

Unlike a regular microscope, the focal spot of a LSCFM is narrowed by a pinhole. Together with the use of a single wavelength laser, this gives a better spatial resolution. In combination with a fluorescent marker, the detection limit approaches the single molecule detection.
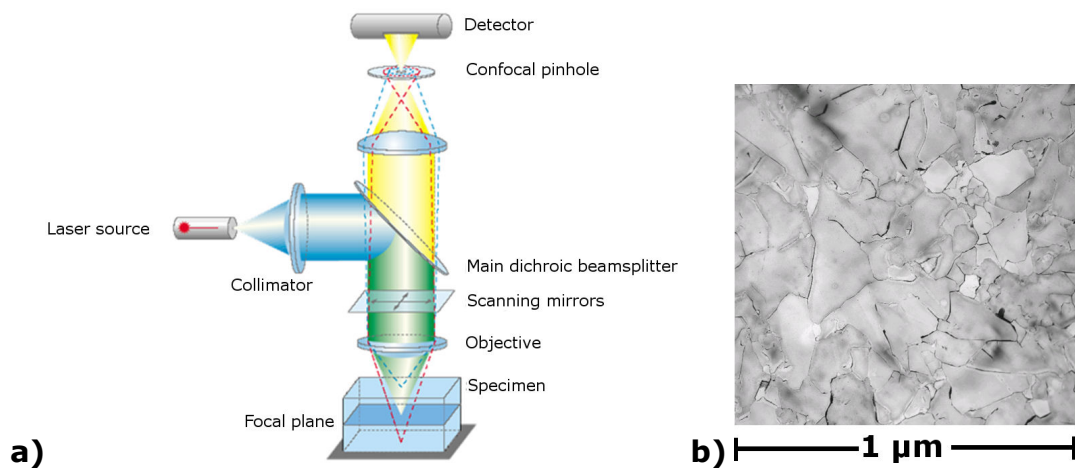
*Figure 3.6.   Optical analysis of diamond surfaces with confocal microscope.
(a) Light path (adapted from Zeiss) (b) visual image showing diamond
microcrystallites.*
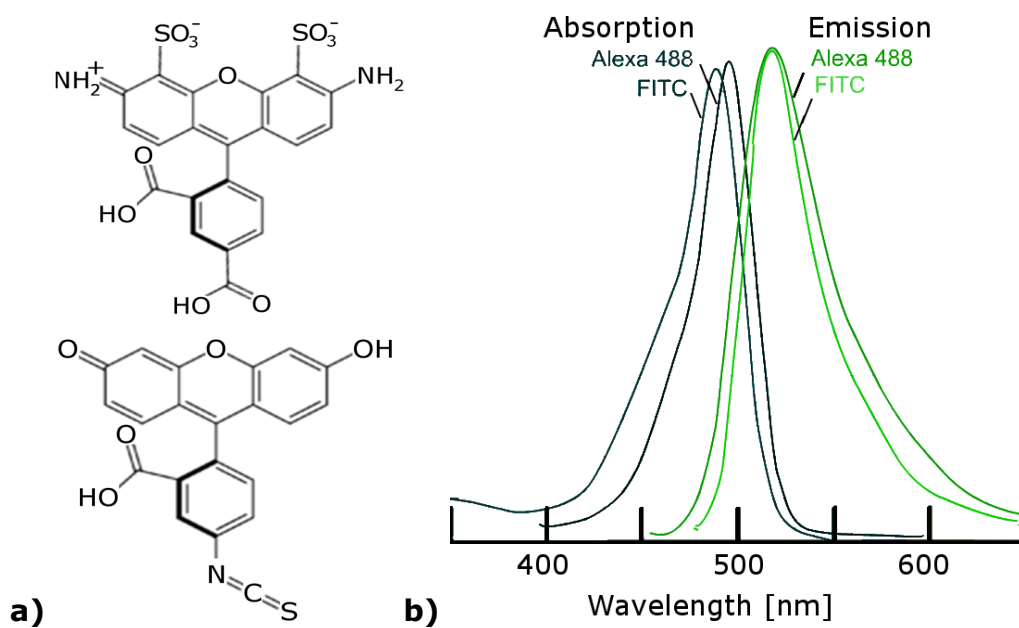
*Figure 3.7.   Structure and spectrum of FITC and Alexa-488 marker molecule.
(a) molecular structure of Alexa-488 (top) and FITC (bottom) (b) absorption and
emission spectrum [adapted from 232]*

Images were recorded with a Zeiss LSM 510 META confocal fluorescence microscope and 488 nm laser light [figure 3.6]. The initially used fluorochrome FITC was later on replaced by Alexa 488 that is more intense and more resistant against photobleaching [figure 3.7] [233].

3.1.5. X-ray photoelectron spectroscopy (XPS)

Surface modifications of diamond can change material properties dramatically. Electrical conductance, electrochemical activity and molecular sensitivity can be altered by different treatments [234]. Therefore, a surface sensitive characterization technique, like XPS is indispensible. XPS uses the photoelectric effect to assess each subsequent surface treatment.

XPS analyses were done at the Laboratory of Chemistry and Electrochemistry of Surfaces at the Facultés Universitaires Notre-Dame de la Paix (FUNDP) in Namur with the XPS instrument SSX-100 from Surface Science Instruments. The setup consists of a vacuum chamber (10^{-8} Pa) where a 0.5 mm spot of an X-ray beam excites the electrons in the sample. Depending on the incidence angle, the penetration depth can be up to 10 nm (at 90°).
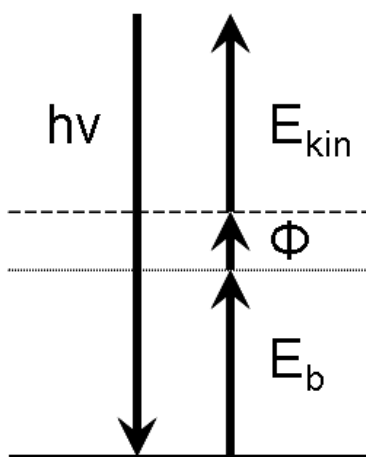
Figure 3.8.   XPS imaging energy diagram.
hv = electromagnetic energy, Φ = work function, Eb = binding energy

In the XPS analysis, the material under examination is irradiated with monochromatic Röntgen radiation. Electrons of the atoms composing the material are excited and emitted. These secondary (Auger) electrons absorb the

X-ray energy and use it to overcome the binding energy from their ground state and the work function i.e. the energy that sticks the electron to the sample surface [figure 3.8]. The recorded kinetic energy is characteristic for the energy level of the chemical element and the chemical bond the electron originates from. The obtained spectrum is the number of counts recorded for a certain binding energy that is reflected by the measured kinetic energy, in the range between 1100 and 0 eV.
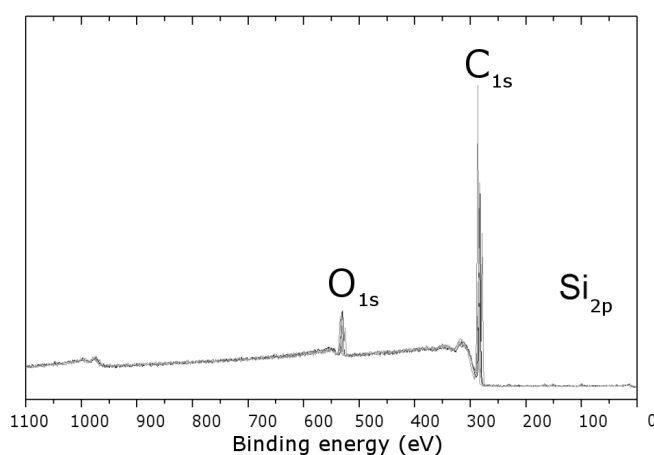
Figure 3.9. *Overview XPS spectra of oxidized NCD indicating the typical element regions.*
Oxygen, carbon, silicon.

After a significant measurement time, the area under the curve (AUC) for different noise-free peaks is multiplied with a weighting factor. This Scolfield factor is dependent on the element (e.g., O: 2.49, C: 1, Si: 0.9) and normalizes the count of each chemical element with respect to carbon [235]. The total count of each spectrum is set to 100%, making comparison between samples possible. An obtained spectrum cannot be directly compared to other spectra because the recording time is different and the signal is also dependent on the vertical position of the sample. Therefore, the Y axis has usually the label "counts (a.u.)", and each spectrum peak has to be compared relatively to other peaks of the same spectrum [figure 3.9].

The XPS technique was used for determination of the surface termination state of diamond after oxidation in acid baths or after plasma hydrogenation. The interesting typical energy peak regions for diamond surfaces are 545-525

eV (O_{1s}), 300-275 eV (C_{1s}) and 110-90 eV (Si). H cannot be detected directly using this technique. The plasma hydrogenation however makes the O_{1s} peak disappear [figure 3.10], while the C_{1s} peak remains [figure 3.9, p. 61]. This analysis proves that oxygenation and hydrogenation treatments are effective.
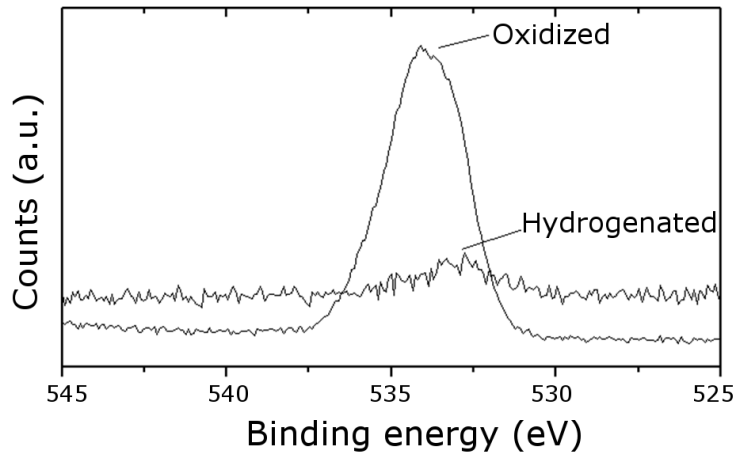
Figure 3.10.   XPS surface element analysis.
Details of O_{1s} region for oxidized and hydrogenated sample groups.
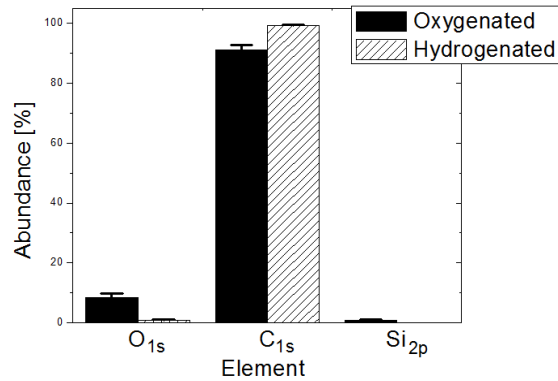
Figure 3.11.   Relative abundance of surface atoms in XPS spectrum.
Oxygenated (left side) and hydrogenated (right side) NCD films. In conclusion, carbon can always be detected. In the oxygenated samples, a large amount of O is clearly present (about 10 at%), in contrary to the hydrogenated samples. Also a small amount of Si can be detected due to interdiffusion and small pinholes.

Residual O remains on the hydrogenated samples because the hydrogenation is not 100% effective [figure 3.11]. Possibly, the O originates from the grain boundaries: accessible for the XPS electron beam, but not attainable for the etching hydrogen plasma ions [236].

4. Materials and methods

4.1. Diamond sample preparation

4.1.1. Synthesis and preparation of NCD substrates

NCD thin films were deposited as described above (see chapter 2.3 *Artificial diamond growth*, p. 35). The obtained wafer was cut in 1 cm^2 pieces using a diamond scribe and cleaned as described in the same chapter.

4.1.2. Sample preparation for concap measurements

The Si substrates were p-Si (ρ = 1-10 Ω cm) and had a several nm thick native oxide or a 50 nm thermally grown SiO$_2$ layer. On top, undoped NCD thin films of 100-500 nm thickness were grown under similar conditions, like described above (see chapter 4.1.1 *Synthesis and preparation of NCD*, p. 65 and chapter 2.3 *Artificial diamond growth*, p. 35), however no Ti was used, and seeding was performed by ultrasonication with 5 nm crystallite size diamond powder suspended in methanol (in solution these crystallites aggregated to 200 nm diamond clusters). A 300 nm Al film was deposited on the rear side of the sensor chip as an electrical contact layer. The chip size of the EDIS sensors was 1 cm^2.

4.2. Methods used for DNA attachment to NCD

4.2.1. Synthesis of FITC-labelled NH$_2$-modified dsDNA

Amino-modified DNA was prepared using amino-modified primers in a PCR amplification reaction. The PCR technique uses thermostable DNA polymerase enzymes and primer oligonucleotides to multiply gene fragments using deoxyribonucleic base building blocks. In a thermal cycling reaction the region, delimited by the binding primer sequences, is multiplied exponentially. A 250 base pair (bp) amplicon of the short tandem repeat (STR)-region of the phenylketonuria (PKU)-gene was obtained using a fluorescein isothiocyanate (FITC)-labelled forward primer and C6-NH$_2$-modified reverse primer. The

fluorescent label FITC was used for detection: it has an excitation maximum at 494 and an emission maximum at 518 nm [figure 3.7]. Introduction of the NH_2 group is needed for the EDC coupling reaction.

Standard 100 µl-PCR reactions contained 200 nmol of each dNTP, 50 pmol of each primer, 5 Units Taq-DNA polymerase, genomic template DNA and PCR buffer [237]. The PCR typically cycled 35 times, each cycle comprising a denaturation phase at 95°C for 20 s, an annealing phase at 52°C for 20 s and an extension phase at 72°C for 30 s. PCR amplicons were purified using phenol-chloroform extraction and were precipitated with ethanol. DNA was dissolved at a concentration of 40 ng/µl.

4.2.2. UV photoattachment of ω-unsaturated fatty acid,

The surface of the diamond samples was covered with a thin layer of 10-undecenoic acid. Subsequently it was irradiated for 20 h with 254 nm light from a Philips TUV G4T4 4W lamp (2.5 mW/cm^2) that was mounted in an EPROM eraser box from Lawtronics (ME5, Edenbridge, UK) under a protective nitrogen atmosphere inside a glove box [figure 5.1]. The samples were rinsed with 10% sodium dodecyl sulfate (SDS) (Acros Organics), an anionic detergent, and with distilled water.

Although the used wavelength is below bandgap (253 nm ~ 4.9 eV photon energy (E_{hv}) versus 5.5 eV diamond bandgap), the reaction can take place [238]. H-induced surface states induce covalent bonding of alkenes, however with low quantum efficiency [61].

4.2.3. EDC linking of dsDNA to carboxylated NCD surfaces

The NCD surfaces that were pretreated with UA, were incubated with a 50 µl droplet of a mixture of 1.2 µg FITC-labelled NH_2-modified dsDNA and 1 mg EDC (50 mg/ml) in a 25 mM 2-[N-morpholino]-ethanesulphonic acid (MES) buffer solution, pH 6, for 2 h at 4°C. NCD samples were placed in a closed box with a droplet of water enclosed, to avoid evaporation. As negative control, other COOH-modified NCD samples were treated with a similar mixture in which EDC was replaced by 25 mM MES, pH 6. Unbound DNA was removed from the diamond samples by thoroughly washing with PBS buffer. These washing steps comprise submersion of NCD samples in PBS buffer and continuous shaking for 5

min. This was repeated 11 times. For the last (12th) washing step, 50 µl of PBS was applied to the surface and was collected after 5 min.

In an analogous experiment, FITC-labelled NH_2-modified dsDNA was also EDC-linked to COOH-modified paramagnetic beads (Dynabeads) to clarify the efficiency of each step. Analogously, COOH-modified beads treated with FITC-labelled NH_2-modified dsDNA without EDC served as a control.

4.3. Concap mode pH measurements on EDIS

4.3.1. Functionalization of the EDIS sensors with polyelectrolyte multilayers

The PE multilayers were obtained, using the layer-by-layer assembly technique by consecutive adsorption of PAH and PSS from the respective PE solution (50 µM PSS or PAH, unbuffered 0.1 M NaCl, pH 5.3) [22,23,280]. During the experiments, the EDIS sensor chips were consecutively exposed to the respective PE solution for a time necessary for the adsorption of a single monolayer (usually 5-15 min), followed by rinsing in buffer solution or ultrapure water. These procedures were repeated until the desired number of layers was obtained (in this study, the maximum number of PE layers was 13). The thickness of the PE layer measured by imaging ellipsometry (EP[3], Nanofilm, Germany) was approximately 2 nm/layer, which is in agreement with the results reported in [23].

4.3.2. Measuring setup

Figure 6.2 shows the measuring setup that has been developed at the Aachen University of Applied Sciences for the electrochemical characterisation of the EDIS sensors. The schematic cross-section of the layer structure of the EDIS sample is also illustrated.

The detailed cross-section of a sample is shown in figure 4.1, illustrating the layer structure of the EDIS sensor with the adsorbed PE layers. These samples were measured in the same setup.

The EDIS sensors have been characterized by means of capacitance-voltage (C-V) and constant capacitance (ConCap) methods [268] after the

functionalization with the mono- and multilayers of charged macromolecules. For comparison, the C-V and ConCap curves of the EDIS structures without PE layer were also measured.
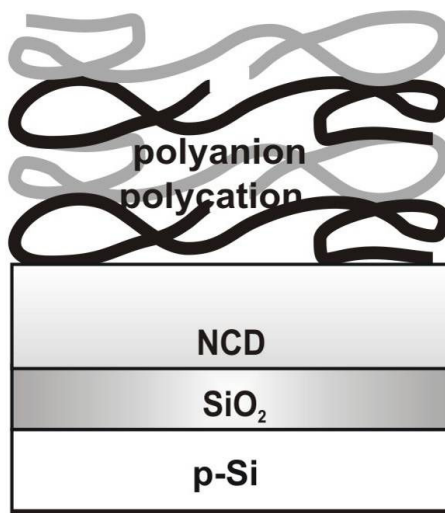
Figure 4.1.   Schematic cross-section of the EDIS structure functionalized with a polyelectrolyte multilayer.

5. DNA attachment to NCD

This chapter is based on the article entitled EDC-mediated DNA Attachment to Nanocrystalline CVD Diamond Films. *Biosensors and Bioelectronics* **22**, 170-177 [248].

5.1. Introduction

Here we present our simple and straightforward two-step method to tether DNA to diamond. This achievement is an essential prerequisite for fabrication of diamond-based biosensors: immobilizing molecules allows for the construction of affinity biosensors that can monitor molecular interactions, like DNA hybridization [239] or antibody-antigen interaction [240] with great sensitivity.

In a first step, a H-terminated diamond surface is carboxylated by photoattachment of undecylenic acid (=10-undecenoic acid) using (sub-bandgap) 254 nm UV light irradiation during 20 h [figure 5.1, p. 69].
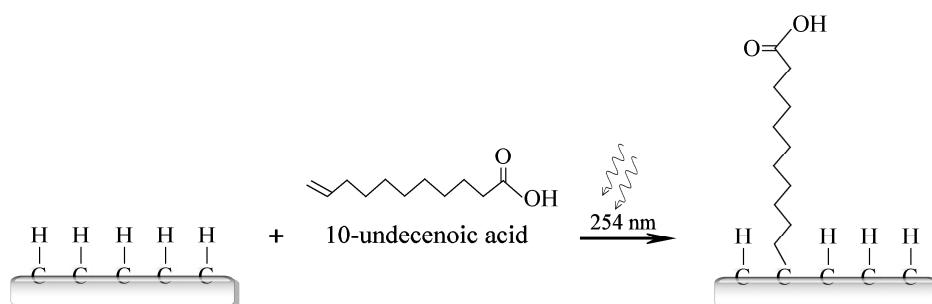
Figure 5.1.   Photoattachment of 10-undecenoic acid to NCD.
The surface is submerged with undecenoic acid and is irradiated with 254 nm UV light.

The second step comprises covalent attachment of NH_2-modified dsDNA to the previously carboxylated surface, using an EDC-mediated reaction [248] [figure 5.2, p. 70].
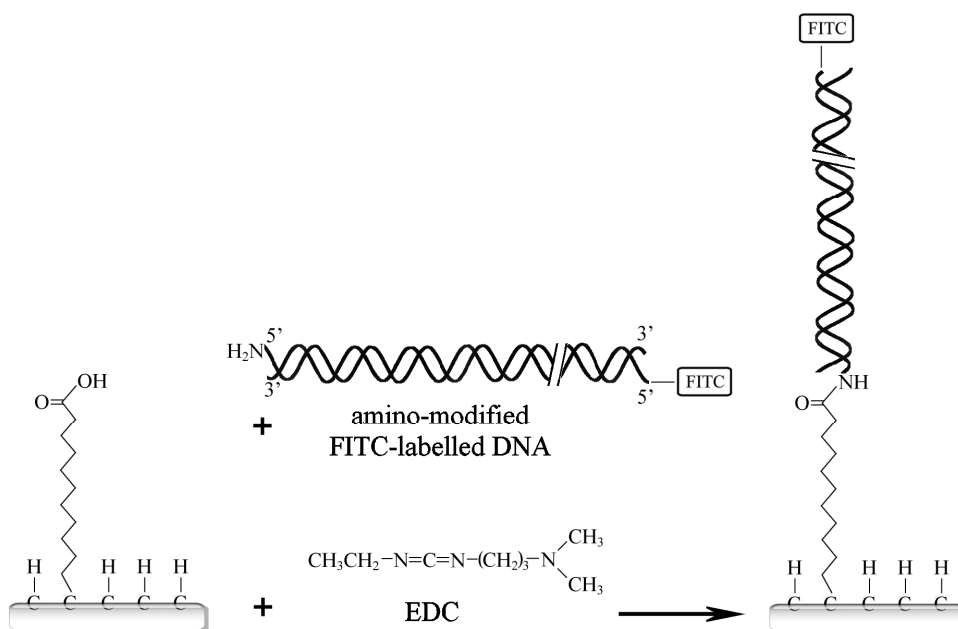
Figure 5.2.   Attachment of DNA to photochemically modified diamond substrates.
FITC-labelled NH₂-modified dsDNA is linked to the 10-undecenoic acid residues on NCD substrate using an EDC-mediated reaction. FITC is used for detection and imaging purposes.

Other groups investigated the validity and efficiency of this new method, confirming [241] and even modifying the method to tether proteins [242]. The protocol can also be applied to carbon nanowalls [243]. Remarkably, a similar protocol can be applied to H-terminated Si substrates that are carboxylate-terminated [244], and subsequently DNA-modified [245].

An advantage of our two-step method is that it discards deprotection described in Yang *et al.* [246], which is essentially a four-step photochemical attachment of ω-unsaturated molecules onto nanocrystalline diamond. The use of a protective group to prevent unwanted side reactions, like in the TFAAD procedure, is even unfavourable since it lowers the bound UA density [241].

Secondly, the crosslinker was omitted using a zero-length carbodiimide-mediated coupling method for amino-modified dsDNA [228]: the OH group of the carboxyl group is a 'bad leaving group', i.e. chemically relatively stable. To

overcome this, OH is chemically transformed into an unstable O-acylisourea intermediate. This is a better leaving group that readily reacts with the NH_2 groups of the FITC-labelled polymerase chain reaction (PCR) amplicons [figure 5.3]. Afterwards, an acid-catalysed nucleophilic substitution with amino-modified DNA results in a simple amide bond between the fatty acid and the dsDNA [figure 5.2].
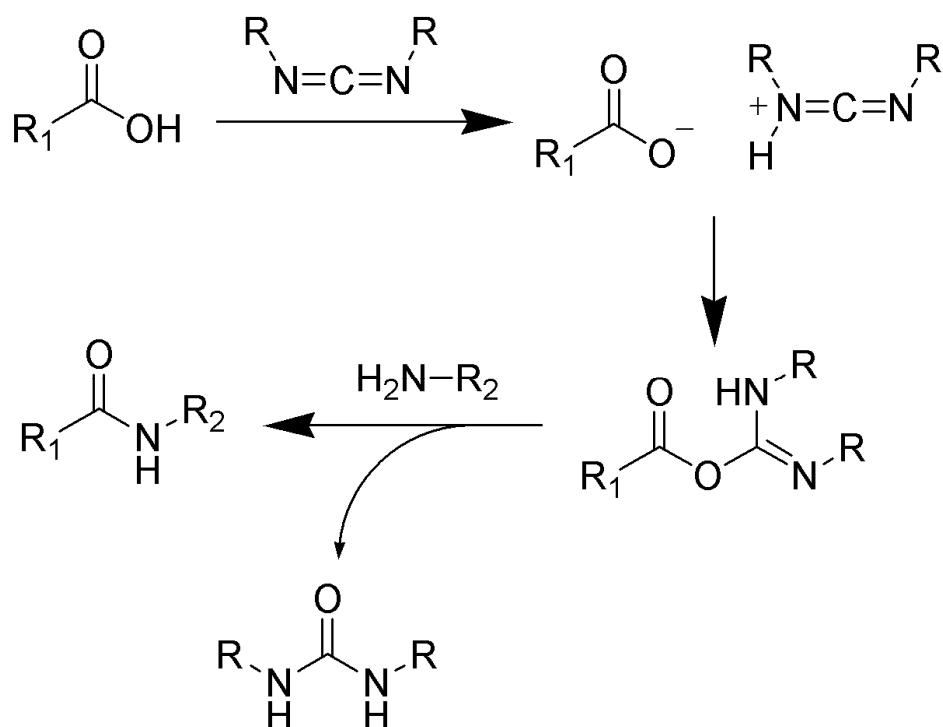
Figure 5.3.   EDC-induced crosslinking chemistry.
The zero-length carbodiimide crosslinker reacts with carboxy and amino groups to form a net amide bond [228] (adapted from [247]).

A third advantage is that the protocol overcomes the problem of insufficient carboxylation that was a problem in the thionyl-route of Ushizawa *et al.* [213]. Via attachment of fatty acid chains to the diamond surface, a universal coupler for amino groups is created.

Other advantages of this method are the formation of a strong C-C bond, the possibility of photopatterning and the high stability of the resulting covalent

functionalisation [49]. The latter was demonstrated in repeated denaturation and rehybridization reactions proving undiminished binding capacity up to 35 cycles [248]: harvested fragments were amplified with PCR, mechanically separated with gel electrophoresis, and visualised with a DNA-staining dye. For DNA, the reversibility of the hybridization process allows regeneration and multiple use of the sensitive surface of DNA sensors [11]. This is in accordance with findings that diamond is a superior material for attachment of biomolecules [214].

5.2. Results

5.2.1. Denaturation-rehybridization experiments
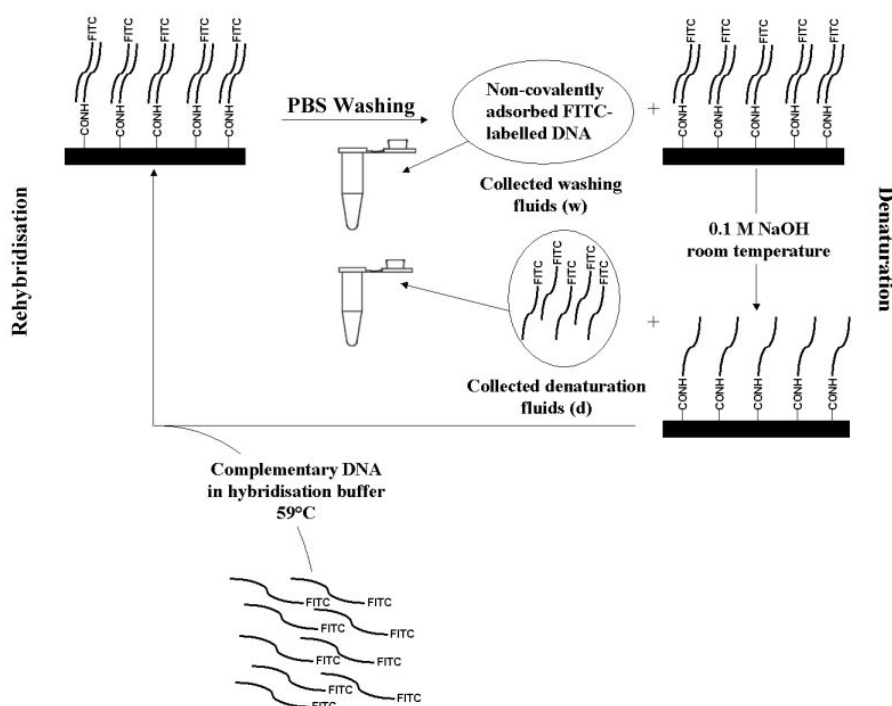
Figure 5.4.　Denaturation-rehybridization-washing (d-r-w) cycle.
FITC-labelled NH$_2$-modified dsDNA was immobilized onto the COOH-modified NCD surface. After thoroughly washing non-bound DNA away, the sample was denatured. Rehybridization was obtained by incubating the sample with new

FITC-labelled complementary ssDNA. In every cycle, fluids from the last washing (w) step and the denaturation step (d) were collected for analysis.

The COOH-modified NCD samples that were treated with an FITC-labelled NH$_2$-modified dsDNA solution, either with or without EDC, were used in a denaturation and rehybridization experiment. Denaturation of immobilized dsDNA was done by application of 50 µl of 0.1 M NaOH on the treated surfaces at room temperature during 5 min. This liquid, containing the FITC-labelled denatured strands, was collected by simply pipetting the drop from the surface. The NaOH was neutralized with 0.1 M HCl. Samples were subsequently submerged in boiling water for 1 min, to make sure all of the surface-bound dsDNA would be denatured.

Rehybridization of the ssDNA that was still bound to the surfaces, was carried out by submerging the samples for 30 min at 59°C in hybridization buffer containing an excess of fresh complementary DNA that was previously denatured for 5 min at 95°C [237]. Hereafter, the samples were thoroughly washed with PBS, as described above.

This cycle of denaturation-rehybridization-washing (d-r-w), which is outlined in figure 5.4, was repeated 35 times, and for each cycle the fluids corresponding to the last washing step and the denaturation step were collected from the EDC-positive and EDC-negative sample batches for further analysis.

5.2.2. Fluorescence measurements

Fluorescence signals were measured with the fluorescence module of the Lightcycler (Roche Diagnostics, Vilvoorde, Belgium). Both denaturation and washing steps of EDC-positive as well as EDC-negative NCD and paramagnetic bead samples were measured. 10 µl of each collected denaturation and washing volume from both diamond sample batches and both bead samples was analysed at 30°C. 10 µl of deionised water was used as a blank reference sample.

FITC-labelled DNA was prepared as described in Section 4.2.1 (Synthesis of FITC-labelled NH$_2$-modified dsDNA, p.65) in a concentration of 40 ng/µl. A dilution series was prepared in triplicate from FITC-labelled dsDNA. Concentrations were 1.5, 0.8, 0.4, 0.2 and 0.1 ng/µl. Deionised water was used as blank. 10 µl of each dilution was analysed with the fluorescence module using a 530/20 nm FWHM (Full Width at Half Maximum) band-pass emission filter. The

sensitivity calibration curve is shown in figure 5.5A. The detection limit of the FITC label is 2 ng (0.2 ng/µl ×10 µl). The fluorescence measurements are expressed as relative values.

The presence of FITC fluorescence in each of the fluids collected from the successive washing and denaturation steps from the EDC-positive and EDC-negative NCD sample batches was analysed [figure 5.5B].
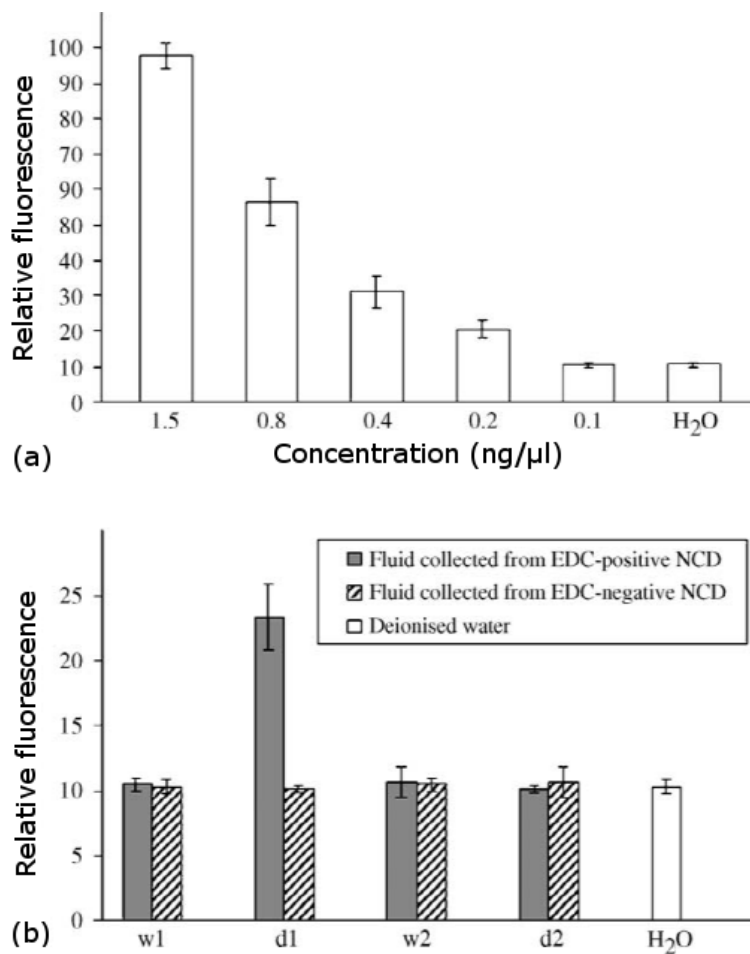
Figure 5.5.   Fluorescence detection of FITC-labelled DNA in supernatant.
(a) Sensitivity curve of Lightcycler fluorimeter for FITC-labelled DNA detection and (b) fluorescence curve obtained from the analysis of the fluids collected from the washing and denaturation steps of cycles 1 and 2 (w1-2 and d1-2, respectively) of the EDC-positive and the EDC-negative NCD sample batches.

For the EDC-positive as well as the EDC-negative NCD sample batch, the fluorescence signal from the last PBS washing step after dsDNA incubation reaction (w1) did not differ from that in water. Also, the fluid obtained from the last washing step after the first rehybridization reaction (w2) remained negative for both sample batches.

In the EDC-positive samples, there was a significant rise in fluorescence in the fluid obtained from the first denaturation step (d1), consistent with the release of the fluorescently labelled ssDNA strand during the alkaline denaturation in NaOH. However, this rise in fluorescence could not be detected in the fluid corresponding to the second denaturation step (d2), or in any of the subsequent denaturation volumes. In the EDC-negative samples, no increase in fluorescence was detected.

Comparable results were obtained from the fluids collected from the last washing steps and the denaturation steps from the EDC-positive and EDC-negative paramagnetic bead samples.

5.2.3. Denaturation and rehybridization monitored by PCR and gel electrophoresis

Because the fluorescence signal dropped below the detection limit after the first denaturation step, parallel PCR amplifications were performed on the same collected fluids. The PCR technique is much more sensitive than the lightcycler.

Fluids were collected from the last (12th) washing steps and the denaturation steps from the EDC-positive and EDC-negative NCD sample batches. In a control experiment performed on the dsDNA-treated EDC-positive and EDC-negative paramagnetic beads, a PCR reaction was performed on the beads themselves after each denaturation reaction. Subsequent to the PCR, the PCR amplicons were checked on a 2% agarose gel electrophoresis: smaller strands migrating due to an applied electric field move faster, while larger are more retained. A DNA ladder was used for calibration [248,249,250,251].

PCR reactions (15 cycles) were performed on 2 µl of dsDNA-treated EDC-positive and EDC-negative paramagnetic beads after two subsequent denaturation reactions. The collected fluids showed clear bands for the EDC-treated sample, but no signal for the EDC-negative sample [figure 5.6].

For the EDC-positive and EDC-negative NCD samples, collected fluids from the last washing steps and the denaturation steps of the denaturation-hybridization cycles from both batches were used in a PCR amplification. The PCR products for the EDC-positive and EDC-negative samples were loaded on an agarose gel. Figure 5.7 shows a representative subset of 10 out of 35 hybridization cycles.
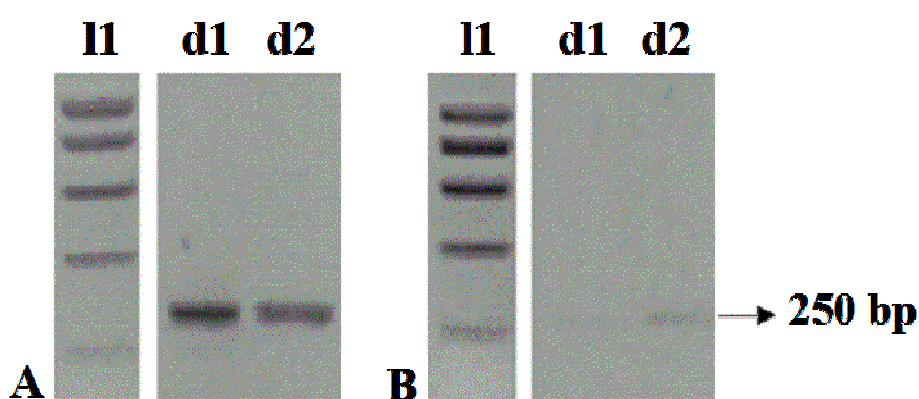
Figure 5.6. *PCR-amplified dehybridized fragments originating from DNA-functionalized carboxylated paramagnetic beads.*
(A) EDC-positive beads and (B) EDC-negative beads. Abbreviations: l1, SMART Ladder; d1, after the denaturation step of cycle 1; d2, after the denaturation step of cycle 2.

Electrophoresis physically separates the charged DNA strands using electromigration: the samples are spotted on one side of a polymer matrix (hydrogel) that is put under an electric field. Molecules carrying more charges (in the given surrounding pH) will migrate faster, while larger molecules experiencing more drag friction will migrate slower. A reference sample containing a mixture of fragments of known length, forms a so-called ladder in the electric field, providing a calibration ruler for molecular weight determination of the sample bands.

As shown in the upper panel of figure 5.7, the bands corresponding to fluids collected during denaturation steps remain visible throughout the entire 35 cycles for the EDC-positive NCD sample. Also, a band corresponding to the fluid collected from the last washing step of cycle 17 can be detected (w17), indicating that some hybridized DNA was still present on the NCD surface during

the last washing step of cycle 17. This attached DNA, however, is certainly removed during the boiling step in between hybridization cycles. In the EDC-negative sample, shown in the lower panel of figure 5.7, some cycles show very weak denaturation bands, suggesting that a very low amount of DNA is also non-covalently attached to the COOH-modified NCD surface.

Control experiments performed on other NCD samples in the EDC-positive and EDC-negative batch gave comparable results.
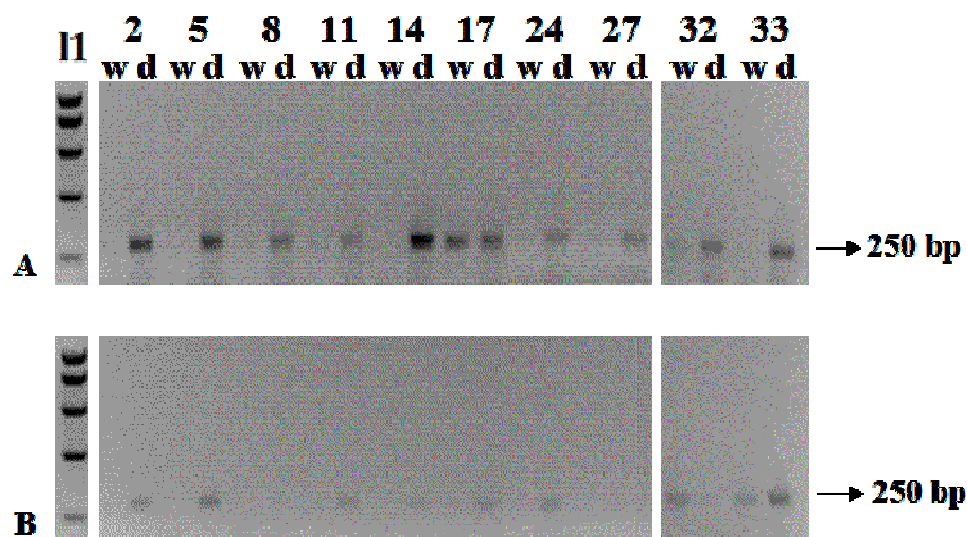
Figure 5.7.   Denaturation-rehybridization cycles on NCD samples.
33 cycles were analysed with 2% agarose gel electrophoresis. (A) EDC-positive NCD and (B) EDC-negative NCD. Abbreviations: l1, SMART Ladder; w2-33, fluids collected from the last washing steps of cycles 2-33; d2-33, fluids collected from the denaturation steps of cycles 2-33.

5.3. Summary

This chapter explains an EDC-based protocol for covalent DNA-binding to NCD diamond surfaces. The DNA molecules are attached through the formation of an amide bond between COOH groups that were photochemically introduced on the diamond surface and NH_2-modified dsDNA molecules.

Functional activity of the obtained samples was demonstrated in a series of 35 denaturations, rehybridizations and washings. Fluids from denaturation step and last washing step of several cycles were analysed for the presence of DNA using both fluorescence and PCR detection. Fluorescence measurements appeared to be not sensitive enough to detect the FITC-labelled DNA in the fluid samples after the various washing and denaturation steps, so a PCR and gel electrophoresis-based approach was used. From the PCR reaction that was performed on the collected last washing steps and the denaturation steps, it was clear that repeated denaturations and rehybridizations remain possible for more than 30 times for the EDC-treated diamond sample [figure 5.7A]. This number of cycles was a practical, but arbitrary limit. More cycles would have been possible. The findings confirm the results obtained by Yang *et al.* [246] who showed preserved denaturation-rehybridization activity for more than 30 cycles for DNA attached to diamond using a SSMCC crosslinker immobilization method.

The systematic lower denaturation signal for the EDC-negative samples [figure 5.7B] indicate that the NH_2-modified DNA was effectively covalently bound to the COOH-modified diamond surface in an EDC-mediated reaction, besides a low amount of DNA that was aspecifically adsorbed to the diamond surface. These results were confirmed on carboxylated paramagnetic bead samples: DNA was only present on the surface of beads that were treated with EDC.

Above results indicate a covalent bond between the DNA and NCD. The initial binding capacity of functionally active dsDNA appears acceptable, as the denatured ssDNA of the EDC-positive NCD-sample was visible with fluorescence measurements in the first cycle. No signal could be detected for the sample without EDC. However, amplification of the DNA present in the collected denaturation and washing fluids by PCR became necessary after this first denaturation-rehybridization cycle. Denaturation and rehybridization of NCD-bound DNA thus appeared to occur with a rather low efficiency. This can be attributed to the physical properties of DNA itself. The length and nature of the DNA molecules that were linked onto the diamond determines their conformation. Conformation is one of the most important parameters affecting surface coverage and hybridization efficiency. Longer molecules, as were used in this study (250 bp) are dynamic, flexible coils that attach themselves aspecifically to the surface on multiple locations. This could lead to a lower DNA surface density and an inaccessibility of various DNA molecules to subsequent hybridizations and denaturations. This implies a lower hybridization efficiency,

resulting in lower, or even no, denaturation signals [252]. dsDNA molecules are more rigid in structure, thereby assuring the accessibility of a considerable amount of DNA molecules for the first denaturation. ssDNA molecules of the same length, however, as produced during this denaturation, are much more flexible and display a greater tendency towards multiple attachment sites on the surface. This might explain the lower hybridization efficiencies in cycles 2-35.

Although no non-covalently attached DNA was visible with paramagnetic beads, a sporadic, nonspecific denaturation signal was present with the EDC-negative NCD sample, corresponding with some non-covalently adsorbed DNA to the NCD surface. The fact that this signal did not appear in every cycle also displays the dynamic nature of this non-covalently attached DNA. Depending on the conformation and orientation of these adsorbed molecules, they become either available or unavailable for denaturation reactions themselves.

After optimization, the functionalisation procedure works, in decreasing order of efficiency, on ultranano-, nano-, micro-, as well as mono-crystalline diamond. These pioneering experiments were performed on 250 bp DNA fragments. Meanwhile, it was shown that shorter fragments with lengths of 29 bp are better because they are standing perpendicular to the surface, without curling [132].

Higher DNA packing densities can theoretically and practically be increased, but are not necessarily desirable since steric hindrance might deteriorate the hybridization capacity.

6. ConCap mode pH measurements on EDIS structures

This chapter is based on the articles Nanocrystalline Diamond-Based Field-Effect Capacitive pH Sensor. *Transducers 2007 and Eurosensors XXI, Digest of technical papers* **1-2**, U954-U955 [271] and pH Sensitivity of Nanocrystalline Diamond Films. *Physica Status Solidi (a)* **204**, 2925-2930 [272].

To gain more fundamental knowledge about the properties of surface phenomena of diamond films, we decided to investigate diamond-modified electrolyte-insulator-semiconductor (EIS) sensor structures, prepared as described in chapter 4.1.2 *Sample preparation for concap measurements* (p. 65). They combine the sensitivity of FETs with the simplicity of impedimetry. This more stable platform only needs two electrical contacts. With this type of sensor, we successfully carried out so-called ConCap measurements on electrolyte-diamond-insulator-semiconductor (EDIS) structures that show a sensitivity for pH and polyelectrolytes as a sensor model system for DNA.

6.1. Introduction to impedimetric sensing

To probe the properties of (non-conductive) biomolecules, the related double layer capacitance can be measured with electrical impedance spectroscopy [24] and the related concap measurement (see chapter 6.2 *Introduction to ConCap measurements*, p. 84). These sensing principles have the advantage that the detection is label-free, abandoning the need for radioactive, fluorescent, enzymatic or electrochemical labelling [253].

Impedimetry measures the current resulting from an alternating (AC) voltage across the structure at different frequencies. The setup is especially sensitive for events at surfaces. By using only small AC voltage amplitudes, this technique offers a gentle way to look at molecular processes without disrupting the structure of the molecules. The only disadvantage is that also the impedance of the buffer solution is measured. This can be solved by differential measurement: this is a setup in twofold, the only difference between the two setups being the specificity of the sensitive part. The accuracy of the measurement increases, and unwanted background effects (e.g., medium composition) and noise (e.g., temperature) of the bulk are filtered out.
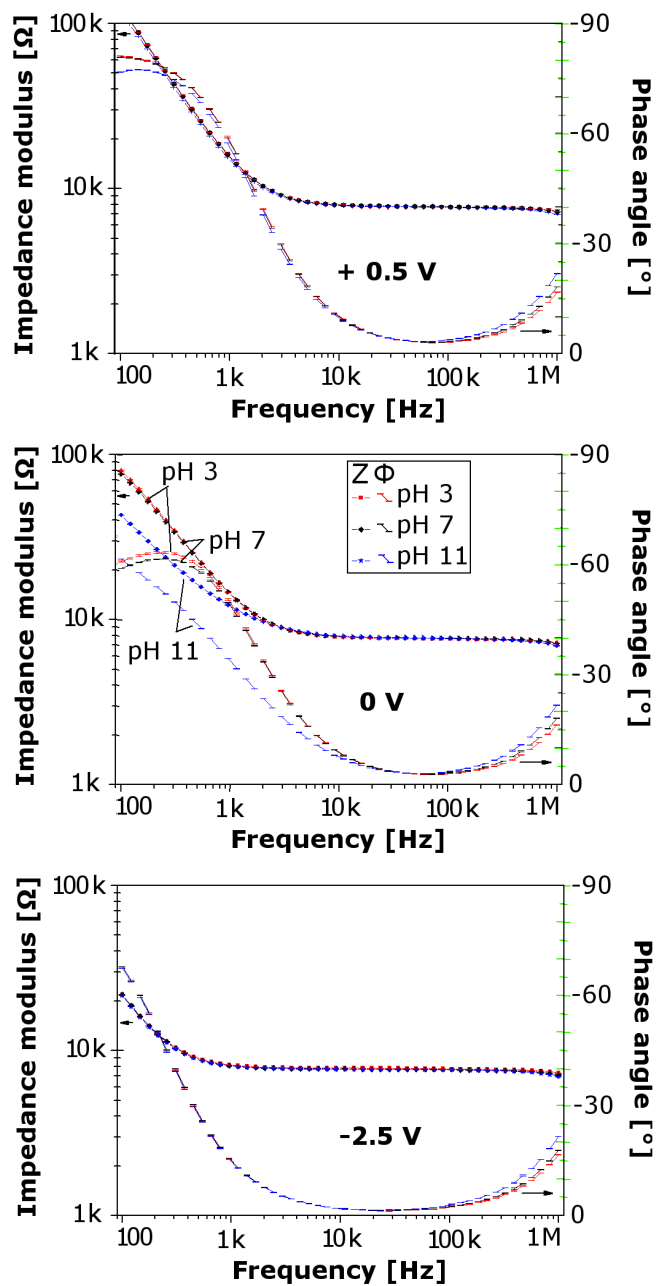
Figure 6.1.   Impedance curves of EDIS sensors at different bias voltages.
Higher pH conditions resemble lower bias voltages: impedance modulus (Z) and phase angle (Φ) obtain lower absolute values when the bias voltage becomes more negative or when the pH of the electrolyte rises.

Like ISFET measurements [figure 2.8, p. 44], electrolyte pH and bias voltages have similar effects on the electrical properties [figure 6.1]. A variety of physicochemical and biological phenomena, like cell migration and viability, can be monitored with impedimetrical measurements [254]. Binding of target molecules to immobilized probe molecules changes the electrical field induced e.g., by the negative charge of hybridizing DNA molecules on the (diamond) space-charge layer, which is also detectable with impedance spectroscopy [24,239,255,256].

There are several ways to represent the measured data. Next to a presentation of the impedance or phase versus frequency, also real and imaginary part versus frequency or imaginary versus real part (Bode diagram) can be shown. For every frequency, the modulus and phase angle between measured current and applied voltage were recorded with a HP 4284A Precision LCR Meter. The impedance spectrum is recorded with a small delay between low and high frequency recording, depending on the number of averaging cycles (e.g., 1 - 1 MHz within 15 s) [240].

The obtained spectrum can be used as a characteristic curve for the empirical state, or an alternative circuit can be modelled [257]. E.g., a lipid bilayer can be modelled as -(CR)- because it electrically behaves in the same way to the applied AC voltage as a capacitance (C) and a resistor (R) in parallel. An extra molecular layer can be fitted as an additional equivalent capacitance element [236]. A (B-doped) diamond film behaves as a Randles-Ershler circuit (-R(CR)-) [258]. And a constant phase element (CPE) models the behaviour of the ion layers and roughness at the solution interface [236,259].

Semiconductor devices can detect charge displacements at the sensor surface caused by DNA hybridization. The electronic behaviour of the interface is frequency-dependent [260]. The use of a two-electrode cell gives similar results as a more complicated three-electrode cell with reference electrode [261,262]. Using small coplanar interdigitated electrodes, increases detection sensitivity because of a higher local current density [263,264].

Impedance spectra were recorded in DNA experiments that were performed lateron. During hybridization and denaturation of DNA, a difference in behaviour was observed for 1-mismatch target DNA and complementary target DNA. A decrease in impedance was observed at lower frequencies when the complementary target DNA was added, while the addition of 1-mismatch target ssDNA caused no significant change. Additional negative charges on the NCD

surface during hybridization influence the depletion region in the diamond resulting in a decrease of the impedance at low frequencies (100 - 1000 Hz) for the complementary ssDNA [132]. Also target-to-antibody binding could be impedimetrically observed [133].

We decided to take the opportunity to relate these findings with ConCap measurements that could be performed in cooperation with Professor Dr. Schöning and Prof. Dr. Poghossian of Aachen University of Applied Sciences and Jülich Research Centre.

6.2. Introduction to ConCap measurements

Surface charge effects, like DNA hybridization and pH sensitivity can be observed in an impedimetric setup using the same field effect as with FET structures, but with a capacitive measurement in a Si-based setup [31]. In contrast to transistor structures, capacitive electrolyte-diamond-insulator-semiconductor (EDIS) sensors are simple in structure, easy and cost-effective in fabrication (usually, no photolithographic process steps nor complicated encapsulation procedures are required) [58,265].

To better understand DNA hybridization, i.e. the interaction of the charged DNA molecules, a more simple model system can be used, with easily obtainable polyelectrolytes (PE), like poly-allylamine (PAH) and poly-styrene sulfonate (PSS) that represent positively, respectively negatively charged macromolecules [41]. Polyelectrolytes can even be used for modification of electrodes to make them sensitive for DNA [266].

The capacitive silicon-based Ta_2O_5-Si setup and ionophore membrane-based electrolyte-membrane-insulator-semiconductor (EMIS) setup were developed as an alternative for the silicon-based ISFET [267,268,269]. The capacitance is measured in function of bias voltage and this curve reflects analyte sensitivity [270]. An advantage of this capacitive setup for future applications is the possibility of multiplexing using the Light-addressable Potentiometric Sensor (LAPS) extension [72]. We combined this setup with electrolyte-diamond-insulator-silicon (EDIS) samples to observe pH sensitivity and polyelectrolyte layer addition (see below in this chapter).

6.3. ConCap principle

In a ConCap measurement, a DC and AC voltage are simultaneously applied over the reference electrode and the metallic backside contact of an electrolyte-insulator-semiconductor (EIS) device under test [figure 6.2].
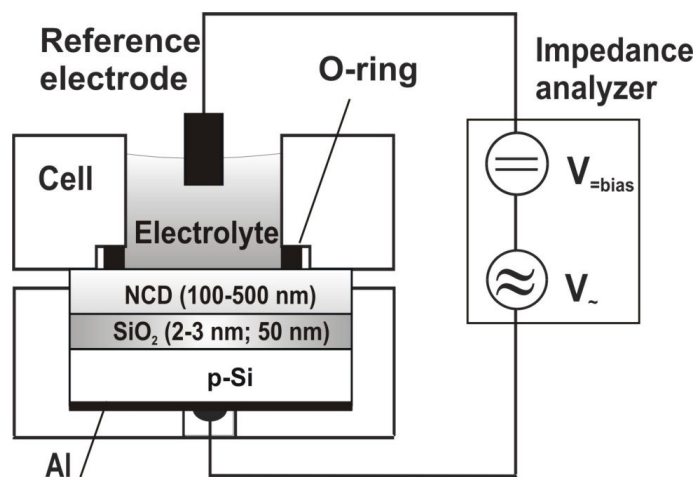
Figure 6.2.   Measuring setup for electrochemical characterisation of EDIS sensors.
The figure also show a schematic cross section of the layer structure.

The capacitance is derived from the impedimetrical measurement using a simple equivalent circuit model -RC- containing a resistor (R) and a capacitor (C) in series. The measurements usually reveal an S-shaped curve [figure 6.3]. Once the initial capacitance versus voltage (C/V) curve is measured, an operation point in the middle of this sigmoid curve is chosen, where the capacitance is very sensitive to small changes in the bias voltage. Here, the space charge in the depletion region evolves from maximum to minimum capacitance.

For these measurements, the chips were staged in a plexi holder [figure 6.4] and measured with a Zahner-Elektrik (Kronach, Germany) IM6 impedance analyzer with built-in software applying an AC voltage (20 mV). In the ConCap mode, the capacitance of the EDIS sensor is kept constant, using a feedback control circuit, and the voltage changes due to the adsorption or binding of charged macromolecules, were directly recorded as a sensor signal. A positive bias voltage means that the counter electrode is positively charged compared to

the sample. The technique principles could be replicated on the HP 4284A Precision LCR Meter with home-made LabVIEW software.
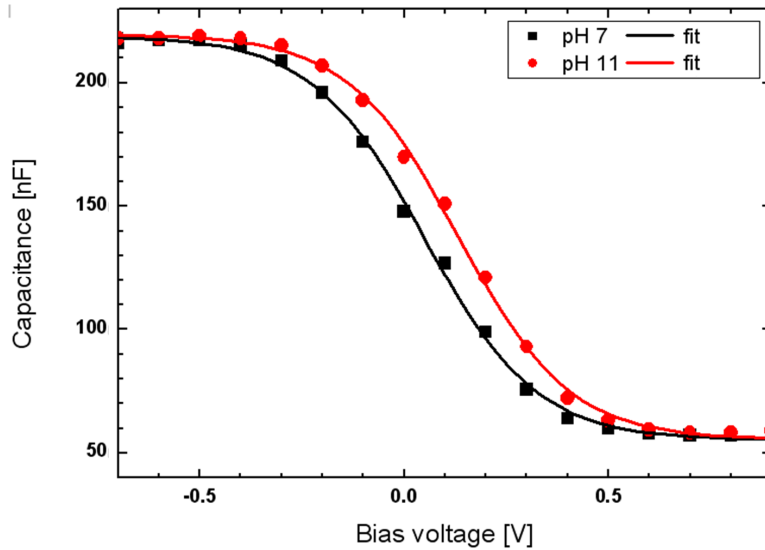
Figure 6.3. *pH-dependent capacitance-voltage characteristic.*
In the negative voltage side (left), charge carriers are attracted and piled up near the surface (accumulation zone), in the transition zone they are depleted (depletion zone), and at the positive voltage side positive charges are left (inversion zone).
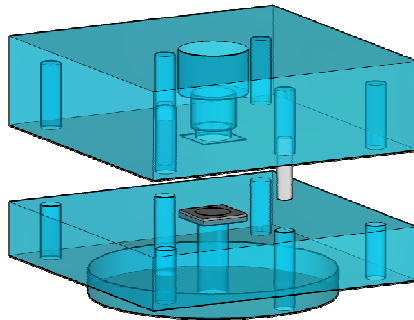
Figure 6.4. *3D view of the capacitive EDIS measurement cell.*
This setup makes sample handling and fixation easy. Top and bottom parts are shown separately (design: FH Aachen, Jülich).
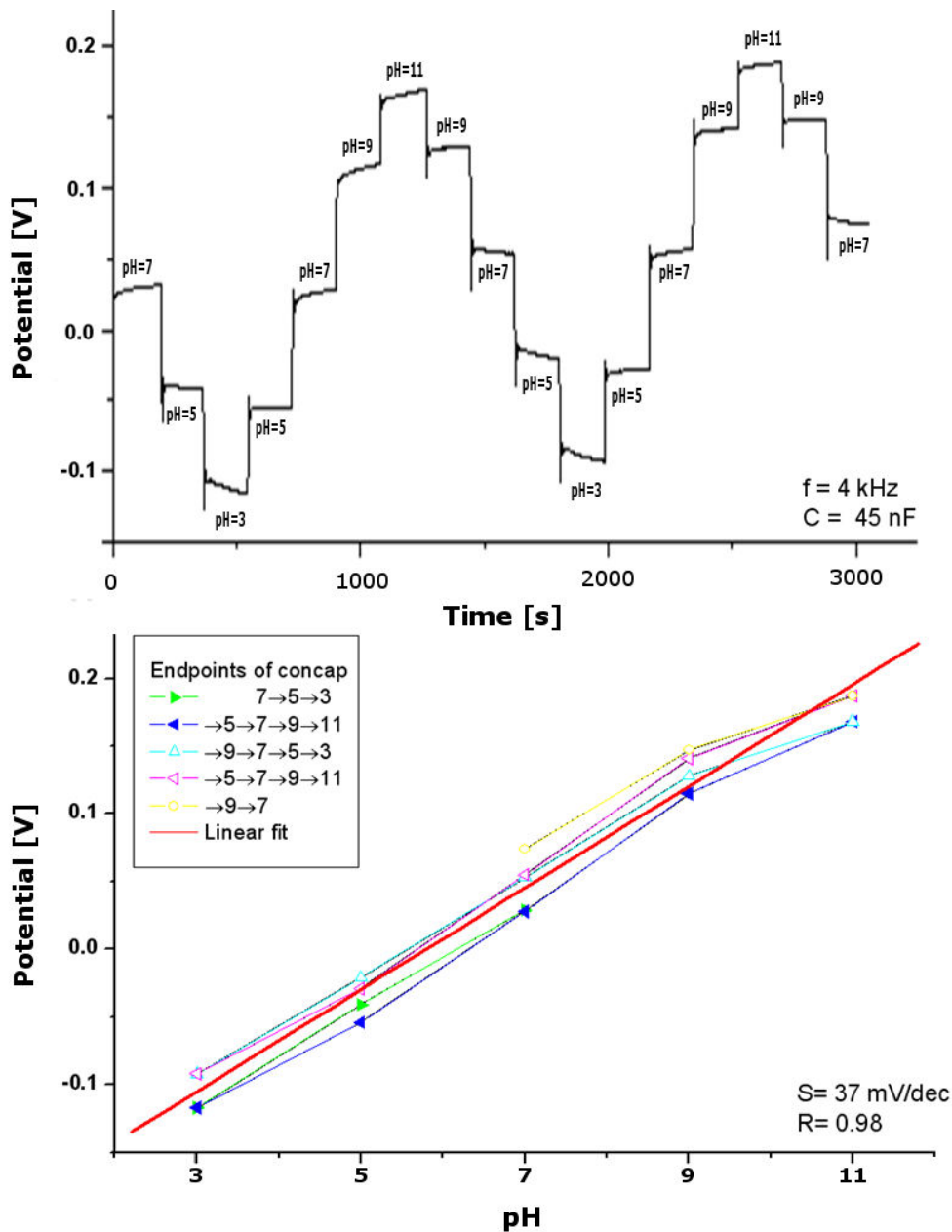
Figure 6.5.   ConCap measurements on EDIS structures.
Stepwise pH-dependent ConCap curves (op) and correlation between ConCap endpoints and pH values (bottom).

The feedback circuit will try to keep the measured capacitance constant starting from this operation point's bias voltage. Therefore, it is called the Constant Capacitance (ConCap) method. During a sensitivity experiment, the bias voltage has to be adjusted in time in order to keep the capacitance at the constant capacitance value, determined by the initially chosen operation point. Different pH values produce stepwise curves [figure 6.5]. From this, an averaged sensitivity value that is expressed in mV/pH can be derived. Also positively and negatively charged poly-electrolytes were subsequently used to influence the electric field at the interface (see chapter 6.5 Introduction to polyelectrolytes, p. 95).

ConCap measurements combine sensitivity of FET measurements with simplicity of execution of electrochemical impedance spectroscopy. Both setups measure conduction channel properties that are influenced by nearby surface charges. Advantage of the latter is that only two contacts are needed instead of three. Whereas the current of this channel is measured in a FET measurement, impedance-induced capacitance is measured in a ConCap measurement. In FET analogy, this corresponds to the opening of the conduction channel. In a recognition experiment, (bio-)chemical reactions inducing chemical or electrical changes at the interface, lead to a shift of these C/V curves to the right or to the left, resulting in ConCap curves analogous to FET constant current curves [figure 2.9, p. 45, and figure 6.9, p. 94].

6.4. Results and discussion

Inspired by the Si-based ConCap measurements in Jülich [267], pH-sensitive capacitive EDIS sensors were made with NCD as hydroxonium binding layer, SiO_2 as insulator and Si as semiconductor [271,272,273]. Diamond was deposited in thin layers (100-500 nm) on Si chips similar to the ones used to fabricate pH sensitive Ta_2O_5-functionalised p-type Si chips [272] [figure 6.6].

6.4.1. Physical characterisation of NCD surfaces

The NCD films have been characterised by ellipsometry, scanning electron microscopy (SEM), atomic force microscopy (AFM) and X-ray photoelectron spectroscopy (XPS) methods. AFM and SEM gave similar results as described in chapter 3.1.1 *Scanning electron microscopy (SEM)* and 3.1.2 *Atomic force microscopy (AFM)*. The results of XPS analysis (see figure 3.11) have shown that

the O_{1s}/C_{1s} atomic concentration ratio for the O-terminated NCD films is about 7-10 at%, as calculated by dividing the relevant peak areas in the recorded spectra by appropriate bulk atomic sensitivity factors. In contrast, the O_{1s}/C_{1s} ratio is about 1 at% for H-terminated NCD films. These values are comparable to those recently reported for B-doped diamond [274,278]. Also, a small trace of Si (~1 at%) has been detected, probably because the NCD film was not completely confluent, exposing the underlying Si layer to the X-ray beam.

Figure 6.6.   EDIS structure cross section (SEM image).

6.4.2. pH-sensitivity of O- and H-terminated NCD films

The pH-sensitive properties of H- and O-terminated nanocrystalline diamond (NCD) films (100-500 nm) have been investigated in the range from pH 3 to pH 11 by means of frequency-dependent capacitance-voltage (C-V) and constant-capacitance (ConCap) methods [268]. An AC voltage with an amplitude of 20 mV has been applied for all types of measurements. For the measurement, the sensor chip was mounted into the measuring cell and contacted on its front side by a standard Titrisol pH buffer solution and a conventional double junction Ag/AgCl electrode (Metrohm, 3 M KCl), and on its rear side an Al evaporated rear side contact by a Au-plated pin. The side walls and backside contact of the EDIS sensor chip were protected from the electrolyte solution by means of an O-ring, thereby circumventing the need for an encapsulation processes. The contact area of the EDIS sensor with the solution is determined by the diameter of the O-ring and was about 0.5 cm^2. The measurements have been carried out in a dark Faraday cage at room temperature.

The EDIS sensors with O-terminated NCD surfaces show an average pH-sensitivity of 30 mV/pH [figure 6.5a]. A slightly smaller pH-sensitivity of 29-36 mV/pH was observed for the EDIS structure with H-terminated NCD surfaces [271]. There is a hysteresis effect probably because of chemical decay effects at extreme pH values. The sensitivity is below Nernst limit (=59 mV/pH).

So far, there have been only a few reports investigating the field-effect in diamond films as platform for chemical and biological sensing. The potential use of diamond for direct electrical sensing of biological binding events such as DNA hybridization and antibody-antigen binding was demonstrated in [150]. An enzyme-modified diamond-based field-effect transistor (FET) has been realised for the detection of urea and glucose [275]. The pH- and ionsensitive properties of an SGFET with monocrystalline and polycrystalline diamond surfaces have been investigated in [127,147,148,153,155,164,276]. Nonetheless, the origin of the pH- and ion-sensitivity of diamond surfaces is still under discussion [127,147,148,276].

The experimental capacitance was compared to the theoretical capacitance of the NCD films of different thicknesses. The calculation was made taking area, thickness and dielectric constant of the two layers into account. Bias voltage was not taken into account. The surface area factor (saf) is the ratio between macroscopical an microscopical surface. It was geometrically calculated from AFM topographical data. The dielectric constant was given the value of hot filament CVD (HFCVD) NCD that ranges from 2.4 to 3.6 and increases with grain size [figure 6.7] [277]. The equivalent capacitance was calculated for different layer thicknesses using the formula for two capacitances in series and the formula for the calculation of the capacitance of one layer, taking in account the extra surface:

$$\frac{1}{C_{eq}} = \sum \frac{1}{C_i} = \frac{1}{C_{NCD}} + \frac{1}{C_{SiO_2}} \quad \text{and} \quad C = \varepsilon_r \varepsilon_0 \frac{A \cdot saf}{d}$$

Within a factor 10, the range of capacitances corresponds to e.g., figure 6.3. The figures shows that the thinner the SiO_2 and/or the NCD layer, the higher the capacitive effect of the total structure. Thinner layers however come at the cost of possible layer defects.

Figure 6.8 shows typical frequency-dependent C-V curves for an EDIS structure with a 100 nm thick O-terminated (left) and H-terminated (right) NCD film measured in a buffer solution of pH 7.
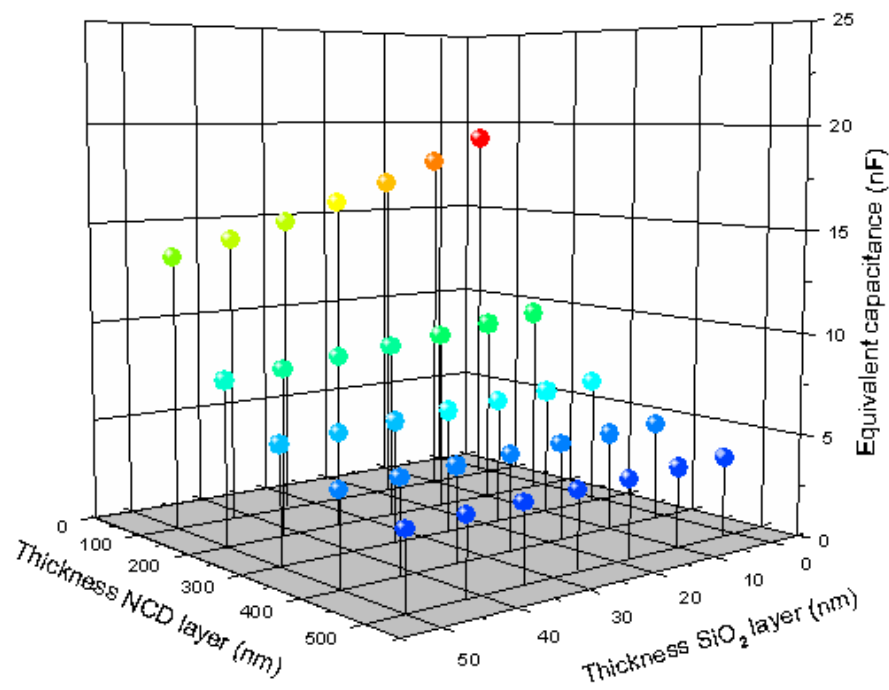
Figure 6.7.   Theoretical calculation of capacitance values.
Colour scale corresponds to the equivalent capacitance value. Simulation for
surface ratio 1.22 and dielectric constant (ε) 3.6 for diamond and 4.1 for SiO_2.
(Figure made with Microcal Origin software)

The complete AC equivalent circuit of an EDIS structure contains
components, like the bulk resistance and space-charge capacitance of the Si,
capacitance of the gate insulator (in this work, SiO_2), resistance and capacitance
of the NCD layer, the double-layer capacitance at the interface electrolyte/NCD,
the electrolyte resistance, and the resistance of the reference electrode.
Generally, any series resistance can lead to a deformation of the C-V curves of
the electrolyte-insulator-semiconductor structure (EIS) [268]. However, for
usual values of insulator thickness (30-100 nm), the electrolyte concentration
($>10^{-4}$-10^{-5} M) and at relatively low measuring frequencies (~1 kHz), the
interferences from several components, like the Si-bulk resistance, the double-
layer capacitance, and the electrolyte resistance can be neglected (see reference
[268] and references herein). In addition, in our experiments, the impedance of
the reference electrode (3-10 kΩ) was much smaller than the impedance of the
NCD (~30-50 kΩ) evaluated from the impedance spectroscopy measurements.
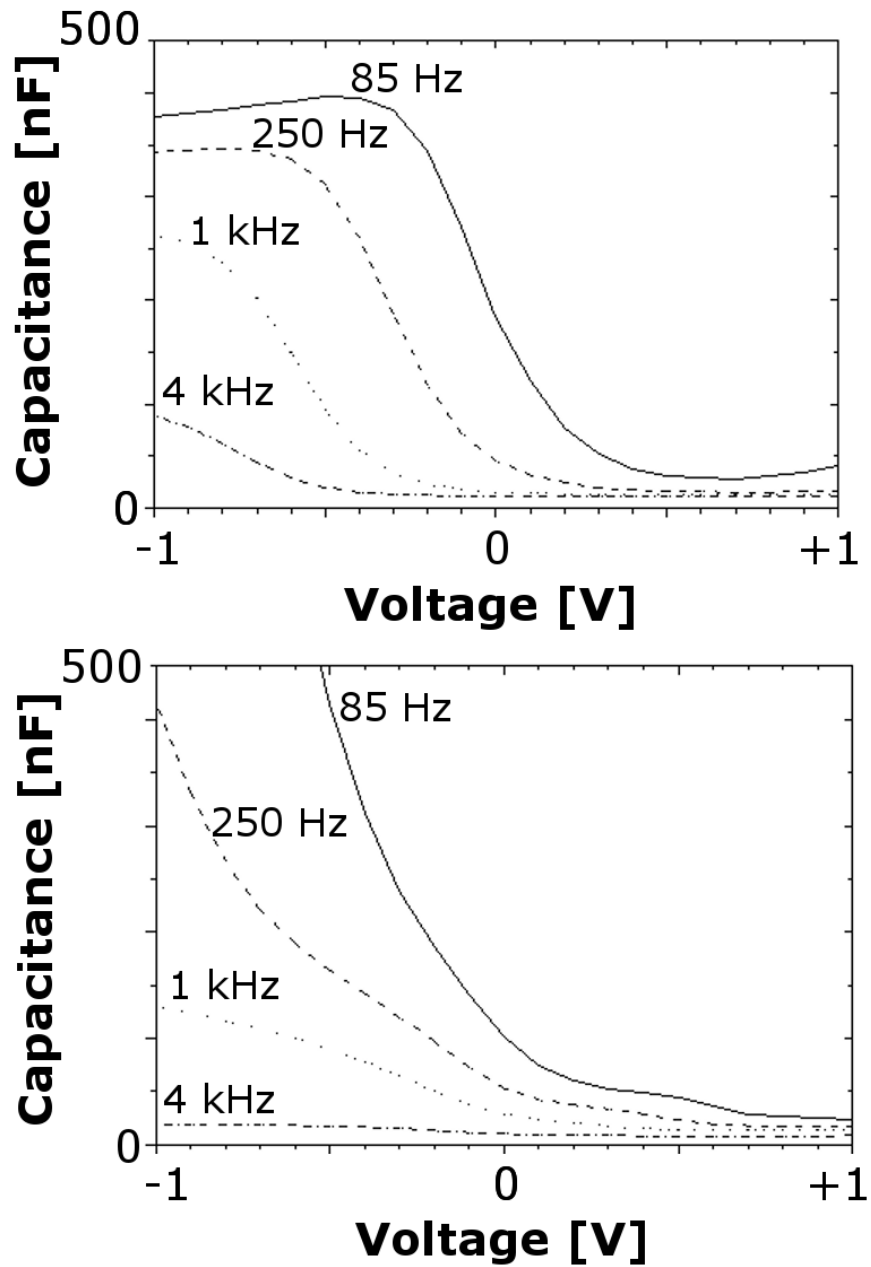
Figure 6.8.   Frequency-dependent C-V curves.
The EDIS structure is covered with a 100 nm thick O-terminated (top) and H-terminated (bottom) NCD film and was measured in a phosphate buffer solution at pH 7.

An impedance effect of the NCD layer is, however, not always negligible, resulting in unusual C-V curves. In a first approximation, the NCD can be described as a parallel network of the NCD resistance and the geometric capacitance, which is in series with the bare EIS structure without NCD layer. Thus, the measured capacitance will be affected by the NCD resistance. The existence of the NCD layer leads to a frequency-dependent distortion of the C-V plots and even practically flat curves at high frequencies (>5-10 kHz).

Figure 6.9 demonstrates the ConCap response of an EDIS structure with a 100 nm thick O-terminated (left) and H-terminated (right) NCD film deposited on a p-Si-SiO$_2$ (50 nm) structure. The ConCap measuring mode allows the investigation of the dynamic behaviour of the sensor signal. In the ConCap mode, by setting the capacitance at a fixed value (usually within the depletion region of the C-V curves at ~60% of the maximum capacitance) using a feedback-control circuit, the potential shift, which results from the pH change at the diamond/electrolyte interface, can be directly recorded.

The EDIS sensors with O-terminated NCD surfaces possess an average pH-sensitivity of 38 mV/pH (evaluated from the ConCap response in figure 6.9) in the range of pH 3 to pH 11. This value is smaller than found for O-terminated polycrystalline diamond field-effect transistors in [147], where a super-Nernstian pH-sensitivity of 63-72 mV/pH has been observed. This high value was lateron partially attributed to the pH sensitivity of the used Pt reference electrode [154]. A possible mechanism for the pH-sensitivity of O-terminated NCD surfaces is described by the site-binding model [143], similar to ion-sensitive field-effect transistors with oxide gate insulators. Similar to the oxide/electrolyte interface, the presence of hydroxyl groups at the oxidised NCD surface can result in pH-dependent changes of the surface charge. Thus, the flat-band voltage (i.e. the voltage that induces zero net charge in the underlying semiconductor) and capacitance of the EDIS structure shifts.

A slightly smaller pH-sensitivity of 29-36 mV/pH was observed for devices with H-terminated NCD surfaces. These values are contrary to results reported in [148,153], where no (or a very small) pH-sensitivity has been observed for H-terminated polycrystalline diamond, and in [127,276], where a nearly-Nernstian pH-sensitivity of 56 mV/pH has been achieved for a FET with H-terminated monocrystalline diamond. On the other hand, the pH-sensitivity of the NCD films in this experiment is higher than found for H-terminated polycrystalline diamond FETs with a poor channel conductivity (~25 mV/pH) [147].
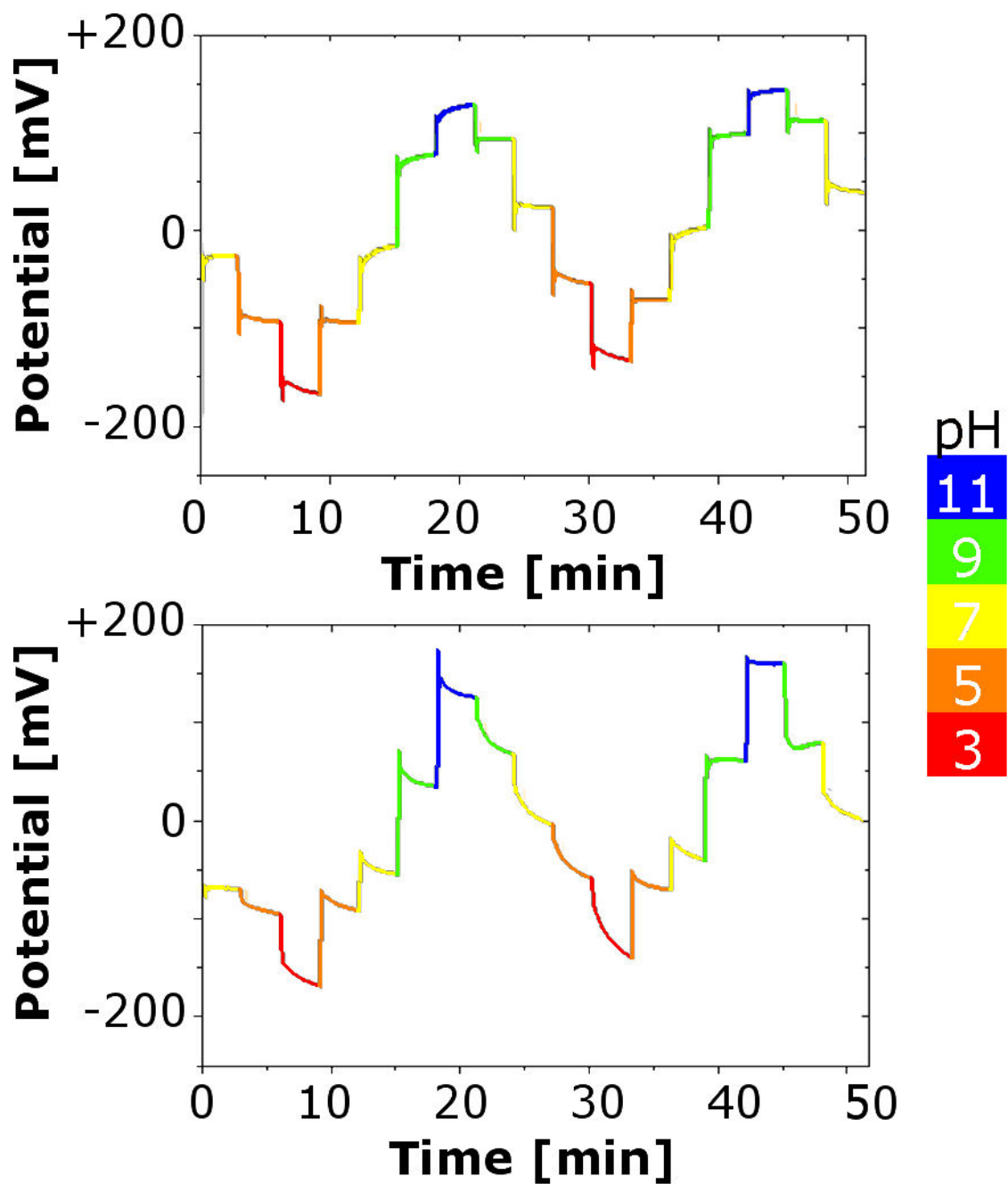
Figure 6.9. pH-dependent ConCap response.
EDIS structure with a 100 nm thick O-terminated (top) and H-terminated (bottom) NCD film.

On ideally H-terminated diamond surfaces, these active surface sites cannot be expected, because C-H bonds are stable and inactive towards H^+ ions [148]. Therefore, the reason for the observed pH-sensitivity of H-terminated diamond is not yet clear. A possible explanation for the relatively high pH-sensitivity of EDIS devices with H-terminated NCD films might be remaining oxidised surface sites due to a suboptimal hydrogenation process. This suggestion is supported by the results of XPS measurements in figure 3.11 (p. 62), where still about 1% O atoms have been observed for H-terminated NCD surfaces. Other possible reasons might be the presence of pores or pinholes within the not completely coalesced NCD layer, allowing a penetration of electrolyte to the underlying pH-sensitive SiO_2 layer or an additional electrochemical oxidation of the H-terminated surface in the solution [278]. In any case, we may conclude that there is a reproducible and significant effect that might be used in future biosensing applications. Additional experiments are needed to explain the pH-sensitive behaviour of the capacitive EDIS devices with H-terminated NCD films.

6.5. Introduction to polyelectrolytes

The ultimate goal is the label-free concap detection of DNA, but in this thesis, polyelectrolytes (PE) were detected as a model system. PE are linear charged macromolecule chains that resemble DNA because they also consist of a long chain with chargeable residues when dissolved in a suitable polar solvent, generally water [279]. They form layer-by-layer adsorbed polyelectrolyte (PE) multilayers. Layer adsorption could be monitored using a field-effect capacitive electrolyte-diamond-insulator-semiconductor (EDIS) sensors with an O-terminated NCD surface. Similar responses were shown with ConCap measurements on Ta_2O_5-modified Si surfaces adsorbed with PSS and PAH layers [23].

PE multilayers (deposited onto the SiO_2 or Ta_2O_5 gate) can be detected using a transistor structure [22], a capacitive EIS (electrolyte-insulator-semiconductor) sensor [22,23,280] or a silicon thin-film resistor [281,282] as transducer. Field-effect devices (FED) in combination with a layer-by-layer self-assembly technique [283,284] can be a powerful tool for a real-time direct electrical monitoring of the adsorption and binding of charged macromolecules. PE, like the positively charged synthetic polyelectrolyte PAH (Poly (allylamine hydrochloride)) and negatively charged PSS (Poly (sodium 4-styrene sulfonate))

[figure 6.10] represent a very useful model system for studying molecular interactions at the liquid/solid state interface.

Application of polyelectrolyte layers can be done by alternated dipping of the diamond samples in PSS and PAH solution [figure 4.1, p. 68]. The charge overcompensation results in a so-called polyelectrolyte multilayer (PEM).

NH_3^+

Cl^-

a)

SO_3^- Na^+

b)
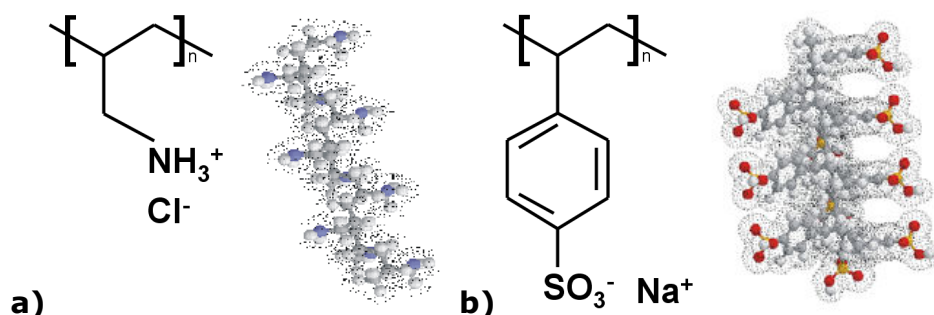
Figure 6.10. Polyelectrolytes.
These charged macromolecules are used as model molecules for detection of DNA. (a) PAH is positively charged (b) PSS is negatively charged.

6.6. Results of measurements with adsorbed PE layers

Figure 6.11 shows typical C-V curves for an EDIS sensor as-prepared and after the adsorption of each PE layer measured at a frequency of 1 kHz. As it can be seen, the adsorption of an additional PE layer shifts the C-V curve of the original EDIS structure along both the capacitance and voltage axis. Small changes (5-10%) in the maximum capacitance (C_{max}) of the C-V curve in the accumulation range are due to an additional series impedance of the molecular layer [268]. For sensor applications, the most interesting part of the C-V curve represents the depletion region, where alternating potential shifts (4-24 mV) have been observed along the voltage axis after the adsorption of each PSS and PAH layer onto the NCD surface. This indicates that the molecular layer may also induce an interfacial potential change (that is in series to the applied gate voltage), resulting in alternating changes of the flat-band voltage, which is defined as the external applied voltage that causes no internal potential difference across the EDIS structure. These shifts can clearly be recognized from the enlarged graph in the depletion region (~60% of C_{max}). The direction of the

shift depends on the sign of the charge of the terminating polyelectrolyte layer. The adsorption of the negatively charged PSS shifts the C-V curve into the direction as for an additional negatively charging of the NCD surface. In contrast, the direction of the potential change after adsorption of the positively charged PAH corresponds to a more positively charged NCD gate surface. Similar changes in the flat-band voltage have also been observed after adsorption of PAH and PSS onto a p-Si-SiO$_2$ or p-Si-SiO$_2$-Ta$_2$O$_5$ structure [22,23,280].
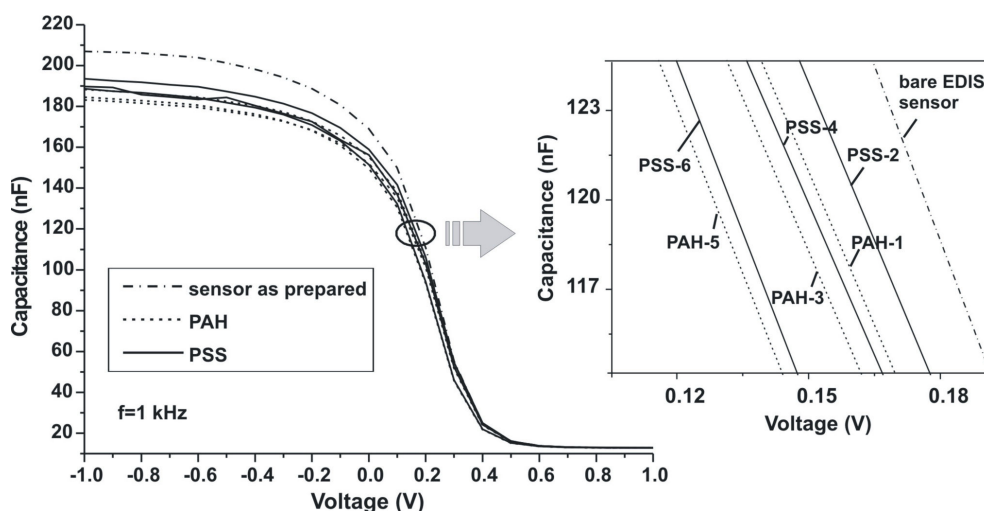
Figure 6.11. Capacitance-voltage characteristic for EDIS structure with layer-by-layer-adsorbed polyelectrolytes.
The inset shows the potential shift zoomed in the depletion region, with typical curves of the sensor as-prepared, and after adsorption of positively charged PAH and negatively charged PSS layers. The numbers indicate the sequence number of the adsorbed layer.

To obtain a picture in which way the characteristics of the functionalized EDIS structures are affected by the number of PE layers, ConCap measurements have been performed after each adsorption. Figure 6.12 depicts the potential changes as a function of the PE layer number evaluated from the ConCap curve. For the EDIS sensor with up to 6-7 adsorbed layers, we have not observed any distinct decrease in the potential shifts with the number of layers deposited that is in agreement with previous results reported for a p-Si-SiO$_2$ and a p-Si-SiO$_2$-Ta$_2$O$_5$ EIS structure without NCD film [22,23,280].

However, after the adsorption of seven layers, the amplitude of the potential shift has the tendency to decrease with increasing number of PE layers. The electric field effect is getting weaker by increasing distance and possibly by worse layering line-up. E.g., potential shifts decrease from 12-15 mV for an EDIS structure with 5-7 PE layers to 2-3 mV for an EDIS structure with 10-13 PE layers. A similar effect has been observed for silicon thin-film resistors functionalized with PE multilayer [281,282].
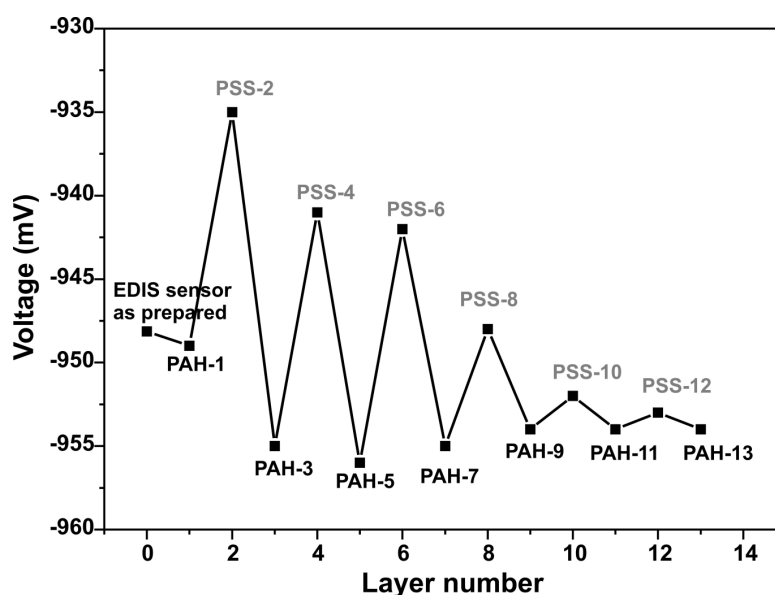
Figure 6.12.   Potential shifts evaluated from the ConCap curve as a function of the PE-layer number.
The maximum number of PE layers was 13.

Despite extensive experimental and theoretical studies of PE adsorption at the solid/liquid interface, a detailed picture of the interfacial behaviour of polymers is far from being complete. From the experiments presented here, as well as those reported in the literature for a $Si-SiO_2$ structure [22,23,280-282], it is obvious that the sign and value of the charge of the outermost layer, the number of adsorbed PE layers and the screening effects inside the adjacent layer of charged macromolecules are the most important parameters that define the characteristics of the field-effect sensors functionalized with charged macromolecules. Nevertheless, the exact mechanism of signal generation is not yet clear in detail and subject to ongoing studies.

Recently, two basic possible mechanisms were proposed which could be responsible for the experimentally observed effects with the FEDs functionalized with charged macromolecules [22,23,280]: on the one hand a change in the flat-band voltage of a capacitive field-effect structure electrostatically induced by the intrinsic charge of adsorbed macromolecules. On the other hand charge or potential effects which are caused from the ion-concentration (including proton concentration) redistribution in the intermolecular spaces or inside a PE multilayer. An alternative mechanism based on the PE adsorption induced reduction of the mobile-ion concentration and, thus, the screening length inside the PE multilayer, has been proposed in [281,282].

The experimental results obtained with the functionalized EDIS structures do not enable us to clearly distinguish between the contributions from each of the above mentioned mechanisms. Therefore, further experiments should be directed to find out the basic mechanism of signal generation. The registration of the overall effect is unequivocally proven and indicates that the concept could also be used in DNA sensor.

7. General conclusions

Biosensor research is becoming more and more important now the need for reliable measuring systems is diversifying to new domains, like biocompatible implantable sensors. Stable platforms for durable long-term implantation are being developed. Diamond is known to be biocompatible, but no implantable diamond-based biosensor application are available yet. We have explored the possible usefulness of diamond as biosensor material. In this thesis, the covalent attachment of DNA to diamond is demonstrated. This is the first but crucial step towards a diamond-based. Secondly, diamond was shown to be a suitable material for detection of surface charge changes, in particular protons (pH) and polyelectrolytes.

In the first step, a biochemical method is developed to immobilize DNA on an NCD diamond surface using ω-unsaturated fatty acids and EDC (see chapter 5, *DNA attachment to NCD*, p. 69). For this, nanocrystalline diamond is grown using microwave plasma-enhanced chemical vapour deposition (MPECVD). After hydrogenation of the surface, 10-undecenoic acid, an ω-unsaturated fatty acid, is tethered by 254 nm photochemical attachment. This is followed by 1-ethyl-3-[3-dimethylaminopropyl]carbodiimide (EDC)-mediated attachment of amino (NH_2)-modified dsDNA. The functionality of the covalently bound dsDNA molecules is confirmed by fluorescence measurements, PCR and gel electrophoresis during 35 denaturation and rehybridization steps.

Compared to other procedures for the attachment of biomolecules to diamond surfaces, the method described has several advantages. First of all, there are many molecules with an NH_2 group which is needed for the amide bond. Proteins (e.g., enzymes, antibodies) contain NH_2 groups both at the amino-terminus as well as at some amino acid residues. However when using the EDC crosslinker with these molecules, internal linking should be prevented by using the N-hydroxy-succinimide (NHS) reagent. Moreover, no deprotection step is necessary with our procedure. The method provides a short and simple link between the DNA and the diamond surface, since no part of EDC is left in the final linker molecule. On the contrary, in the SSMCC approach a part of the crosslinker remains in the final linkage. Therefore, the EDC-based method prevents unwanted side reactions. This approach also maintains the proximity-to-the-surface criterion, which is required for the electrical detection sensitivity during impedance measurements.

The results indicate an EDC-mediated attachment of dsDNA to NCD was established by formation of a covalent bond. However, the binding capacity and/or the denaturation/rehybridization efficiency of functionally active DNA still remains low. Also some non-covalently adsorbed DNA can be detectedThese findings are due to conformational aspects: long molecules (250 bp) show more coiling and aspecific binding, leading to a decreased number of binding places. Smaller molecules (8 b) show higher efficiencies. Also the washing steps were optimized by using hot acetic acid to remove non-covalently bonded undecylenic acid [233, 285].

In a second step, several sensing mechanisms were investigated. Constant capacitance measurements on EDIS structures were most successful, both for pH and polyelectrolyte detection. The pH-sensitive behaviour of H- and O-terminated nanocrystalline diamond (NCD) thin films (100-500 nm) using a field-effect capacitive EDIS structure as transducer was demonstrated. The NCD films were grown on p-Si-SiO$_2$ substrates by a microwave plasma-enhanced chemical vapour deposition. The developed EDIS sensors with O-terminated NCD surfaces show an average pH-sensitivity of 38 mV/pH. A slightly smaller pH-sensitivity of 29-36 mV/pH was observed for the EDIS structure with H-terminated NCD surfaces. While the pH-sensitivity of O-terminated NCD surfaces can be explained by using the site-binding model, additional experiments are needed to understand the origin of pH-sensitivity of the H-terminated NCD surfaces.

To obtain a higher number and more homogeneous diamond samples, larger 3" wafer growth will be developed. Other improvements could be made to the native oxide layer, since holes in the SiO$_2$ layer might be the cause of the limited reproducibility.

The results obtained in chapter 6 *ConCap mode pH measurements on EDIS structures* demonstrate the feasibility of EDIS structures for a label-free electrical detection of adsorption and binding of charged macromolecules. Although with increasing thickness of the polyelectrolyte multilayer (PEM), the effect of polyelectrolyte adsorption decreases, this is not a disadvantage because in our eventual measurement DNA will not accumulate in several layers. It can even be seen as an advantage because the confined proximity sensing region excludes non-specific interactions occurring further away from the sensor surface. The immobilization of charged biomolecules, like DNA and proteins on NCD films will be the subject of future works for extending the biosensor capabilities.

Thanks to the simple coupling of DNA to diamond, it is possible to link biomolecules and diamond for future applications, like DNA sensors for detection of single point mutations [132]. Moreover, the proposed reaction mechanism inspired the use of the attachment technique on other sensor platforms, like carbon nanowalls that are possibly more sensitive due to their higher surface area [243]. Methods for covalent orientated binding of antibodies using this protocol, are being investigated.

The proof that concap measurements work on diamond-covered EDIS sensors revealed that diamond films could, even in non-functionalized setups, be used as sensor platform. This inspired the label-free detection technique using physically adsorbed antibodies that was lateron developed [133,286].

A focus for future developments will be on refinements of the setups leading towards point-of-care diagnostics, like simultaneous measurement of several biomarkers in serum samples. Therefore, a miniaturized impedance spectroscopy device as possible sensor platform for biosensor applications is being developed [287]. Moreover, diamond layers are patterned on glass substrates, forming an array of working electrodes, for parallel measurements. And for simultaneous fluorescence measurements, transparent electrochemical cells are developed, allowing the study correlation between simultaneous impedance and confocal fluorescence imaging.

Summarizing, we can conclude that we succeeded in attaching biomolecules to NCD surfaces as a first step for biosensor construction. As a second step, several sensing principles were evaluated and the most reliable ConCap method was found suitable for detection of charged macromolecules. These results are being further developed towards useful applications.

References

[1]   Shah J., and Wilkins E. (2003) Electrochemical biosensors for detection of biological warfare agents. *Electroanalysis* **15**, 157-167.

[2]   Zhu Z., Zha ng J., and Zhu J. (2005) An overview of Si-based biosensors. S*ensor Letters* **3**, 71-88.

[3]   Han Y., Offenhäusser A., and Ingebrandt S. (2006) Detection of DNA hybridization by a field-effect transistor with covalently attached catcher molecules. *Surface and Interface Analysis* **38**, 176-181.

[4]   Ong K.G., Wang J., Singh R.S., Bachas L.G., and Grimes C.A. (2001) Monitoring of bacteria growth using a wireless, remote query resonant-circuit sensor: Application to environmental sensing. *Biosensors and Bioelectronics* **16**, 305-312.

[5]   Stenger D.A., Gross G.W., Keefer E.W., Shaffer K.M., Andreadis J.D., Ma W., and Pancrazio J.J. (2001) Detection of physiologically active compounds using cell-based biosensors. *Trends in Biotechnology* **19**, 304-309.

[6]   Schöning M.J., Schroth P., and Schütz S. (2000) The use of insect chemoreceptors for the assembly of biosensors based on semiconductor field-effect transistors. *Electroanalysis* **12**, 645-652.

[7]   Inscentinel Ltd., inscentinel.com, Rothamsted Research Harpenden, Hertfordshire AL5 2JQ, UK

[8]   Rains G.C., Utley S.L., and Lewis W.J. (2006) Behavioral monitoring of trained insects for chemical detection. *Biotechnology Progress* **22**, 2-8.

[9]   Tsuda S., Zauner K.P., and Gunji Y.P. (2007) Robot control with biological cells. *Biosystems* **87**, 215-23.

[10]   Medzhitov R. (2001) Toll-like receptors and innate immunity. *Nature Reviews* **1**, 135-145.

[11]   Baumann W.H., Lehmann M., Schwinde A., Ehret R., Brischwein M., and Wolf B. (1999) Microelectronic sensor system for microphysiological application on living cells. *Sensors and Actuators B* **55**, 77-89.

[12]   Vermeeren V., Wenmackers S., Wagner P., and Michiels L. (2009) DNA sensors with diamond as a promising alternative transducer material. *Sensors* **9**, 5600-5636.

[13] Hernando J., Pourrostami T., Garrido J.A., Williams O.A., Gruen D.M., Kromka A., Steinmüller D., and Stutzmann M. (2007) Immobilization of horseradish peroxidase via an amino silane on oxidized ultrananocrystalline diamond. *Diamond and Related Materials* **16**, 138-143.

[14] Fu Y., Yuan R., Xu L., Chai Y., Zhong X., and Tang D. (2005) Indicator free DNA hybridization detection via EIS based on self-assembled gold nanoparticles and bilayer two-dimensional 3-mercaptopropyltrimethoxysilane onto a gold substrate. *Biochemical Engineering* **23**, 37-44.

[15] Notsu H., Fukazawa T., Tatsuma T., Tryk D.A., and Fujishima A. (2001) Hydroxyl groups on boron-doped diamond electrodes and their modification with a silane coupling agent. *Electrochemical and Solid-State Letters* **4**, H1-H3

[16] Pividori M.I., Merkoçi A., and Alegret S. (2000) Electrochemical genosensor design: Immobilisation of oligonucleotides onto transducer surfaces and detection methods. *Biosensors and Bioelectronics* 291-303.

[17] Shen Z., Mernaugh R.L., Yan H., Yu L., Zhang Y., and Zeng X. (2005) Engineered recombinant single-chain fragment variable antibody for immunosensors. *Analytical Chemistry* **77**, 6834-6842.

[18] Frederix F., Bonroy K., Reekmans G., Laureyn W., Campitelli A., Abramov M.A., Dehaen W., and Maes G. (2004) Reduced nonspecific adsorption on covalently immobilized protein surfaces using poly(ethylene oxide) containing blocking agents. *Journal of Biochemical and Biophysical Methods* **58**, 67-74.

[19] Lasseter Clare T., Clare B.H., Nichols B.M., Abbott N.L., and Hamers R.J. (2005) Temperature-dependent transport properties of hydrogen-induced diamond. Oligo(ethylene glycol)-modified silicon and diamond surfaces
. *Langmuir* **21**, 6344-6355.

[20] Lasseter T.L., Clare B.H., Abbott N.L., and Hamers R.J. (2004) Covalently modified silicon and diamond surfaces: Resistance to nonspecific protein adsorption and optimization for biosensing. *Journal of The American Chemical Society* **126**, 10220-10221.

[21] Kharitonov A.B., Wasserman J., Katz E., and Willner I. (2001) The use of impedance spectroscopy for the characterization of protein-modified ISFET devices: Application of the method for the analysis of biorecognition processes. *Journal of Physical Chemistry B* **105**, 4205-4213.

[22] Poghossian A., Abouzar M.H., Sakkari M., Kassab T., Han Y., Ingebrandt S., Offenhäusser A., and Schöning M.J. (2006) Field-effect sensors for monitoring the layer-by-layer adsorption of charged macromolecules. S*ensors and Actuators B* **118**, 163-170.

[23] Poghossian A., Abouzar M.H., Amberger F., Mayer D., Han Y., Ingebrandt S., Offenhäusser A., and Schöning M.J. (2007) Field-effect Sensors with Charged Macromolecules: Characterisation by capacitance-voltage, constant-capacitance, impedance spectroscopy and atomic-force microscopy methods. *Biosensors and Bioelectronics* **22**, 2100-2107.

[24] Hamers R.J., Butler J.E., Lasseter T., Nichols B.M., Russell J.N., Tsea K.-Y., and Yang W. (2005) Molecular and biomolecular monolayers on diamond as an interface to biology. *Diamond and Related Materials* **14**, 661-668.

[25] Fritz J., Cooper E.B., Gaudet S., Sorger P.K., and Manalis S.R. (2002) Electronic detection of dNA by its intrinsic molecular charge. *Proceedings of The National Academy of Science* **99**, 14142-14146.

[26] Nelissen H., Fleury D., Bruno L., Robles P., De Veylder L., Traas J., Micol J.L., Van Montagu M., Inzé D., and Van Lijsebettens M. (2005) The elongata mutants identify a functional elongator complex in plants with a role in cell proliferation during organ growth. *Proceedings of The National Academy of Science* **102**, 7754-7759.

[27] Tachiki M., Kaibara Y., Sumikawa Y., Shigeno M., Banno T., Song K.S., Umezawa H., and Kawarada H. (2003) Diamond nanofabrication and characterization for biosensing application. *Physica Status Solidi* **199**, 39-43.

[28] Wang J. (2000) From DNA biosensors to gene chips. *Nucleic Acids Research* **28**, 3011-3016.

[29] Ingebrandt S., Hana Y., Nakamura F., Poghossian A., Schöning M.J., and Offenhäusser A. (2006) Label-free detection of single nucleotide polymorphisms utilizing the differential transfer function of field-effect transistors. *Biosensors and Bioelectronics* **22**, 2834-2840.

[30] Butte A. (2004) The use and analysis of microarray data. *Nature Reviews* **1**, 951-960.

[31] Berney H., West J., Haefele E., Alderman J., Lane W., and Collins J.K. (2000) A DNA diagnostic biosensor: Development, characterisation and performance. *Sensors and Actuators B* **68**, 100-108.

[32] Fodor S.P., Read J.L., Pirrung M.C., Stryer L., Lu A.T., and Solas D. (1991) Light-directed, spatially addressable parallel chemical synthesis. *Science* **251**, 767-773.

[33] Gillmor S.D., Thiel A.J., Strother T.C., Smith L.M., and Lagally M.G. (2000) Hydrophilic/hydrophobic patterned surfaces as templates for DNA arrays. *Langmuir* **16**, 7223-7228.

[34] MAF-VIB Facility Website (http://www.microarrays.be)

[35] Johnston M. (1998) Gene chips: Array of hope for understanding gene regulation. *Current Biology* **8**, R171-R174

[36] Lopez M.F., and Pluskal M.G. (2003) Protein micro- and macroarrays: Digitizing the proteome. *Journal of Chromatography* **787**, 19-27.

[37] Wang J. (1998) DNA biosensors based on peptide nucleic acid (PNA) recognition layers. A review. *Biosensors and Bioelectronics* **13**, 757–762.

[38] Klug S.J., and Famulok M. (1994) All you wanted to know about SELEX. *Molecular Biology Reports* **20**, 97-107.

[39] Tombelli S., Minunni M., and Mascini M. (2005) Analytical applications of aptamers. *Biosensors and Bioelectronics* **20**, 2424-2434.

[40] Hoppe-Seyler F., and Butz K. (2000) Peptide aptamers. Powerful new tools for molecular medicine. *Journal of Molecular Medicine* **78**, 426-430.

[41] Uslu F., Ingebrandt S., Mayer D., Böcker-Meffert S., Odenthal M., and Offenhäusser (2004) Labelfree fully electronic nucleic acid detection system based on a field-effect transistor device. *Biosensors and Bioelectronics* **9**, 1723-1731.

[42] Alcami A. (2003) Structural basis of the herpesvirus m3-chemokine interaction. *Trends in Microbiology* **11**, 191-193.

[43] Muyldermans S. (2001) Single domain camel antibodies: Current status. *Reviews in Molecular Biotechnology* **74**, 277-302.

[44] Lauwereys M., Arbabi Ghahroudi M.A., Desmyter A., Kinne J., Hölzer W., De Genst E., Wyns L., and Muyldermans S. (1998) Potent enzyme inhibitors derived from dromedary. *The EMBO Journal* **17**, 3512-3520.

[45] Holt L.J., Herring C., Jespers L.S., Woolven B.P., Tomlinson I.M. (2003) Domain antibodies: Proteins for therapy. *Trends in Biotechnology* **21**, 484-490.

[46] Poghossian A., Cherstvy A., Ingebrandt S., Offenhäusser A., and Schöning M.J. (2005) Possibilities and limitations of label-free detection of DNA hybridization with field-effect-based devices. *Sensors and Actuators B* **111-112**, 470-480.

[47] Bergveld P. (2003) ISFET, theory and practice. I*EEE Sensor Conference Toronto* 1-26.

[48] Yang W., and Hamers R.J. (2004) Fabrication and characterization of a biologically sensitive field-effect transistor using a nanocrystalline diamond thin film. *Applied Physics Letters* **85**, 3626-3628.

[49] Strother T., Knickerbocker T., Russell J.N.Jr., Butler J.E., Smith L.M., and Hamers R.J. (2002) Photochemical functionalization of diamond films. *Langmuir* **18**, 968-971.

[50] Piletsky S., and Turner A. (2006) Molecular imprinting of polymers - Landes Bioscience, USA. ISBN 1-58706-219-4.

[51] Vo-Dinh T., and Cullum B. (2000) Biosensors and biochips: Advances in biological and medical diagnostics. *Fresenius' Journal of Analytical Chemistry* **366**, 540-551

[52] Bossi A., Bonini F., Turner A.P.F., and Piletsky S.A. (2007) Molecularly imprinted polymers for the recognition of proteins: The state of the art. *Biosensors and Bioelectronics* **22**, 1131-1137.

[53] Clark L.C.Jr. (1956) Monitor and control of blood and tissue oxygen tensions. *Transactions - American Society for Artificial Internal Organs* **2**, 41-48.

[54] Clark L.C.Jr. (1962) Electrode systems for continuous monitoring in cardiovascular surgery. *Annals New York Academy of Sciences* **102**, 29-45.

[55] Vikas A., and Pundir C.S. (2007) Biosensors: Future analytical tools. *Sensors and Transducers* **76**, 935-936.

[56] Abouzar M., Poghossian A., Razavi A., Besmehn A., Bijnens N., Williams O., Haenen K., Wagner P., Schöning M.J. (2008) Penicillin detection with nanocrystalline-diamond field-effect sensor. *Physica Status Solidi A* **205**(9), 2141-2145

[57] Rolka D., Poghossian A., and Schöning M.J. (2004) Integration of a capacitive EIS sensor into a FIA system for pH and penicillin determination. *Sensors* **4**, 84-94.

[58] Poghossian A., Yoshinobu T., Simonis A., Ecken H., Lüth H., and Schöning M.J. (2001) Penicillin detection by means of field-effect based sensors: EnFET, capacitive EIS sensor or LAPS? *Sensors and Actuators B* **78**, 237.

[59] Poghossian A., Abouzar M.H., Razavi A., Bäcker M., Bijnens N., Williams O.A., Haenen K., Moritz W., Wagner P., and Schöning M.J. (2009) Nanocrystalline-diamond thin films with high pH and penicillin sensitivity prepared on a capacitive Si–SiO$_2$ structure. *Electrochimica Acta* **54**, 5981-5985.

[60] Abouzar M.H., Poghossian A., Razavi A., Williams O.A., Bijnens N., Wagner P., Schöning M.J. (2009) Characterisation of capacitive field-effect sensors with a nanocrystalline-diamond film as transducer material for multi-parameter sensing. *Biosensors and Bioelectronics* **24**, 1298–1304.

[61] Shin D., Rezek B., Tokuda N., Takeuchi D., Watanabe H., Nakamura T., Yamamoto T., and Nebel C.E. (2006) Photo- and electrochemical bonding of DNA to single crystalline CVD diamond. *Physica Status Solidi A* **203**, 3245-3272.

[62] Choi K.H., Friedt J.M., Frederix F., Campitelli A., and Borghs G. (2002) Simultaneous atomic force microscope and quartz crystal microbalance measurements: Investigation of human plasma fibrinogen adsorption. *Applied Physics Letters* **81**, 1335-1337.

[63] Shen Z., Stryker G.A., Mernaugh R.L., Yu L., Yan H., and Zeng X. (2005) Single-chain fragment variable antibody piezoimmunosensors. *Analytical Chemistry* **77**, 797-805.

[64] Vercoutere W., and Akeson M. (2002) Biosensors for DNA sequence detection. *Current Opinion in Chemical Biology* **6**, 816-822.

[65] Akkoyun Akin (2002) Detection of low molecular weight molecules by using optical biosensors. Technical University Carolo-Wilhelmina, Braunschweig.

[66] Lazcka O., Del Campo F.J., and Muñoz F.X. (2007) Pathogen detection: A perspective of traditional methods and biosensors. *Biosensors and Bioelectronics* **22**, 1205-1217.

[67] Baker S.E., Tse K.Y., Lee C.S., and Hamers R.J. (2006) Fabrication and characterization of vertically aligned carbon nanofiber electrodes for biosensing applications. *Diamond and Related Materials* **15**, 433-439.

[68] Poh W.C., and Loh K.P. (2004) Biosensing properties of diamond and carbon nanotubes. *Langmuir* **20**, 5484-5492.

[69] Cvacka J., Quaiserova V., Show P.J., Muck A.J., and Swain G.M. (2003) Boron-doped diamond microelectrodes for use in capillary electrophoresis with electrochemical detection. *Analytical Chemistry* **75**, 2678-2687.

[70] Umek R.M., Lin S.W., Vielmetter J., Terbrueggen R.H., Irvine B., Yu C.J., Kayyem J.F., Yowanto H., Blackburn G.F., Farkas D.H., and Chen Y.P. (2001) Electronic detection of nucleic acids. *Journal of Molecular Diagnostics* **3**, 74-84.

[71] Cahill D.J. (2001) Protein and antibody arrays and their medical applications. *Journal of Immunological Methods* **250**, 81-91.

[72] Yoshinobu T., Iwasaki H., Ui Y., Furuichi K., Ermolenko Y., Mourzina Y., Wagner T., Näther N., and Schöning M.J. (2005) The light-addressable potentiometric sensor for multi-ion sensing and imaging. *Methods* **37**, 94-102.

[73] Kasemo B. (2002) Biological Surface Science. *Surface Science* **500**, 656-677.

[74] Wilson G.S., and Gifford R. (2005) Biosensors for real-time in vivo measurements. *Biosensors and Bioelectronics* **20**, 2388-2403.

[75] Oelßner W., Zosel J., Guth U., Pechstein T., Babel W., Connery J.G., Demuth C., Grote Gansey M., and Verburg J.B. (2005) Encapsulation of ISFET sensor chips. *Sensors and Actuators B* **105**, 104-117.

[76] Gómez R., Bashir R., Sarikaya A., Ladisch M.R., Sturgis J., Robinson J.P., Geng T., Bhunia A.K., Apple H.L., and Wereley S. (2001) Microfluidic biochip for impedance spectroscopy of biological species. *Biomedical Microdevices* **3**, 201-209.

[77] Beebe D.J., Moore J.S., Bauer J.M., Yu Q., Liu R.H., Devadoss C., and Jo B.H. (2000) Functional hydrogel structures for autonomous flow control inside microfluidic channels. *Nature* **404**, 588-590.

[78] Yu B., Longa N., Moussy Y., Moussy F. (2005) Functional hydrogel structures for autonomous flow control inside microfluidic channels. *Biosensors and Bioelectronics* **21** 2275–2282.

[79] Chung H.Y., Weinberger M.B., Levine J.B., Kavner A., Yang J.M., Tolbert S.H., and Kaner R.B. (2007) Synthesis of ultra-incompressible superhard rhenium diboride at ambient pressure. *Science* **316**, 436-439.

[80] Spear K.E., and Frenklach M. (1994) Synthetic diamond: Emerging CVD *science* and technology. *Wiley-Interscience, New York* 244-249; 260-265.

[81] Smisdom N., Smets I., Williams O.A., Daenen M., Wenmackers S., Haenen K., Nesládek M., D'Haen J., Wagner P., Rigo J-M., Ameloot M., and vandeVen M. (2009) Chinese hamster ovary cell viability on hydrogen and oxygen terminated nano- and microcrystalline diamond surfaces. *Physica Status Solidi A* **206**, 2042-2047.

[82] Huaert R. (2003) A review of modified dLC coatings for biological applications. *Diamond and Related Materials* **12**, 583-589.

[83] Catledge S.A., Fries M.D., Vohra Y.K., Lacefield W.R., Lemons J.E., Woodard S., and Venugopalan R. (2002) Nanostructured ceramics for biomedical implants. *Journal of NanoScience and Nanotechnology* **2**, 293-312.

[84] Bąkowicz K., and Mitura S. (2002) Biocompatibility of NCD. *Journal of Wide Bandgap Materials* **9**, 261-272.

[85] Schrand A.M., Huang H., Carlson C., Schlager J.J., Osawa E, Hussain S.M., and Dai L. (2007) Are diamond nanoparticles cytotoxic? *Journal of Physical Chemistry B Letters* **111**, 2-7.

[86] Aspenberg P., Anttila A, Konttinen Y.T., Lappalainen R., Goodman S.B., Nordsletten L., and Santavirta S. (1996) Benign response to particles of diamond and SiC: Bone chamber studies of new joint replacement coating materials in rabbits. *Biomaterials* **17**, 807-812.

[87] Specht C.G., Williams O.A., Jackman R.B., and Schoepfer R. (2004) Ordered growth of neurons on diamond. *Biomaterials* **25**, 4073-4078.

[88] Ariano P., Baldelli P., Carbone E., Gilardino A., Lo Giudice A., Lovisolo D., Manfredotti C., Novara M., Sternschulte H., and Vittone E. (2005) Cellular adhesion and neuronal excitability on functionalised diamond surfaces. *Diamond and Related Materials* **14**, 669-674.

[89] Krüger A. (2006) Hard and soft: Biofunctionalized diamond. *Angewandte Chemie International Edition* **45**, 6426-6427.

[90] Kalbacova M., Michalikova L., Baresova V., Kromka A., Rezek B., and Kmoch S. (2008) Adhesion of osteoblasts on chemically patterned nanocrystalline diamonds. *Physica Status Solidi B* **245**, 2124–2127.

[91] Tang L., Tsai C., Gerberich W.W., Kruckeberg L., and Kania D.R. (1995) Biocompatibility of chemical-vapor-deposited diamond. *Biomaterials* **16**, 483-488.

[92] Khanna P., Villagra A., Kim S., Seto E., Jaroszeski M., Kumar A., and Bhansali S. (2006) Use of nanocrystalline diamond for microfluidic lab-on-a-chip. *Diamond and Related Materials* **15**, 2073-2077.

[93] Eversole W.G. (1962) Synthesis of diamond. U.S. Patent 3030188.

[94] Spitsyn B.V., Bouilov L.L., and Derjaguin B.V. (1981) Vapor growth of diamond on diamond and other surfaces. *Journal of Crystal Growth* **52**, 219-226.

[95] Meykens K. (2002) Study by means of photothermal deflection methods of the opto-electronic properties of CVD diamond in relation to the defect population. PhD Thesis, 5-27.

[96] Daenen M., Williams O.A., D'Haen J., Haenen K., and Nesládek M. (2006) Seeding, growth and characterization of nanocrystalline diamond films on various substrates. *Physica Status Solidi A* **203**, 3005-3010.

[97] John P., Lee J.-K., Anderson M., Gray F., and Wilson J. (2006) The fabrication of diamond microshells. *Chemical Vapor Deposition* **12**, 714-717

[98] Adamschik M., Hinz M., Maier C., Schmid P., Seliger H., Hofer E.P., and Kohn E. (2001) Diamond micro system for bio-chemistry. *Diamond and Related Materials* **10**, 722-730.

[99] Siew P.S., Loh K.P., Poh W.C., and Zhang H. (2005) Biosensing properties of nanocrystalline diamond film grown on polycrystalline diamond electrodes. *Diamond and Related Materials* **14**, 426-431.

[100] Carlisle J.A. (2004) Precious biosensors. *Nature Materials* **3**, 668-669.

[101] May P.W. (2000) Diamond thin films: a 21st-century material. *Philosophical Transactions of the Royal Society of London* **358**, 473-495.

[102] Nesterenko P.N., Fedyanina O.N and Volgin Y.V. (2007) Microdispersed sintered nanodiamonds as a new stationary phase for high-performance liquid chromatography. *The Analyst* 132, 403-405

[103] Rubio-Retama J., Hernando J., López-Ruiz B., Härtl A., Steinmüller D., Stutzmann M., López-Cabarcos E., and Garrido J.A. (2006) Microdispersed sintered nanodiamonds as a new stationary phase for high-performance liquid chromatography. *Langmuir* **22**, 5837-5842.

[104] Yan C., Vohra Y.K., Mao H., and Hemley R.J. (2002) Very high growth rate chemical vapor deposition of single-crystal diamond. *Proceedings of The National Academy of Science of The USA* **99**, 12523-12525.

[105] Williams O.A., and Nesládek M. (2006) Growth and properties of nanocrystalline diamond films. *Physica Status Solidi A* **203**, 3375-3386.

[106] Feliciangeli M.C., Conte G., Rossi M.C., Giorgi L., Giorgi R., and Lisi N. (2007) Impedance and modulus spectroscopy of nanocrystalline diamond films. *Sensors and Actuators B* **126**, 245-251.

[107] Davies R.F. (1994) Handbook on semiconductors. *Elsevier Science, Amsterdam* 454-483.

[108] Mortet V., D'Haen J., Potmesil J., Kravets R., Drbohlav I., Vorlicek V., Rosa J., and Vanecek M. (2005) Thin nanodiamond membranes and their microstructural, optical and photoelectrical properties. *Diamond and Related Materials* **14**, 393-397.

[109] Iijima S., Aikawa Y., and Baba K. (1990) Early formation of chemical vapor deposition diamond films. *Applied Physics Letters* **57**, 2646.

[110] Daenen M., Nesládek M., Potocky S., Mortet V., D'Haen J., Rosa J. and Vanecek M. (2004) Nucleation of nanocrystalline diamond on thin titanium films, presented at the 15th European Conference on Diamond, Diamond-like Materials, Carbon Nanotubes, Nitrides and Silicon Carbide, Palacongressi, Riva del Garda, Italy, September 7-12.

[111] Kawarada H. (1996) Hydrogen-terminated diamond surfaces and interfaces. *Surface Science Reports* **26**, 205-259

[112] Maier F., Riedel M., Mantel B., Ristein J., and Ley L. (2000) Origin of surface conductivity in diamond. *Physical Review Letters* **85** (16), 3472-3475.

[113] Cannaerts M., Nesládek M., Haenen K., Stals L.M., De Schepper L., and Van Haesendonck C. (2001) Reversible switching of the surface conductance of hydrogenated cVD diamond films. *Physica Status Solidi* **186**, 235-240.

[114] Garrido J.A., Heimbeck T., and Stutzmann M. (2005) Temperature-dependent transport properties of hydrogen-induced diamond surface conductive channels. *Physical Review B* **71**, 245310

[115] Looi H.J., Pang L.Y.S., Molloy A.B., Jones F., Foord J.S., and Jackman R.B. (1998) An insight into the mechanism of surface conductivity in thin film diamond. *Diamond and Related Materials* **7**, 550-555.

[116] Rezek B., Watanabe H., and Nebel C.E. (2006) High carrier mobility on hydrogen terminated <100> diamond surfaces. *Applied Physics Letters* **88**, 042110

[117] Tachiki M., Fukuda T., Sugata K., Seo H., Umezawa H., and Kawarada H. (2000) Control of adsorbates and conduction on CVD-grown diamond surface, using scanning probe microscope. A*pplied Surface Science* **159-160**, 578

[118] Cannaerts M. (2002) Scanning probe microscopy for thin film characterization. PhD Thesis, 11-16; 37-62

[119] Cannaerts M., Nesládek M., Haenen K., De Schepper L., Stals L.M., and Van Haesendonck C. (2002) Influence of annealing on the electronic properties of chemical vapor deposited diamond films studied by high vacuum scanning tunneling microscopy and spectroscopy. *Diamond and Related Materials* **11**, 212-217.

[120] Maier F., Riedel M., Mantel B., Ristein J., and Ley L. (2000) Origin of surface conductivity in diamond. *Physical Review Letters* **85**, 3472-3475.

[121] Denisenko A., Aleksov A., Pribil A., Gluche P., Ebert W., and Kohn E. (2000) Hypothesis on the conductivity mechanism in hydrogen terminated diamond films. *Diamond and Related Materials* **9**, 1138-1142.

[122] Fausett B., Granger M.C., Hupert M.L., Wang J., Swain G.M., and Gruen D.M. (2000) The electrochemical properties of nanocrystalline diamond thin-films deposited from C60/argon and methane/nitrogen gas mixtures. *Electroanalysis* **12**, 7-15.

[123] van Staden R.I.S., and Bokretsion R.G. (2006) Simultaneous determination of creatine and creatinine using monocrystalline diamond paste-based amperometric biosensors. *Analytical Letters* **39**, 2227-2233.

[124] Rezek B., Shin D., Watanabe H., and Nebel C.E. (2007) Intrinsic hydrogen-terminated diamond as ion-sensitive field effect transistor. *Sensors and Actuators B* **122**, 596-599.

[125] Strobel P., Riedl M., Ristein J., and Ley L. (2004) Surface transfer doping of diamond. *Nature* **430**, 439-441.

[126] Shirafuji J., and Sugino T. (1996) Electrical properties of diamond surfaces. *Diamond and Related Materials* **5**, 706-713.

[127] Rezek B., Watanabe H., Shin D., Yamamoto T., and Nebel C.E. (2006) Ion-sensitive field effect transistor on hydrogenated diamond. *Diamond and Related Materials* **15**, 673-677

[128] Garrido J.A., Nebel C.E., and Stutzmann M. (2002) Capacitance-voltage studies of Al-Schottky contacts on hydrogen-terminated diamond. *Applied Physics Letters* **81**, 637-639.

[129] Garrido J.A., Nebel C.E., Stutzmann M., Rösel G., Todt R., Amann M.C., Snidero E., and Bergonzo P. (2002) Characterization of sub-micron in-plane devices in H-terminated diamond. *Physica Status Solidi* **193**, 517-522.

[130] Qureshi A., Gurbuz Y., Howell M., Kang W.P., and Davidson J.L. (2010) Nanocrystalline diamond film for biosensor applications. *Diamond and Related Materials* **19**(5-6), 457-461.

[131] Yang J.-H., Song K.-S., Kuga S., and Kawarada H. (2006) Characterization of direct immobilized probe DNA on partially functionalized diamond solution-gate field-effect transistors. *Japanese Journal of Applied Physics* **45**, L1114.

[132] Vermeeren V., Bijnens N., Wenmackers S., Daenen M., Haenen K., Williams O.A., Ameloot M., vandeVen M., Wagner P. and Michiels L. (2007) Towards a real-time, label-free diamond-based DNA sensor. *Langmuir* **23**, 13193-13202.

[133] Bijnens N., Vermeeren V., Daenen M., Grieten L., Haenen K., Wenmackers S., Williams O.A., Ameloot M., vandeVen M., Michiels L., and Wagner P. (2009) Synthetic diamond films as a platform material for label-free protein sensors. *Physica Status Solidi A* **206**, *520-526*.

[134] Chen S.C., Su Y.K., and Tzeng J.S. (1986) The fabrication and characterisation of ion-sensitive field-effect transistors with a silicon dioxide gate. *Journal of Physics D* 1951-1956.

[135] Bergveld P. (2003) Thirty years of ISFETOLOGY what happened in the past 30 years and what may happen in the next 30 years. *Sensors and Actuators B* **88**, 1-20.

[136] van Hal R.E.G., Eijkel J.C.T., Bergveld P. (1995) A novel description of ISFET sensitivity with the buffer capacity and double-layer capacitance as key parameters. *Sensors and Actuators B* **24-25**, 201-205.

[137] Ariano P., Lo Giudice A., Marcantoni A., Vittone E., Carbone E., Lovisolo D. (2008) A diamond-based biosensor for the recording of neuronal activity. *Biosensors and Bioelectronics* **24**, 2046–2050.

[138] Yuqing M., Jianguo G., and Jianrong C. (2003) Ion sensitive field effect transducer-based biosensors. *Biotechnology Advances* **21**, 527-534.

[139] Baur B., Howgate J., Von Ribbeck H.G., Gawlina Y., Bandalo V., Steinhoff G., Stutzmann M., and Eickhoff M. (2006) Catalytic activity of enzymes immobilized on AlGaN/GaN solution gate field-effect transistors. *Applied Physics Letters* **89**, 183901

[140] Steinhoff G., Baur B., Wrobel G., Ingebrandt S., Offenhäusser A., Dadgar A., Krost A., Stutzmann M., and Eickhoff M. (2005) Recording of cell action potentials with AlGaN/GaN field-effect transistors. *Applied Physics Letters* **86**, 033901

[141] Natarajan A., Oskam G., and Searson P.C. (1998) The potential distribution at the semiconductor/solution interface. *Journal of Physical Chemistry B* **102**, 7793-7799.

[142] Gerischer H. (1990) The impact of semiconductors on the concepts of electrochemistry. *Electrochimica Acta* **35**, 1677-1699.

[143] Yates D.E., Levine S., and Healy T.W. (1973) Site-binding Model of The electrical double layer at the oxide/water interface. *Journal of The Chemical Society, Faraday Transactions* **70**, 1807-1818.

[144] Bard A.J., and Faulkner L.R. (1980) Electrochemical methods, fundamentals and applications. *Wiley, New York.*

[145] Bartic C., and Borghs G. (2006) Organic thin-film transistors as transducers for (bio) analytical applications. *Analytical and BioAnalytical Chemistry* **384**, 354-365.

[146] Song K.-S., Hiraki T., Umezawa H., and Kawarada H. (2007) Miniaturized diamond field-effect transistors for application in biosensors in electrolyte solution. *Applied Physics Letters* **90**, 063901

[147] Garrido J.A., Härtl A., Kuch S., Stutzmann M., Williams O.A., and Jackmann R.B. (2005) pH sensors based on hydrogenated diamond surfaces. *Applied Physics Letters* **86**, 073504

[148] Kawarada M., Araki Y., Sakai T., Ogawa T., and Umezawa H. (2001) Electolyte-solution-gate FETs using diamond surface for biocompatible ion sensors. *Physica Status Solidi* **185**, 79-83.

[149] Dankerl M., Eick S., Hofmann B., Hauf M., Ingebrandt S., Offenhäusser A., Stutzmann M., and Garrido J.A. (2009) Diamond transistor array for extracellular recording from electrogenic cells. *Advanced Functional Materials* **19**, 2915 – 2923.

[150] Song K.S., Zhang G.J., Nakamura Y., Furukawa K., Hiraki T., Yang J.H., Funatsu T., Ohdomari I., and Kawarada H. (2006) Label-free DNA sensors using ultrasensitive diamond field-effect transistors in solution. *Physical Review E* **74**, 1-7.

[151] Hammond P.A., Ali D., and Cumming D.R.S. (2002) A single-chip pH sensor fabricated by a conventional CMOS process. *Eurosensors XVI* **1**, 350-355.

[152] Denisenko A., Aleksov A., and Kohn E. (2001) pH sensing by surface-doped diamond and effect of the diamond surface termination. *Diamond and Related Materials* **10**, 667-672.

[153] Song K.-S., Sakai T., Kanazawa H., Araki Y., Umezawa H., Tachiki M., and Kawarada H. (2003) Cl⁻ sensitive biosensor used electrolyte-solution-gate diamond FETs. *Biosensors and Bioelectronics* **19**, 137-140.

[154] Dankerl M., Reitinger A., Stutzmann M., and Garrido J.A. (2008) Resolving the controversy on the pH sensitivity of diamond surfaces. Physica Status Solidi **2**, 31-33.

[155] Song K.S., Nakamura Y., Sasaki Y., Degawa M., Yang J.H., and Kawarada H. (2006) pH-sensitive diamond field-effect transistors (FETs) with directly aminated channel surface. *Analytica Chimica Acta* **573-574**, 3-8.

[156] Garrido J.A., Nebel C.E., Todt R., Amann M.C., Williams O.A., Jackman R., Nesládek M., and Stutzmann M. (2003) Novel in-plane gate devices on hydrogenated diamond surfaces. *Physica Status Solidi* **199**, 56-63

[157] Müller R., Denisenko A., and Kohn E. (2003) Effect of surface quality on ion sensitivity of H-terminated diamond. *Diamond and Related Materials* **12**, 554-559.

[158] Müller R., Denisenko A., Adamschik M., and Kohn E. (2002) On the ion-sensitivity of H-terminated surface channel devices on diamond. *Diamond and Related Materials* **11**, 651-656.

[159] Song K.S., Degawa M., Nakamura Y., Kanazawa H., Umezawa H., and Kawarada H. (2004) Surface-modified diamond field-effect transistors for enzyme-immobilized biosensors. *Japanese Journal of Applied Physics* **43**, L814-L817.

[160] Shang L., Clare T.L., Eriksson M.A., Marcus M.S., Metz K.M., and Hamers R.J. (2005) Electrical characterization of nanowire bridges incorporating biomolecular recognition elements. *Nanotechnology* **16**, 2846-2851.

[161] Cui Y., Wei Q., Park H., and Lieber C.M. (2001) Nanowire nanosensors for highly sensitive and selective detection of biological and chemical species. *Science* **293**, 1289-1292.

[162] Staii C., and Johnson A.T.Jr. (2005) DNA-decorated carbon nanotubes for chemical sensing. *Nano Letters* **5**, 1774-1778.

[163] Aleksov A., Kubovic M., Kaeb N., Spitzberg U., Bergmaier A., Dollinger G., Bauer Th., Schreck M., Stritzker B., and Kohn E. (2003) Diamond field effect transistors - Concepts and challenges. *Diamond and Related Materials* **12**, 391-398.

[164] Kanazawa H., Song K.-S., Sakai T., Nakamura Yu., Umezawa H., Tachiki M., and Kawarada H. (2003) Effect of iodide ions on the hydrogen-terminated and partially oxygen-terminated diamond surface. *Diamond and Related Materials* **12**, 618-622.

[165] Kichambare P.D., and Star A. (2007) Biosensing using carbon nanotube field-effect transistors. *Nanomaterials for Biosensors Nanotechnologies for The Life Sciences* **8**, 1-16.

[166] Pouthas F., Gentil C., Côte D., and Bockelmann U. (2004) DNA detection on transistor arrays following mutation-specific enzymatic amplification. *Applied Physics Letters* **84**, 1594-1596.

[167] Chatterjee A., Compton R.G., Foord J.S., Hiramatsu M., and Marken F. (2003) Electrochemical and related processes at surface conductive diamond-solution interfaces. *Physica Status Solidi A* **199**, 49-55.

[168] Voigt H., Schitthelm F., Lange T., Kullick T., and Ferretti R. (1997) Diamond-like carbon-gate pH-ISFET. *Sensors and Actuators B* **44**, 441-445.

[169] Latto M.N., Riley D.J., and May P.W. (2000) Impedance studies of boron-doped CVD diamond electrodes. *Diamond and Related Materials* **9**, 1181-1183.

[170] Ivandini T.A., Sarada B.V., Terashima C., Rao T.N., Tryk D.A., Ishiguro H., Kubota Y., and Fujishima A. (2002) Electrochemical detection of tricyclic antidepressant drugs by HPLC using highly boron-doped diamond electrodes. *Journal of ElectroAnalytical Chemistry* **521**, 117-126.

[171] Sirés I., Cabot P.L., Centellas F., Garrido J.A., Rodríguez R.M., Arias C., and Brillas E. (2006) Electrochemical degradation of clofibric acid in water by anodic oxidation. Comparative study with platinum and boron-doped diamond electrodes. *Electrochimica Acta* **52**, 75-85

[172] Spetz A.L., Nakagomi S., Wingbrant H., Andersson M., Salomonsson A., Roy S., Wingqvist G., Katardjiev I., Eickhoff M., Uvdal K., and Yakimova R. (2006) New materials for chemical and biosensors. *Materials and Manufacturing Processes* **21**, 253-256.

[173] Härtl A., Garrido J.A., Nowy S., Zimmermann R., Werner C., Horinek D., Netz R., and Stutzmann (2007) The ion sensitivity of surface conductive single crystalline diamond. *Journal of The American Chemical Society* **129**, 1287-1292.

[174] Koizumi S. (2003) In: Nebel, C.E., Ristein J. (Eds.), Semiconductors and semimetals, Thin film diamond I, **76**. *Elsevier Academic Press, Amsterdam,* pp. 239-259.

[175] Nesládek M. (2005) Conventional N-type doping in diamond. State of the art and recent progress. *Semiconductor Science and Technology* **20**, R19-R27

[176] Achatz P., Williams O.A., Bruno P., Gruen D.M., Garrido J.A., and Stutzmann M. (2006) Effect of nitrogen on the electronic properties of ultrananocrystalline diamond thin films grown on quartz and diamond substrates. *Physical Review B* **74**, 155429

[177] Gheeraert E., Koizumi S., Teraji T., Kanda H., and Nesládek M. (1999) Electronic states of boron and phosphorus in diamond. *Physica Status Solidi* **174**, 39-51.

[178] Sternschulte H., Schreck M., Stritzker B., Bergmaier A., and Dollinger G. (2000) Lithium addition during cVD diamond growth. Influence on the optical emission of the plasma and properties of the films. *Diamond and Related Materials* **9**, 1046-1050.

[179] Williams O.A. (2006) Ultrananocrystalline diamond for electronic applications. *Semiconductor Science and Technology* **21**, R49-R56

[180] Yamanaka S., Takeuchi D., Watanabe H., Okushi H., and Kajimura K. (2000) Low-compensated boron-doped homoepitaxial diamond films. *Diamond and Related Materials* **9**, 956-959.

[181] Teraji J., Hamada M., Wada H., Yamamoto M., Arima K. and Ito T. (2005) High rate growth and electrical-optical properties of high-quality homoepitaxial diamond (100) films. *Diamond and Related Materials* **14**, 255-260.

[182] Yamanaka S, Takeuchi D, Watanabe H, Okushi H and Kajimura K (2000) Low-compensated boron-doped homoepitaxial diamond films. *Diamond and Related Materials* **9**, 956-959.

[183] Aleksov A., Vescan A., Kunze M., Gluche P., Ebert W., Kohn E., Bergmaier A., and Dollinger G. (1999) Diamond junction FETs based on δ-doped channels. *Diamond and Related Materials* **8**, 941-945.

[184] Koizumi S., Watanabe K., Hasegawa M., and Kanda H. (2001) Ultraviolet emission from a diamond pn junction. *Science* **292**, 1899-1901.

[185] Amaratunga G.A.J. (2002) A dawn for carbon electronics. *Science* **297**, 1657

[186] Xu J., Granger M.C., Chen Q., Strojek J.W., Lister T.E., and Swain G.M. (1997) Diamond thin films could be an electrochemist's best friend. *Analytical Chemistry* **69**, 591A-597A.

[187] Miller J.B., and Brown D.W. (1996) Photochemical modification of diamond surfaces. *Langmuir* **12**, 5809-5817.

[188] Wenmackers S., Haenen K., Nesládek M., Wagner P., Michiels L., vandeVen M., and Ameloot M. (2003) Covalent immobilization of DNA on CVD diamond films. *Physica Status Solidi* **199**, 44-48.

[189] Garrido J.A., Nebel C.E., Todt R., Rösel G., Amann M.C., and Stutzmann M. (2003) Fabrication of in-plane gate transistors on hydrogenated diamond surfaces. *Applied Physics Letters* **82**, 988-990.

[190] Sakai T., Song K.S., Kanazawa H., Nakamura Y., Umezawa H., Tachiki M., and Kawarada H. (2003) Ozone-treated channel diamond field-effect transistors. *Diamond and Related Materials* **12**, 1971-1975.

[191] Ando T., Yamamoto K., Ishil M., Kamo M., and Sato Y. (1993) Vapour-phase oxidation of diamond surfaces in O_2 studied by diffuse reflectance FTIR and temperature-programmed desorption spectroscopy. *Journal of the Chemical Society, Faraday Transactions* **89**, 3635-3640.

[192] Banno T., Tachiki M., Seo H., Umezawa H., and Kawarada H. (2002) Fabrication of diamond single-hole transistors using AFM anodization process. *Diamond and Related Materials* **11**, 387-391.

[193] Tachiki M., Ishizaka H., Banno T., Sakai T., Song K.S., Umezawa H., and Kawarada H. (2002) Low-temperature operation of diamond surface-channel field-effect transistors. *Materials Research Society Symposium Proceedings* **719**, 1-5.

[194] Rezek B., Sauerer C., Garrido J.A., Nebel C.E., and Stutzmann M. (2003) Scribing into hydrogenated diamond surfaces using AFM. *Applied Physics Letters* **82**, 3336-3338

[195] Nebel C.E., Rezek B., Shin D., and Watanabe H. (2006) Surface electronic properties of H-terminated diamond in contact with adsorbates and electrolytes. *Physica Status Solidi A* **203**, 3273-3298.

[196] Takahashi K., Tanga M., Takai O., and Okamura H. (2003) DNA preservation using diamond chips. *Diamond and Related Materials* **12**, 572-576.

[197] Ida S., Tsubota T., Hirabayashi O., Nagata M., Matsumoto Y., and Fujishima A (2003) Chemical reaction of hydrogenated diamond surface with peroxide radical initiators. *Diamond and Related Materials* 601-605.

[198] Finstad C.C., Thorsness A.G., and Muscat A.J. (2006) The mechanism of amine formation on Si(100) activated with chlorine atoms. *Surface Science* **600**, 3363-3374.

[199] Zhang G.J., Song K.-S., Nakamura Y., Ueno T., Funatsu T., Ohdomari I., and Kawarada H. (2006) DNA micropatterning on polycrystalline diamond via one-step direct amination. *Langmuir* **22**, 3728-3734.

[200] Baker S.E., Cai W., Lasseter T.L., Weidkamp K.P., and Hamers R.J.(2002) Covalently bonded adducts of deoxyribonucleic acid (DNA) oligonucleotides with single-wall carbon nanotubes: Synthesis and hybridization. *Nano Letters* **2**, 1413–1417.

[201] Williams K.A., Veenhuizen P.T.M., de la Torre B.G., Eritja R., and Dekker C. (2002) Carbon nanotubes with DNA recognition. *Nature* **420**, 761.

[202] Nakamura T., Suzuki M., Ishihara M., Ohana T., Tanaka A., and Koga Y. (2004) Photochemical modification of diamond films: Introduction of perfluorooctyl functional groups on their surface. *Langmuir* **20**, 5846-5849.

[203] Takahashi K. (2000) Substrates for immobilizing and amplifying dNA, dNA-immobilized chips having DNA immobilized on the substrates, and method for amplifying DNA. *European Patent Application* EP 1063286 A1

[204] Tanga M., and Takahashi K. (2001) Supports for immobilizing DNA or the like. E*uropean Patent A*pplication EP 1 122 309 A1

[205] Nakamura E., and Kenichi S. (2002) Method for producing DNA chip, and DNA chip obtained thereby. *U.S. Patent Application* US 2002/0197417 A1.

[206] Tanga M., and Takahashi K. (2003) Supports for immobilizing DNA or the like. *US Patent Application* US 006607908 B1

[207] Strother T., Hamers R.J., and Smith L.M. (2000) Covalent attachment of oligodeoxyribonucleotides to amine-modified Si (001) surfaces. *Nucleic Acids Research* **28**, 3535-3541.

[208] Troupe C.E., Drummond I.C., Graham C., Grice J., John P., Wilson J.I.B., Jubber M.G., and Morrison N.A. (1998) Diamond-based glucose sensors. *Diamond and Related Materials* **7**, 575-580.

[209] Baker S.E., Tse K.Y., Hindin E., Nichols B.M., Lasseter T., and Hamers R.J. (2005) Covalent functionalization for biomolecular recognition on vertically aligned carbon nanofibers. *Chemistry of Materials* **17**, 4971-4978.

[210] Lud S.Q., Steenackers M., Jordan R., Bruno P., Gruen D.M., Feulner P., Garrido J.A., and Stutzmann M. (2006) Chemical grafting of biphenyl self-assembled monolayers on ultrananocrystalline diamond. *Journal of The American Chemical Society* **128**, 16884-16891.

[211] Ida S., Tsubota T., Tanii S., Nagata M., and Matsumoto Y. (2003) Chemical modification of the diamond surface using benzoyl peroxide and dicarboxylic acids. *Langmuir* **19**, 9693-9698.

[212] Uetsuka H., Shin D., Tokuda N., Saeki K., and Nebel C.E. (2007) Electrochemical grafting of boron-doped single-crystalline chemical vapor deposition diamond with nitrophenyl molecules. *Langmuir* **23**, 3466-3472.

[213] Ushizawa K., Sato Y., Mitsumori T., Machinami T., Ueda T., and ando T. (2002) Covalent immobilisation of dNA on diamond and its verification by diffuse reflectance infrared spectroscopy. *Chemical Physics Letters* **351**, 105-108.

[214] Yang W., Auciello O., Butler J.E., Cai W., Carlisle J.A., Gerbi J.E., Gruen D.M., Knickerbocker T., Lasseter T.L., Russell J.N., Smith L.M., and Hamers R.J. (2002) DNA-modified nanocrystalline diamond thin-films as stable, biologically active substrates. *Nature Materials* **1**, 253-257.

[215] Knickerbocker T., Strother T., Schwartz M.P., Russell J.N.Jr., Butler J.E., Smith L.M., and Hamers R.J. (2003) DNA-modified diamond surfaces. *Langmuir* **19**, 1938-1942 .

[216] Sun B., Colavita P.E., Kim H., Lockett M., Marcus M.S., Smith L.M., and Hamers R.J. (2006) Covalent photochemical functionalization of amorphous carbon thin films for integrated real-time biosensing. *Langmuir* **22**, 9598-9605.

[217] Yang W., Butler J.E., Russell J.N.Jr., and Hamers R.J. (2007) Direct electrical detection of antigen-antibody binding on diamond and silicon substrates using electrical impedance spectroscopy. *The Analyst* **132**, 296-306.

[218] Härtl A., Schmich E., Garrido J.A., Hernando J., Catharino S.C.R., Walter S., Feulner P., Kromka A., Steinmüller D., and Stutzmann M. (2004) Protein-modified nanocrystalline diamond thin films for biosensor applications. *Nature Materials* **3**, 736-742.

[219] Lasseter T. L., Clare B. H., Abbott N. L., and Hamers R. J. (2004) Covalently modified silicon and diamond surfaces: Resistance to nonspecific protein adsorption and optimization for biosensing. *Journal of the American Chemical Society* **126**, 10220-10221.

[220] Stutzmann M., Garrido J.A., Eickhoff M., and Brandt M.S. (2006) Direct biofunctionalization of semiconductors: A survey. *Physica Status Solidi A* **14**, 3424-3437.

[221] Coffinier Y., Szunerits S., Jama C., Desmet R., Melnyk O., Marcus B., Gengembre L., Payen E., Delabouglise D., and Boukherroub R. (2007) Peptide immobilization on amine-terminated boron-doped diamond surfaces. *Langmuir* **23**, 4494-4497.

[222] Lu M., Knickerbocker T., Cai W., Yang W., Hamers R.J., and Smith L.M. (2004) Invasive cleavage reactions on DNA-modified diamond surfaces. *Biopolymers* **73**, 606-613.

[223] Yang N., Uetsuka H., Watanabe H., Nakamura T., and Nebel C.E. (2007) Photochemical amine layer formation on H-terminated single-crystalline CVD diamond. *Chemistry of Materials* **19**, 2852-2859.

[224] Krueger A., Stegk J., Liang Y., Lu L., and Jarre G. (2008) Biotinylated nanodiamond: Simple and efficient functionalization of detonation diamond. *Langmuir* **24**, 4200-4204.

[225] Gajovic-Eichelmann N., Ehrentreich-Förster E., and Bier F.F. (2003) Directed immobilization of nucleic acids at ultramicroelectrodes using a novel electro-deposited polymer. *Biosensors and Bioelectronics* **19**, 417-422.

[226] Huang T.S., Tzeng Y., Liu Y.K., Chen Y.C., Walker K.R., Guntupalli R., and Liu C. (2004) Immobilization of antibodies and bacterial binding on nanodiamond and carbon nanotubes for biosensor applications. *Diamond and Related Materials* **13**, 1098-1102.

[227] Yang J.H., Song K.S., Zhang G.J., Degawa M., Sasaki Y., Ohdomari I., and Kawarada H. (2006) Characterization of DNA hybridization on partially aminated diamond by aromatic compounds. *Langmuir* **22**, 11245-11250.

[228] Grabarek Z., and Gergely J. (1990) Zero-length crosslinking procedure with the use of active esters. *Analytical Biochemistry* **185**, 131-135.

[229] Nettikadan S.R., Johnson J.C., Vengasandra S.G., Muys J., and Henderson E. (2004) Virichip: A solid phase assay for detection and identification of viruses by atomic force microscopy. *Nanotechnology* **15**, 383-389.

[230] Tachiki M., Seo H., Banno T., Sumikawa Y., Umezawa H. and Kawarada H. (2002) Fabrication of single-hole transistors on hydrogenated diamond surface using AFM. *Applied Physics Letters* **61**, 2854-2856.

[231] Kaibara Y., Sugata K., Tachiki M., Umezawa H., and Kawarada H. (2003) Control wettability of the hydrogen-terminated diamond surface and the oxidized diamond surface using AFM. *Diamond and Related Materials* **12**, 560-564.

[232] University of Arizona, Department of Molecular & Cellular Biology (http://www.mcb.arizona.edu/IPC/spectra_page.htm)

[233] Vermeeren V., Wenmackers S., Daenen M., Haenen K., Williams O.A., Ameloot M., vandeVen M., Wagner P., and Michiels L. (2008) Topographical and functional characterization of the ssDNA probe layer generated through EDC-mediated covalent attachment to nanocrystalline diamond using fluorescence microscopy. *Langmuir* **24**, 9125-9134.

[234] Ghodbane S., Deneuville A., Tromson D., Bergonzo P., Bustarret E., and Ballutaud D. (2006) Sensitivity of raman excited at 325 nm to surface treatments of undoped polycrystalline diamond films. *Physica Status Solidi A* **203**, 2397-2402.

[235] Ghodbane S., Ballutaud D., Deneuville A., and Baron C. (2006) Influence of boron concentration on the XPS spectra of the (100) surface of homoepitaxial boron-doped diamond films. *Physica Status Solidi A* **203**, 3147-3151.

[236] Tse K.Y., Nichols B.M., Yang W., Butler J.E., Russell J.N.Jr., and Hamers R.J. (2005) Electrical properties of diamond surfaces functionalized with molecular monolayers. *Journal of Physical Chemistry B* **109**, 8523-8532.

[237] Sambrook, and Russell (2001) Molecular cloning, a laboratory manual. **1-3**. *Cold Spring Harbor Laboratory Press*.

[238] Nichols B.M., Butler J.E., Russell J.N., and Hamers R.J. (2005) Photochemical functionalization of hydrogen-terminated diamond surfaces: A structural and mechanistic study. *Journal of Physical Chemistry B* **109**, 20938-20947.

[239] Cai W., Peck J.R., Van Der Weide D.W., and Hamers R.J. (2004) Direct electrical detection of hybridization at DNA-modified silicon surfaces. *Biosensors and Bioelectronics* **19**, 1013-1019.

[240] Cooreman P., Thoelen R., Manca J., vandeVen M, Vermeeren V., Michiels L., Ameloot M., and Wagner P. (2005) Impedimetric immunosensors based on the conjugated polymer PPV. *Biosensors and Bioelectronics* **20**, 2151-2156.

[241] Zhong Y.L., Chong K.F., May P.W., Chen Z.K., and Loh K.P. (2007) Optimizing biosensing properties on undecylenic acid-functionalized diamond. *Langmuir* **23**, 5824-5830.

[242] Chong K.W., Long K.P., Vedula S.R.K., Lim C.T., Sternschulte H., Steinmüller D., Sheu F.S., and Zhong Y.L. (2007) Cell adhesion properties on photochemically functionalized diamond. *Langmuir* **23**, 5615-5621.

[243] Vansweevelt R., Malesevic A., Van Gompel M., Vanhulsel A., Wenmackers S., D'Haen J., Vermeeren V., Ameloot M., Michiels L., Van Haesendonck C., and Wagner P. (2010) Biological modification of carbon nanowalls with DNA strands and hybridization experiments with complementary and mismatched DNA. *Chemical Physics Letters* **485**, 196-201.

[244] Faucheux A., Gouget-Laemmel A.C., De Villeneuve C.H., Boukherroub R., Ozanam F., Allongue P., and Chazalviel J.N. (2006) Well-defined carboxyl-terminated alkyl monolayers grafted onto H-Si(111): Packing density from a combined AFM and quantitative IR study. *Langmuir* **22**, 153-162.

[245] Voicu R., Boukherroub R., Bartzoka V., Ward T., Wojtyk J.T.C., and Wayner D.M. (2004) Formation, characterization, and chemistry of undecanoic acid-terminated silicon surfaces: Patterning and immobilization of DNA. *Langmuir* **20**, 11713-11720.

[246] Yang W., Auciello O., Butler J.E., Cai W., Carlisle J.A., Gerbi J.E., Gruen D.M., Knickerbocker T., Lasseter T.L., Russell J.N., Smith L.M., Hamers R.J. (2002) DNA-modified nanocrystalline diamond thin-films as stable, biologically active substrates. *Nature Materials* **1**, 253-257.

[247] http://commons.wikimedia.org/ - GNU Free Documentation License

[248] Christiaens P., Vermeeren V., Wenmackers S., Daenen M., Haenen K., Nesládek M., vandeVen M., Ameloot M., Michiels L., and Wagner P. (2006) EDC-mediated DNA attachment to nanocrystalline CVD diamond films. *Biosensors and Bioelectronics* **22**, 170-177.

[249] Vermeeren V., Christiaens P., Wenmackers S., vandeVen M., Ameloot M., Wagner P. and Michiels L. (2005) EDC-mediated DNA attachment to nanocrystalline diamond. *Communications in Agricultural and Applied Biological Sciences* **70**, 285-288.

[250] Wenmackers S., Christiaens P., Daenen M., Haenen K., Nesládek M., vandeVen M., Vermeeren V., Michiels L., Ameloot M., and Wagner P. (2005) DNA attachment to nanocrystalline diamond films. *Physica Status Solidi* **202**, 2212-2216.

[251] Wenmackers S., Christiaens P., Deferme W., Daenen M., Haenen K., Nesládek M., Wagner P., Vermeeren V., Michiels L., vandeVen M., Ameloot M., Wouters J., Naelaerts L., and Mekhalif Z. (2005) Head-on immobilization of dNA fragments on CVD-diamond layers. *Materials Science Forum* **492-493**, 267-272.

[252] Steel A.B., Levicky R.L., Herne T.M., and Tarlov M.J. (2000) Immobilization of nucleic acids at solid surfaces: Effect of oligonucleotide length on layer assembly. *Biophysics Journal* **79**, 975-981.

[253] Yang W., Butler J.E., Russell J.N. , and Hamers R.J. (2004) Interfacial electrical properties of dNA-modified diamond thin films: Intrinsic response and hybridization-induced field effects. *Langmuir* **20**, 6778-6787.

[254] Wegener J., Keese C.R., and Giaever I. (2000) Electric Cell-Substrate Impedance Sensing (ECIS) As A Noninvasive Means to Monitor The Kinetics of Cell Spreading to Artificial Surfaces. *Experimental Cell Research* **259**, 158-166.

[255] Ma K.S., Zhou H., Zoval J., and Madou M. (2006) DNA hybridization detection by label free versus impedance amplifying label with impedance spectroscopy. *Sensors and Actuators B* **114**, 58-64.

[256] Gu H., Su X., and Loh K.P. (2005) Electrochemical impedance sensing of dNA hybridization on conducting polymer film-modified diamond. *Journal of Physical Chemistry B* **109**, 13611-13618.

[257] Curat S., Ye H., Gaudin O., and Jackman R.B. (2005) An impedance spectroscopic study of n-type phosphorus-doped diamond. *Journal of Applied Physics* **98**, 073701

[258] Pleskov Y.V. (2002) Electrochemistry of diamond: A review. *Russian Journal of Electrochemistry* **38**, 1275-1291.

[259] Carrara S., Gürkaynak F.K., Guiducci C., Stagni C., Benini L., Leblebici Y., Samori B., and De Micheli G. (2007) Interface layering phenomena in capacitance detection of DNA with biochips. *Sensors and Transducers* **76**, 969-977.

[260] Lasseter T.L., Cai W., and Hamers R.J. (2004) Frequency-dependent electrical detection of protein binding events. *Analyst* **129**, 3-8.

[261] Zebda A., Stambouli V., Labeau M., Guiducci C., Diard J.P., and Le Gorrec B. (2006) Metallic oxide $CdIn_2O_4$ films for the label free electrochemical detection of DNA hybridization. *Biosensors and Bioelectronics* **22**, 178-184.

[262] Stambouli V., Zebda A., Appert E., Guiducci C., Labeau M., Diard J.P., Le Gorrec B., Brack N., and Pigram P.J. (2006) Semiconductor oxide based electrodes for the label-free electrical detection of DNA hybridization: Comparison between Sb doped SnO_2 and $CdIn_2O_4$. *Electrochimica Acta, Special Issue On BES-ISE Symposium 2005* **51**, 5206-5214.

[263] Van Gerwen P., Laureyn W., Laureys W., Huyberechts G., Op De Beeck M., Baert K., Suls J., Sansen W., Jacobs P., Hermans L., and Mertens R. (1998) Nanoscaled interdigitated electrode arrays for biochemical sensors. *Sensors and Actuators B* **49**, 73-80.

[264] Laureyn W., Nelis D., Van Gerwen P., Baert K., Hermans L., Magnee R., Pireaux J.J., and Maes G. (2000) Nanoscaled interdigitated titanium electrodes for impedimetric biosensing. *Sensors and Actuators B* **68**, 360-370.

[265] Poghossian A., and Schöning M.J. (2006) Silicon-based chemical and biological field-effect sensors. *Encyclopedia of Sensors* **9**, 463-534.

[266] Weng J., Zhang J., Li H., Sun L., Lin C., and Zhang Q. (2008) Label-free DNA sensor by boron-doped diamond electrode using an ac impedimetric approach. *Anal. Chem.* **80**, 7075–7083.

[267] Schöning M.J., Tsarouchas D., Beckers L., Schubert J., Zander W., Kordos P., and Lüth H. (1996) A highly long-term stable silicon-based pH sensor fabricated by pulsed laser deposition technique. *Sensors and Actuators B* **35**, 228-232.

[268] Poghossian A., Mai D.-T., Mourzina Yu., and Schöning M.J. (2004) Impedance effect of an ion-sensitive membrane: Characterisation of an EMIS sensor by impedance spectroscopy, capacitance-voltage and constant-capacitance method. *Sensors and Actuators B* **103**, 423-428.

[269] Bäcker M., Beging S., Biselli M., Poghossian A., Wang J., Zang W., Wagner P., and Schöning M.J. (2009) Concept for a solid-state multi-parameter sensor system for cell-culture monitoring. Electrochimica Acta 54, 6107-6112.

[270] Fabry P., and Laurent-Yvonnou L. (1990) The C-V method for characterizing ISFET or EOS devices with ion-sensitive membranes. *Journal of ElectroAnalytical Chemistry* **286**, 23-40.

[271] Poghossian A., Christiaens P., Abouzar M.H., Wagner T., Bijnens N., Williams O.A., Daenen M., Haenen K., Wagner P. and Schöning M.J. (2007) Nanocrystalline diamond-based field-effect capacitive pH sensor. *Transducers 2007 and Eurosensors XXI, Digest of technical papers, 1 and 2, U954-U955*. ISBN 978-1-4244-0841-2.

[272] Christiaens P., Abouzar M.H., Poghossian A., Wagner T., Bijnens N., Williams O.A., Daenen M., Haenen K., Douhéret O., D'Haen J., Mekhalif Z., Schöning M.J., and Wagner P. (2007) pH sensitivity of nanocrystalline diamond films. *Physica Status Solidi A* **204**, 2925-2930.

[273] Poghossian A., Abouzar M.H., Christiaens P., Williams O.A., Haenen K., Wagner P. and Schöning M.J. (2008) Sensing charged macromolecules with nanocrystalline diamond-based field-effect capacitive sensors. *Journal of Contemporary Physics (Armenian Academy of Sciences)* **43**, 77-81.
Original publication in Russian: Погосян А., Абузар М.Г., Кристиенс П., Уилъямс О.А., Хенен К., Вагнер П., Шёнинг М.Дж. (2007) Зондирование заряженных макромолекул нанокристаллическими емкостными полевыми датчиками на основе алмаза. *Известия НАН Армении, Физика* **43**, 120-127.

[274] Liu F.B., Wang J.D., Liu B., Li X.M., and Chen D.R. (2007) Effect of electronic structures on electrochemical behaviors of surface-terminated boron-doped diamond film electrodes *Diamond and Related Materials* **16**, 454.

[275] Song K.-S., Degawa M., Nakamura Y., Kanazawa H., Umezawa H., and Kawarada H. (2004) Surface-modified diamond field-effect transistors for enzyme-immobilized biosensors. *Japanese Journal of Applied Physics* **43**, L814.

[276] Nebel C.E., Rezek B., Shin D., Watanabe H., and Yamamoto T. (2006) Electronic properties of H-terminated diamond in electrolyte solutions. *Journal of Applied Physics* **99**, 033711.

[277] Wang Z.L., Li J.J., Sun Z.H., Li Y.L., Luo Q., Gu C.Z., and Cui Z. (2007) Effect of grain size and pores on the dielectric constant of nanocrystalline diamond films. *Applied Physics Letters* **90**, 133118

[278] Rao T.N., Tryk D.A., Hashimoto K., and Fujishima A. (1999) Band-edge movements of semiconducting diamond in aqueous electrolyte induced by anodic surface treatment. *Journal of the Electrochemical Society* **146**, 680-684.

[279] Lvov Y. (2001) Thin film nanofabrication by alternate adsorption of polyions, proteins and nanoparticles. In: Handbook for Surfaces and Interfaces **3**: Nanostructured Materials, Ed: H. Nalwa, Academic Press, NY, 170-189.

[280] Poghossian A., Ingebrandt S., Abouzar M.H., and Schöning M.J. (2007) Label-free detection of charged macromolecules by using a field-effect-based sensor platform: Experiments and possible mechanisms of signal generation. *Applied Physics A* **87**, 517.

[281] Neff P.A., Naji A., Ecker C., Nickel F., Klitzing R., and Bausch A.R. (2006) Electrical detection of self-assembled polyelectrolyte multilayers by a thin film resistor. *Macromolecules* **39**, 463-466.

[282] Neff P.A., Wunderlich B.K., Lud S.Q., and Bausch A.R. (2006) Silicon-on-insulator based thin film resistors for quantitative biosensing applications. *Physica Status Solidi A*, **14**, 3417.

[283] Decher G., Eckle M., Schmitt J., and Struth B. (1998) Layer-by-layer assembled multicomposite films. *Current Opinion in Colloid and Interface Science* **3**, 32.

[284] Schönhoff M. (2003) Self-assembled polyelectrolyte multilayers. *Current Opinion in Colloid and Interface Science* **8**, 86-95.

[285] Wenmackers S., Vermeeren V., vandeVen M., Ameloot M., Bijnens N., Haenen K., Michiels L., and Wagner P. (2009) Diamond-based DNA sensors: surface functionalization and read-out strategies. *Physica Status Solidi A* **206**, 391–408.

[286] Wenmackers S., Pop S.D., Roodenko K., Vermeeren V., Williams O.A., Daenen M., Douhéret O., D'Haen J., Hardy A., Van Bael M.K., Hinrichs K., Cobet C., vandeVen M., Ameloot M., Haenen K., Michiels L., Esser N., and Wagner P. (2008) Structural and optical properties of DNA layers covalently attached to diamond surfaces. *Langmuir* **24**, 7269-7277 (2008).

[287] van Grinsven B., Vandenryt T., Duchateau S., Gaulke A., Grieten L., Thoelen R., Ingebrandt S., De Ceuninck W., Wagner P. (2009) Customized impedance spectroscopy device as possible sensor platform for biosensor applications. *Physica Status Solidi A* **207**, 919-923.

International publications

[01] Vermeeren V., Christiaens P., Wenmackers S., vandeVen M., Ameloot M., Wagner P. and Michiels L. (2005) EDC-mediated DNA attachment to nanocrystalline diamond. *Communications in Agricultural and Applied Biological Sciences* **70**, 285-288.

[02] Wenmackers S., Christiaens P., Daenen M., Haenen K., Nesládek M., vandeVen M., Vermeeren V., Michiels L., Ameloot M., and Wagner P. (2005) DNA attachment to nanocrystalline diamond films. *Physica Status Solidi* **202**, 2212-2216.

[03] Wenmackers S., Christiaens P., Deferme W., Daenen M., Haenen K., Nesládek M., Wagner P., Vermeeren V., Michiels L., vandeVen M., Ameloot M., Wouters J., Naelaerts L., and Mekhalif Z. (2005) Head-on immobilization of DNA fragments on CVD-diamond layers. *Materials Science Forum* **492-493**, 267-272.

[04] Christiaens P., Vermeeren V., Wenmackers S., Daenen M., Haenen K., Nesládek M., vandeVen M., Ameloot M., Michiels L., and Wagner P. (2006) EDC-mediated DNA attachment to nanocrystalline CVD diamond films. *Biosensors and Bioelectronics* **22**, 170-177.

[05] Poghossian A., Christiaens P., Abouzar M.H., Wagner T., Bijnens N., Williams O.A., Daenen M., Haenen K., Wagner P. and Schöning M.J. (2007) Nanocrystalline diamond-based field-effect capacitive pH sensor. *Transducers 2007 and Eurosensors XXI, Digest of technical papers* **1-2**, U954-U955. ISBN 978-1-4244-0841-2.

[06] Christiaens P., Abouzar M.H., Poghossian A., Wagner T., Bijnens N., Williams O.A., Daenen M., Haenen K., Douhéret O., D'Haen J., Mekhalif Z., Schöning M.J., and Wagner P. (2007) pH sensitivity of nanocrystalline diamond films. *Physica Status Solidi A* **204**, 2925-2930.

[07] Abouzar M.H., Poghossian A., Schöning M.J., Christiaens P., Williams O., Wagner P., Haenen K. (2009), Field effect sensor on nanocristalline diamond base - Feldeffektsensor auf nanokristalliner Diamantbasis, *VDI-Berichte* **2011**, 549-558.

[08] Poghossian A., Abouzar M.H., Christiaens P., Williams O.A., Haenen K., Wagner P. and Schöning M.J. (2008) Sensing charged macromolecules with nanocrystalline diamond-based field-effect capacitive sensors. *Journal of Contemporary Physics (Armenian Academy of Sciences)* **43**, 77-81.

[08'] Original publication in Russian: Погосян А., Абузар М.Г., Кристиенс П.,
       Уилъямс О.А., Хенен К., Вагнер П., Шёнинг М.Дж. (2007)
       Зондирование заряженных макромолекул нанокристаллическими
       емкостными полевыми датчиками на основе алмаза. *Известия НАН
       Армении, Физика* **43**, 120-127.